

---

Electronic Thesis and Dissertation Repository

---

9-14-2021 5:00 PM

## 4DCT analysis of in-vivo carpal kinematics during FEM

Manisha R. Mistry, *The University of Western Ontario*

Supervisor: Suh, Nina, *The University of Western Ontario*

Co-Supervisor: Lalone, Emily, *The University of Western Ontario*

A thesis submitted in partial fulfillment of the requirements for the Master of Science degree in Surgery

© Manisha R. Mistry 2021

Follow this and additional works at: <https://ir.lib.uwo.ca/etd>



Part of the [Orthopedics Commons](#), [Other Biomedical Engineering and Bioengineering Commons](#), [Plastic Surgery Commons](#), and the [Surgery Commons](#)

---

### Recommended Citation

Mistry, Manisha R., "4DCT analysis of in-vivo carpal kinematics during FEM" (2021). *Electronic Thesis and Dissertation Repository*. 8227.

<https://ir.lib.uwo.ca/etd/8227>

This Dissertation/Thesis is brought to you for free and open access by Scholarship@Western. It has been accepted for inclusion in Electronic Thesis and Dissertation Repository by an authorized administrator of Scholarship@Western. For more information, please contact [wlsadmin@uwo.ca](mailto:wlsadmin@uwo.ca).

# Abstract

A consensus, detailed understanding of carpal kinematics remains elusive. 4-dimensional CT (4DCT) is a validated modality capable of accurately studying *in-vivo* kinematic motion. The objective of this work is to quantify normal, *in-vivo* kinematic motion of the carpus through a flexion-extension arc of motion using 4DCT. Ten healthy, un-injured volunteers underwent a 4DCT scanning protocol through a complete arc of flexion-extension motion. Kinematic changes in motion were quantified using helical axis motion data for each carpal bone. Helical axes were compared between bones and statistical analysis performed using repeated-measures ANOVA to identify difference in kinematic motion between bones ( $p < 0.05$ ). The carpus can be divided into four main kinematic blocks: the distal carpal block, the proximal carpal block and individual scaphoid and trapezium blocks. This work supports an additional segmentation of the trapezium from the distal carpal row, which suggests some modulation between the scaphoid and distal carpal row.

**Keywords:** Kinematics, Carpal Kinematics, 4DCT, Computational Modelling, Kinematic Modelling

# Lay Summary

Two of the most impactful health interventions of the 20<sup>th</sup> centuries have been joint replacement surgery of both the hip and the knee. A crucial element of the success of these surgeries stems from thorough understanding of the normal way the joint moves, also known as its normal kinematics. The wrist is comprised of the most complex series of joints in the body, and is heavily relied upon for day-to-day human functions and activities. Although several theories regarding carpal kinematics exist, a consensus understanding remains elusive. Our understanding draws largely from biomechanical cadaver analysis, or static non-invasive imaging modalities. Without truly the understanding the native motion and interactions of a joint, we do not have precise targets to tailor interventions to; nor can we truly recreate normal function in the setting of pathology or injury.

We use 4-dimensional Computerized Tomography (4DCT) technology, to define normal, *in-vivo* kinematics of the carpus. 4DCT presents the opportunity to study *in-vivo*, real-time motion and kinematics in a non-invasive manner. This, all whilst preserving muscle tone and soft tissue stabilizers present during functional range of motion of a patient's wrist. Four-dimensional CT allows the inclusion of time, and can analyze changes in 3-dimensional orientation over time or throughout a movement or activity. The accuracy of this method of measurement is high and unparalleled by older modalities. Additionally, it provides a lower-cost model of study than cadaveric samples, and lower risk profile to participants than implantable trackers; making it an ideal modality.

This work contributes data needed to thoroughly understand the way in which the wrist and carpus move. By understanding the complex kinematics of the wrist, we can set our sights on optimizing implants and surgical interventions aimed to restore peak function in patients burdened with injury and pathology.

# Co-Authorship Statement

## **Chapter 1:**

Sole Authorship: Manisha R. Mistry

Manuscript Review: Nina Suh, Emily Lalone

## **Chapter 2:**

Sole Authorship: Manisha R. Mistry

Manuscript Review: Nina Suh, Emily Lalone

## **Chapter 3:**

Study Design: Manisha R. Mistry, Elizabeth Norman, Nina Suh, Emily Lalone

Manuscript Preparation: Manisha R. Mistry

Manuscript Review: Nina Suh, Emily Lalone

## **Chapter 4:**

Data Collection: Manisha R. Mistry, Elizabeth Norman, Danning Li, Nicole Stachura,  
Alexandra Munn, Winston Jin, Alex Rocha, Hanshin Lee

Data Analysis: Manisha R. Mistry, Elizabeth Norman

Statistical Analysis: Manisha R. Mistry

Manuscript Preparation: Manisha R. Mistry

Manuscript Review: Nina Suh, Emily Lalone

## **Chapter 5:**

Sole Authorship: Manisha R. Mistry

Manuscript Review: Nina Suh, Emily Lalone



# Acknowledgements

I'd like to acknowledge that this work would not be possible without the assistance, guidance, support and contribution of many outstanding individuals. Firstly, I'd like to extend an immense thank you to my supervisors Drs. Emily Lalone and Nina Suh. Your leadership, knowledge and insight have been truly invaluable. Emily, you have created a supportive and productive team environment within your lab, and I'd like to thank you for allowing me to contribute and be a part of it. Nina, your mentorship and friendship is something I truly value, and I appreciate you taking this fledgeling under your wing and helping me move to the next level professionally, clinically and academically.

Elizabeth Norman was vital to the success of this project. Elizabeth, not only were you a wealth of information, but I cannot begin to emphasize how crucial your role in coordinating our team was. Thanks for all that you taught me and for always being reliable and enthusiastic regarding this project. You truly are the lynch-pin of our endeavour, and this work is a credit to your efforts. To the team on the ground, I sincerely express my gratitude. Danning, Nicole, Alex M., Alex R., Jason and Winston, your steadfast effort in the segmentation, modelling and registration of countless scans, and hours of investment have been the backbone of this project. Additionally, would not have been able to complete this project without the expertise and ground work that Sydney has contributed within the lab. I'd like to recognize and thank her for her assistance with this particular project.

Finally, the moral support of my colleagues, family and friends has been instrumental. Mom, your daily text messages were always read and appreciated, regardless of if they were responded to. Kendrick and Eva, thanks for taking this journey with me and treating it as a team sport. Lastly, to Liz and Rafo – your unwavering support and friendship, throughout years rife with all sorts of challenges and uncertainty, have made all the difference.

# Table of Contents

Abstract .....	i
Summary for Lay Audience .....	ii
Co-Authorship Statement .....	iii
Acknowledgements .....	iv
List of Tables .....	viii
List of Figures .....	ix
List of Appendices.....	xii
List of Abbreviations .....	xiii
<b>Chapter 1: Introduction .....</b>	<b>1</b>
1.1 Hand and Wrist Anatomy .....	2
1.1.1 Summary of the Bones and Joints Comprising the Hand and Wrist .....	2
1.1.2 Relevant Osteology .....	5
1.1.2.1 Scaphoid .....	5
1.1.2.2 Lunate .....	7
1.1.2.3 Triquetrum .....	8
1.1.2.4 Trapezium .....	9
1.1.2.5 Trapezoid .....	10
1.1.2.6 Capitate .....	11
1.1.2.7 Hamate .....	12
1.1.2.8 Distal Radius .....	14
1.1.3 Soft Tissue Stabilizers of the Carpus .....	15
1.1.3.1 Static Stabilizers .....	15
1.1.3.1.1 Extrinsic Carpal Ligaments .....	15
1.1.3.1.1.1 Volar Radiocarpal Ligaments .....	15
1.1.3.1.1.2 Volar Ulnocarpal Ligaments .....	16
1.1.3.1.1.3 Dorsal Radiocarpal Ligaments .....	17
1.1.3.1.2 Intrinsic Carpal Ligaments .....	18
1.1.3.2 Dynamic Stabilizers .....	18

1.1.3.2.1	Volar Muscles .....	18
1.1.3.2.2	Dorsal Muscles .....	21
1.2	Carpal Kinematics .....	23
1.2.1	Prevailing Theories of Carpal Kinematics .....	25
1.2.1.1	Column Theory .....	25
1.2.1.2	Row Theory .....	27
1.2.1.3	Oval Ring Theory .....	27
1.2.1.4	Applied Forces to a Balanced Lunate .....	29
1.2.1.5	Central Column Theory .....	30
1.2.2	Challenges and Controversies in the Study and Characterization of Carpal Kinematics .....	32
1.3	Thesis Rationale .....	34
1.3.1	Objective and Hypothesis .....	35
1.3.2	Overview .....	36
<b>Chapter 2:</b>	<b>Review of Literature: Techniques in the Study of Carpal Kinematics &amp; the Use of Helical Axes .....</b>	<b>37</b>
2.1	Earlier Modalities for the Study of Wrist Kinematics .....	38
2.1.1	2-Dimensional Imaging Techniques .....	38
2.1.2	3-Dimensional Imaging with Implantable Trackers .....	40
2.1.3	Marker-less Bone Registration in 3-Dimensional Imaging .....	42
2.2	4-Dimensional CT in Carpal Kinematic Analysis .....	44
2.2.1	Accuracy & Resolution .....	44
2.2.2	4DCT Radiation Dose & Safety .....	45
2.2.3	Uses of 4DCT to Analyze Carpal Kinematics in Healthy Patients to Date .....	45
2.3	The Use of Helical Axes in Kinematic Study .....	47
2.3.1	Helical Axes to Describe Kinematic Motion .....	47
2.3.2	Helical Axis in Joint Kinematics .....	49
2.4	Summary .....	50
<b>Chapter 3:</b>	<b>Methodology for in-<i>Vivo</i> Carpal Kinematic Analysis using 4-Dimensional CT Acquisition .....</b>	<b>51</b>

3.1 Image Acquisition and Scanning Protocol .....	52
3.1.1 Pre-Scanning Protocol .....	52
3.1.2 4DCT Image Acquisition and Scanning Protocol .....	52
3.1.3 Radiation Exposure .....	53
3.2 Scan Processing and Data Analysis .....	54
3.2.1 3D Image Reconstruction and Modelling .....	54
3.2.2 Registration and Helical Axes .....	56
3.2.3 Statistical Analysis .....	57
3.2.4 Inter-Joint Distance Analysis .....	58
<b>Chapter 4: Results .....</b>	<b>59</b>
4.1 Participant Demographics .....	60
4.2 Degree of Flexion-Extension by Carpal Bone Through FEM .....	61
4.3 Grouping of Carpal Bones by Kinematic Blocks Based on Degree of Rotation Through FEM.....	66
4.4 Analysis of Kinematic Blocks .....	72
4.5 Joint Distances Around the Trapezial Block .....	78
<b>Chapter 5: General Discussion &amp; Conclusions .....</b>	<b>81</b>
5.1 Overview and Discussion of Results .....	82
5.2 Strengths and Limitations .....	86
5.3 Current and Future Directions .....	88
5.4 Significance and Conclusion .....	90
<b>References .....</b>	<b>91</b>
<b>Appendices .....</b>	<b>96</b>
Appendix A: Ethics Approval .....	96
Appendix B: Glossary of Terms .....	97
Appendix C: Repeated-Measures ANOVA Pairwise Comparison by Kinematic Block ..	101
<b>Curriculum Vitae .....</b>	<b>103</b>

# List of Tables

<b>Table 1.1:</b>	Volar Musculature Imparting Dynamic Stabilization of the Carpus. ....	20
<b>Table 1.2:</b>	Dorsal Musculature Imparting Dynamic Stabilization of the Carpus. ....	22
<b>Table 4.1</b>	Demographic Summary of Participants. ....	60
<b>Table 4.2.1:</b>	Rotation in Degrees of Carpal Bones from Wrist Extension to Flexion. ....	62
<b>Table 4.2.2:</b>	Rotation in Degrees of Carpal Bones from Wrist Flexion to Extension. ....	63
<b>Table 4.3.1:</b>	Mean Sagittal Rotation in Degrees of Each Kinematic Block from Wrist Extension to Flexion. ....	73
<b>Table 4.3.2:</b>	Mean Sagittal Rotation in Degrees of Each Kinematic Block from Wrist Flexion Extension. ....	73
<b>Table 4.4:</b>	Repeated-Measures ANOVA for Differences in Mean Rotation (Degrees) Between Kinematic Blocks. ....	74

# List of Figures

## CHAPTER 1:

<b>Figure 1.1:</b>	Anatomic Divisions of the Osseous Hand and Wrist. ....	3
<b>Figure 1.2:</b>	Osseous Anatomy of the Carpus. ....	4
<b>Figure 1.3:</b>	Osseous Features of the Scaphoid. ....	6
<b>Figure 1.4:</b>	Osseous Features of the Lunate. ....	7
<b>Figure 1.5:</b>	Osseous Features of the Triquetrum. ....	8
<b>Figure 1.6:</b>	Osseous Features of the Trapezium. ....	9
<b>Figure 1.7:</b>	Osseous Features of the Trapezium. ....	10
<b>Figure 1.8:</b>	Osseous Features of the Capitate. ....	11
<b>Figure 1.9:</b>	Osseous Features of the Hamate. ....	13
<b>Figure 1.10:</b>	Osseous Features of the Distal Radius. ....	14
<b>Figure 1.11:</b>	Volar Intrinsic and Extrinsic Ligaments. ....	16
<b>Figure 1.12:</b>	Major Dorsal Wrist Ligaments. ....	17
<b>Figure 1.13:</b>	Volar Extrinsic Muscles of the Wrist and Forearm. ....	19
<b>Figure 1.14:</b>	Dorsal Extrinsic Muscles of the Wrist and Forearm. ....	21
<b>Figure 1.15:</b>	Flexion-Extension Motion of the Wrist. ....	23
<b>Figure 1.16:</b>	Radioulnar Deviation (RUD) of the Wrist. ....	24
<b>Figure 1.17:</b>	Dart Thrower's Motion (DTM) of the Wrist. ....	24
<b>Figure 1.18:</b>	Functional Kinematic Units as Described in Row and Column Theory. ...	26
<b>Figure 1.19:</b>	Oval Ring Theory as Described by Litchman et al. ....	28
<b>Figure 1.20:</b>	Forces Applied to a Balanced Lunate as Described by Garcia-Elias et al. ....	29

<b>Figure 1.21:</b> Four-Gear, Two-Bar Linkage Concept of Central Column Theory. ....	30
<b>Figure 1.22:</b> Central Column Theory as Described by Sandow et al. ....	31

**CHAPTER 2:**

<b>Figure 2.1:</b> Xray Imaging to Compare Carpal Morphology in Radioulnar Deviation. ....	39
<b>Figure 2.2:</b> Implantable Trackers Used to Measure Kinematic Motion in Cadaveric Study. ....	41
<b>Figure 2.3:</b> Marker-less Bone Registration as Developed by Crisco et al. ....	43
<b>Figure 2.4:</b> Depiction of Helical Axis of Rotation of the Scaphoid as Demonstrated by deRoo et al. ....	48

**CHAPTER 3:**

<b>Figure 3.1:</b> Identifying Global Carpal Motion and Frames of Interest During Wrist FEM. ....	55
<b>Figure 3.2:</b> Visual Representation of Helical Axes of the Scaphoid, Lunate and Distal Radius from Neutral to 40 Degrees of Wrist Extension.....	57

**CHAPTER 4:**

<b>Figure 4.1.1:</b> Rotation of Each Carpal Bone from Wrist Extension to Flexion. ....	64
<b>Figure 4.1.2:</b> Rotation of Each Carpal Bone from Flexion to Extension. ....	65
<b>Figure 4.2.1:</b> Rotation of the Distal Carpal Row Bones from Wrist Extension to Flexion. ....	67
<b>Figure 4.2.2:</b> Rotation of the Distal Carpal Row Bones Axes from Wrist Flexion to Extension. ....	68
<b>Figure 4.2.3:</b> Rotation of Each Carpal Bone from Wrist Extension to Flexion. ....	69

<b>Figure 4.2.4:</b> Rotation of Each Carpal Bone from Wrist Flexion to Extension. ....	70
<b>Figure 4.3:</b> Division of Carpal Kinematic Blocks. ....	71
<b>Figure 4.4.1:</b> Coronal Visualization of Kinematic Blocks During FEM. ....	75
<b>Figure 4.4.2:</b> Superior-Oblique Visualization of Kinematic Blocks During FEM. ....	76
<b>Figure 4.4.3:</b> Coronal Visualization of Kinematic Blocks During FEM. ....	77
<b>Figure 4.5.1:</b> Inter-Joint Distance at the Trapeziotrapezoid Joint Through FEM. ....	79
<b>Figure 4.5.1:</b> Inter-Joint Distance at the Scaphotrapezoidal Joint Through FEM. ....	80



# List of Appendices

<b>Appendix A:</b> Ethics Approval .....	96
<b>Appendix B:</b> Glossary .....	97
<b>Appendix C:</b> Repeated-Measures ANOVA Pairwise Comparison by Kinematic Block ...	101

# List of Abbreviations

2D	Two-Dimensional
3D	Three-Dimensional
3DCT	Three-Dimensional Computerized Tomography
3MC	Third Metacarpal
4D	Four-Dimensional
4DCT	Four-Dimensional Computerized Tomography
APB	Abductor Pollicis Brevis
CI	Confidence Interval
CMC	Carpometacarpal
CT	Computerized Tomography
DICL	Dorsal Intercarpal Ligament
DIP	Distal Interphalangeal
DISI	Dorsal Intercalated Segmental Instability
DRCL	Dorsal Radiocarpal Ligament
DRUJ	Distal Radioulnar Joint
DTM	Dart-thrower's Motion
FCR	Flexor Carpi Radialis
FCU	Flexor Carpi Ulnaris

FDP	Flexor Digitorum Profundus
FDS	Flexor Digitorum Superficialis
FHA	Finite Helical Axis
FPL	Flexor Pollicis Longus
FEM	Flexion-Extension Motion
HAM	Helical Axis of Motion
GCFA	Global Carpal Flexion Angle
ICP	Iterative Closest Point
IHA	Instantaneous Helical Axis
IP	Interphalangeal
ISB	International Society of Biomechanics
LC	Lunocapitate
LRL	Long Radiolunate Ligament
LT	Lunotriquetral
LTL	Lunotriquetral Ligament
MCP	Metocarpophalangeal
MRI	Magnetic Resonance Imaging
PIP	Proximal Interphalangeal
PL	Palmaris Longus
PQ	Pronator Quadratus

PRUJ	Proximal Radioulnar Joint
PT	Pisotriquetral
RSCL	Radioscaphocapitate Ligament
RSLL	Radioscapholunate Ligament
RUD	Radioulnar Deviation
REB	Research Ethics Board
SRL	Short Radiolunate Ligament
STTL	Scaphotrapeziotrapezoid Ligament
SC	Scaphocapitate
SCL	Scaphocapitate Ligament
SD	Standard Deviation
SL	Scapholunate
SLL	Scapholunate Ligament
STT	Scaphotrapeziotrapezoid
TFCC	Triangular Fibrocartilage Complex
TH	Triquetrohamate
UCL	Ulnocapitate Ligament
ULL	Ulnolunate Ligament
UTL	Ulnotriquetral Ligament
VISI	Volar Intercalated Segmental Instability

# Chapter 1

## **1 Introduction**

*This chapter provides an introduction to wrist and carpal anatomy and carpal kinematics. A review of carpal and wrist anatomy, including osteology, ligamentous and musculotendinous stabilizers is provided. The current understanding of carpal kinematics is presented, with an overview of prevalent and widely-accepted theories of carpal kinematics. Particular attention is drawn to the challenges involved in the definitive study of wrist and carpal kinematics, controversies, and the implications of this knowledge gap. Finally, a rationale for study, objectives and hypothesis for this work is given.*

## 1.1 Hand and Wrist Anatomy

The wrist “joint” is a specialized series of articulations that allows intricate and complex movement of the hand. Its synchronous motion of multiple articulations, soft tissue stabilizers and the muscles acting upon those joints is what provides the ability to perform a plethora of functional tasks on a daily basis. This section provides an overview to the relevant anatomy.

### 1.1.1 Summary of the Bones and Joints Comprising the Hand and Wrist

There are a total of 27 bones that make up the hand and wrist. These can be grouped into the forearm, carpus, metacarpals and phalanges (**Figure 1.1**). The forearm is comprised of the radius and ulna long bones. The carpus is comprised of 8 carpal bones, divided into a distal and proximal carpal row. Bones comprising the proximal carpal row, from radial to ulnar are the scaphoid, lunate, triquetrum and pisiform (**Figure 1.2**). The distal carpal row includes the trapezium most radially, followed by the trapezoid, capitate, and hamate most ulnarly. There are 5 metacarpal bones, numbered 1 through 5 from radial to ulnar; all of which articulate with the distal carpal row and form the base for an associated group of phalanges. The combination of the metacarpal and its associated phalanges is referred to as a “ray”. Alternatively, the 1<sup>st</sup> ray is called the thumb, the 2<sup>nd</sup> the index, 3<sup>rd</sup> the middle, 4<sup>th</sup> the ring, and 5<sup>th</sup> the small or little. Each phalanx is comprised of a proximal, middle and distal phalanx, and are named with the same convention as their ray and associated metacarpal. The thumb is unique as it only has a proximal and distal phalanx. Meanwhile, the radius and ulna have two articulations with each other: the proximal radioulnar joint (PRUJ), and distal radioulnar joint (DRUJ). This work focusses on the carpus as it is the main component of the “wrist joint”.

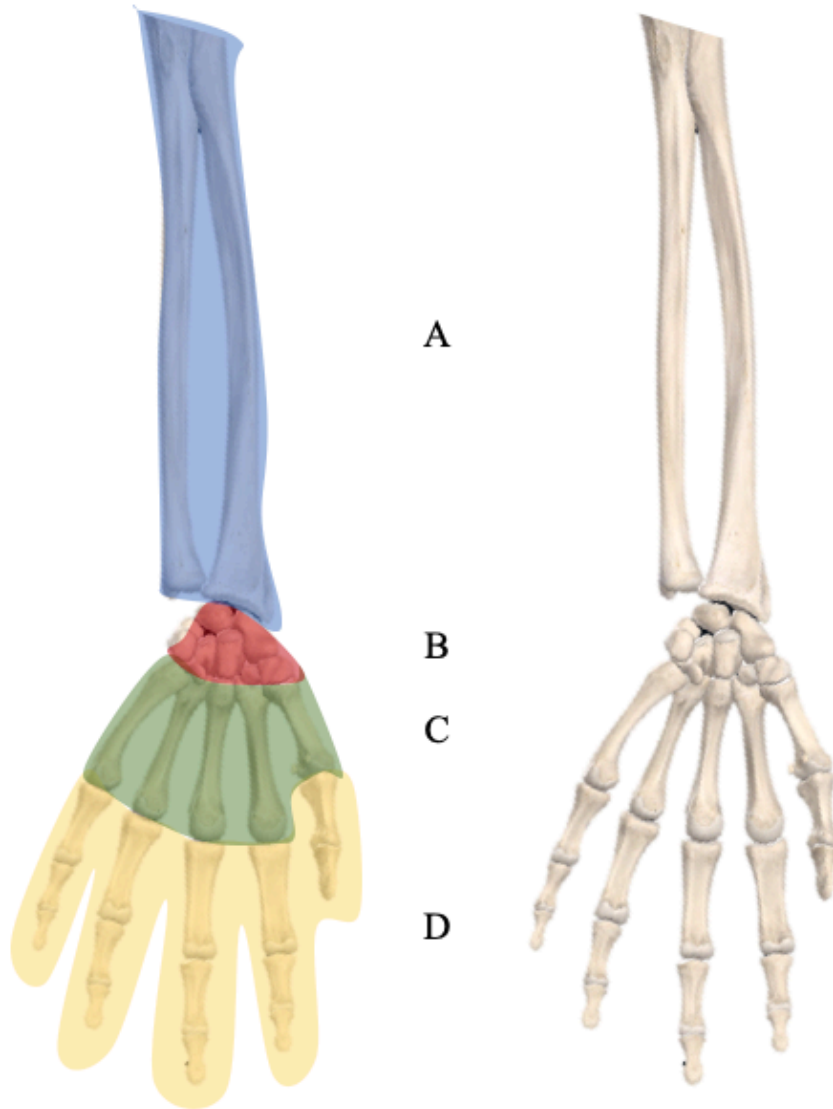


**Figure 1.1: Anatomic Divisions of the Osseous Hand and Wrist.** The hand and wrist can be anatomically divided into four main sections. From proximal to distal, these are the forearm (A) the carpus (B), the metacarpals (C), and the phalanges (D). (Reused with permission from Chambers SB. *The Impact of scaphoid malunion on wrist kinematics & kinetics: a biomechanical investigation*. The University of Western Ontario; 2019. <https://ir.lib.uwo.ca/etd/6707>).

The wrist and carpus are comprised of numerous joints and each bone within has up to seven articulations with adjacent bones (**Figure 1.2**). The radius and ulna articulate both proximally and distally with each other at the proximal radioulnar joint (PRUJ), and distal radioulnar joint (DRUJ). The forearm articulates with the proximal carpal row at the radiocarpal joint (distal radius with the lunate and scaphoid), and at the ulnocarpal joint (ulna and triquetrum). The distal and proximal carpal rows articulate at the midcarpal joint, which is made up of the triquetrohamate (TH), lunocapitate (LC) joint, and scaphotrapeziotrapezoid (STT) joints. The metacarpals articulate proximally with the distal carpal bones at the carpometacarpal (CMC) joints, and distally with the proximal phalanx at the metacarpophalangeal (MCP) joint. In rays 2-5, the proximal interphalangeal (PIP) joints form the articulation between the metacarpal and the proximal and middle phalanx, and the distal interphalangeal (DIP) joint, between the middle and distal phalanx. The thumb has a single interphalangeal (IP) joint between its proximal and distal phalanges. The specific intercarpal articulations are outlined in greater detail, by each bone, in **Section 1.1.2**

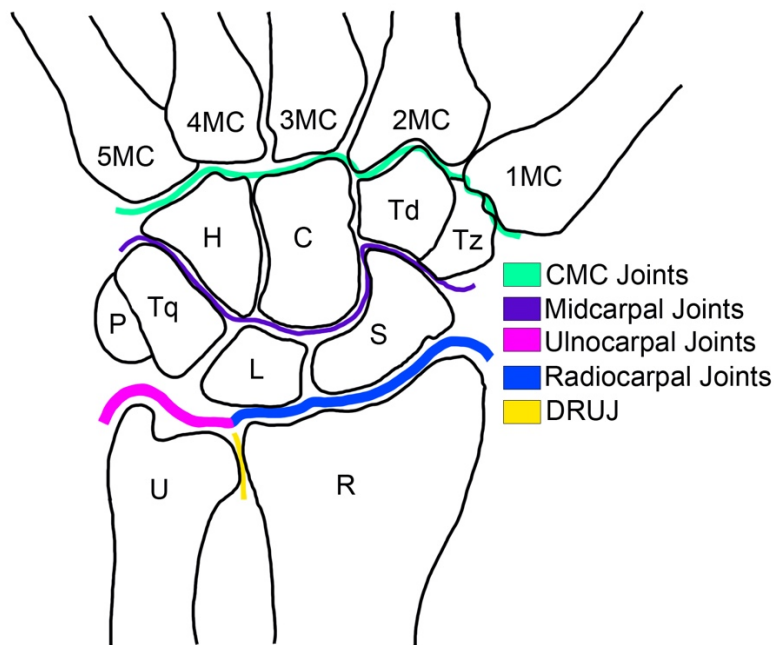


**Figure 1.2: Osseous Anatomy of the Carpus.** The bones of the hand and wrist are depicted here with focus on the carpal bones including scaphoid (S), lunate (L), triquetrum (T), pisiform (P), trapezium (Tz), trapezoid (Td), capitate (C) and hamate (H). Proximally the distal radius (R), and distal ulna articulate with the carpus, and distally the 1<sup>st</sup> through 5<sup>th</sup> metacarpals (MC). Major articulations between the bony units are shown, but intercarpal articulations are not depicted.



## 1.1.2 Relevant Osteology

This section reviews the shape and surfaces of each carpal bone and the distal radius. The distal ulna and pisiform have been excluded due to their negligible kinematic contribution to the motions of interest in this work <sup>1,2</sup>.

### 1.1.2.1 Scaphoid

The scaphoid is the largest bone of the proximal carpal row. It is curved in shape with a concave volar surface, and convex dorsal surface (**Figure 1.3**). Approximately 75-80% of the scaphoid is covered in cartilage for articulation <sup>1</sup>. The non-articulating portion of the scaphoid includes a large tubercle is found on the distal, radial portion of its volar surface, which serves as the insertion of the abductor pollicis brevis (ABP), and transverse carpal ligament. Superficial to the scaphoid tubercle, on the volar surface, runs the flexor carpi radialis (FCR), tendon on route to its insertion on the base of the 2<sup>nd</sup> metacarpal. Additionally the radial surface contains a rough surface for attachment of the radial collateral ligament (RCL) of the wrist <sup>1,3</sup>.

The remaining surfaces of the scaphoid are articular. It articulates with the capitate on its concave surface forming the scaphocapitate (SC) joint. Proximally on its flat surface it articulates with the lunate forming the scapholunate (SL) joint. On its convex surface it articulates with the scaphoid facet of the radius forming the radioscaphoid joint. Distally it articulates with both the trapezium and trapezoid at the STT joint <sup>1,3</sup>.

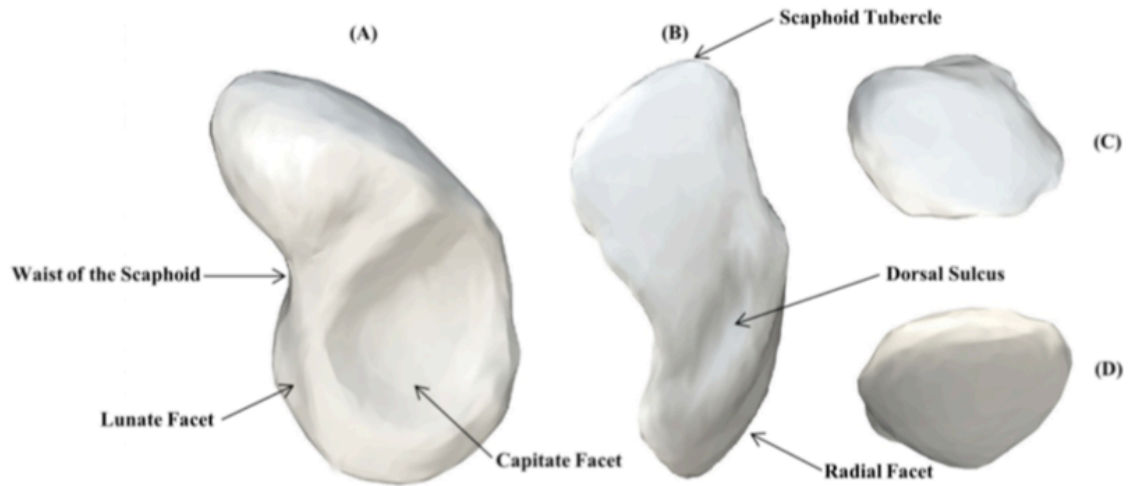


**Figure 1.3: Osseous Features of the Scaphoid.** Osseous anatomy of the scaphoid is depicted with relevant landmarks. (A) Ulnar View, (B) Dorsal View, (C) Distal Articular Surface, (D) Proximal Articular Surface. (Reused with permission from Chambers SB. *The Impact of scaphoid malunion on wrist kinematics & kinetics: a biomechanical investigation*. The University of Western Ontario; 2019. <https://ir.lib.uwo.ca/etd/6707>).

### 1.1.2.2 Lunate

The lunate is the central bone of the proximal carpal row and is named for its semi-lunar shape on a sagittal projection (**Figure 1.4**). It is wedge-shaped with a smaller dorsal surface than volar surface. It is particularly important in kinematic motion as it plays a role in all movements of the wrist in the coronal and sagittal planes <sup>1</sup>. Its convex proximal surface articulates with the lunate facet of the radius, forming the radiolunate joint. Distally its concave surface it articulates with the capitate at the capitulunate joint. Radially it articulates with the scaphoid at the SL joint and ulnarly with the triquetrum at the lunotriquetral (LT) joint. In 65% of cases, there is an additional facet for articulation with the hamate; this is known as a type II lunate <sup>1</sup>.

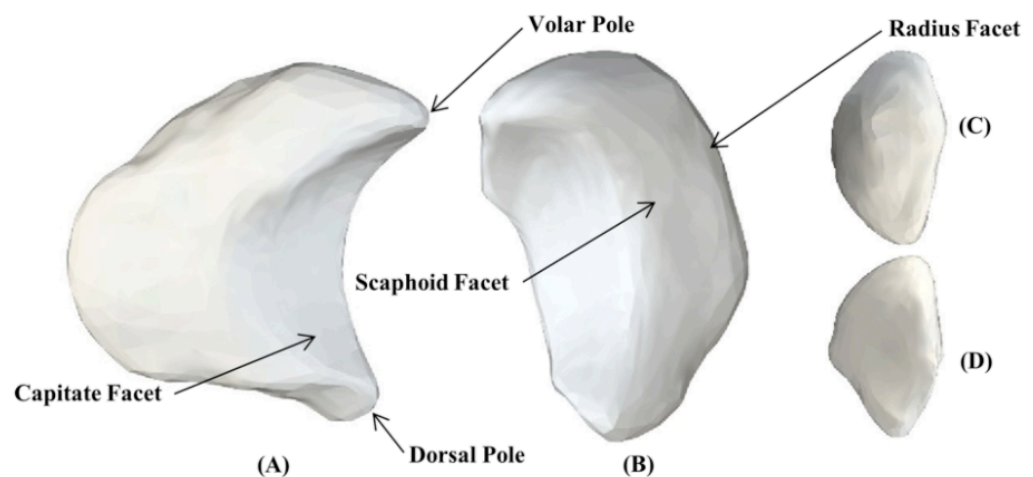


**Figure 1.4: Osseous Features of the Lunate.** Osseous anatomy of the lunate is depicted with relevant landmarks. (A) Distal Articular Surface, (B) Proximal Articular Surface, (C) Ulnar View, (D) Radial View. (Reused with permission from Chambers SB. *The Impact of scaphoid malunion on wrist kinematics & kinetics: a biomechanical investigation*. The University of Western Ontario; 2019. <https://ir.lib.uwo.ca/etd/6707>).

### 1.1.2.3 Triquetrum

The triquetrum is the most ulnar bone of the proximal carpal row and is pyramidal in shape<sup>3</sup> (**Figure 1.5**). It has a non-articular ulnar and dorsal facet for insertion of the ulnar collateral ligament of the wrist. Additionally, dorsally it has a large non-articular portion for insertions of the dorsal intercarpal ligament (DICL) and dorsal radiocarpal ligaments (DRCL), and volarly for insertion of the transverse carpal ligament. Proximally it articulates with the triangular fibrocartilage complex (TFCC), a fibrocartilaginous articular disc between the distal ulna and proximal carpal row. Radially, it articulates with the lunate at the LT joint. Most interestingly, its distal ulnar articulation with the hamate has a convex and concave shape allowing a corkscrew motion at the TH joint, particularly seen in radioulnar deviation<sup>1</sup>. Additionally, there is a distal radial facet for articulation with the head of the capitate, and a volar concave articulation with the pisiform at the pisotriquetral (PT) joint.

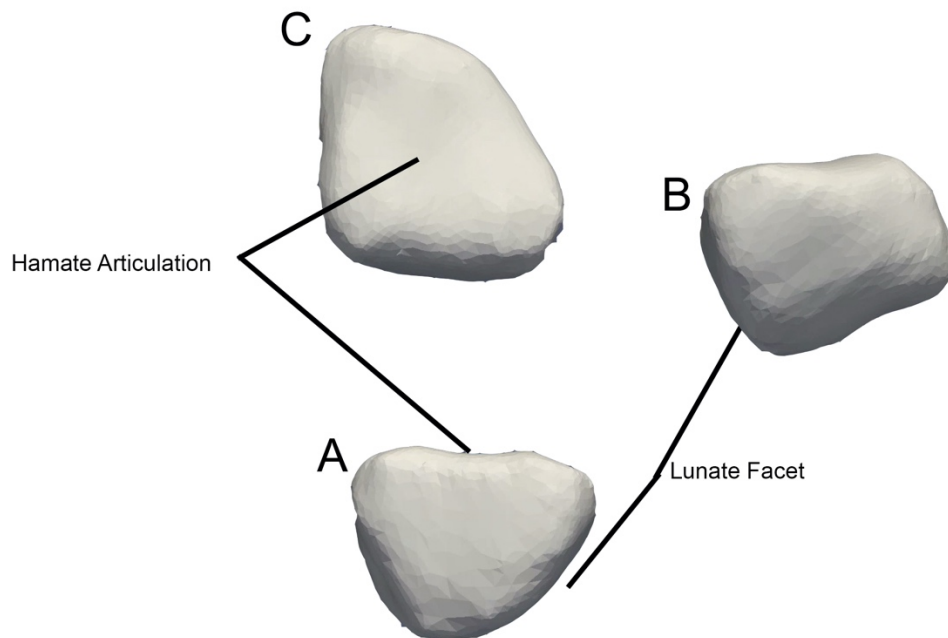


**Figure 1.5: Osseous Features of the Triquetrum.** Osseous anatomy of the triquetrum is depicted with relevant landmarks. (A) Volar View, (B) Radial View, (C) Distal Articular Surface.

### 1.1.2.4 Trapezium

The trapezium is the most radial bone of the distal carpal row (**Figure 1.6**). It is non-articular on the volar, radial and dorsal surfaces; all sites for ligamentous attachment. The radial collateral ligament of the wrist inserts on the radial side. Volarly, it has a groove for the FCR tendon as it traverses from the scaphoid tubercle towards the base of the 2<sup>nd</sup> metacarpal. On the distal and radial aspect of the bone there is a large saddle-shaped articulation for the 1<sup>st</sup> metacarpal of the thumb. The biconcave saddle joint provides the increased degrees of freedom allowed for thumb dexterity and opposition grip, and is considered one of the most important joints in the hand <sup>1</sup>. Ulnarly, it articulates with the trapezoid, and proximally with the scaphoid.

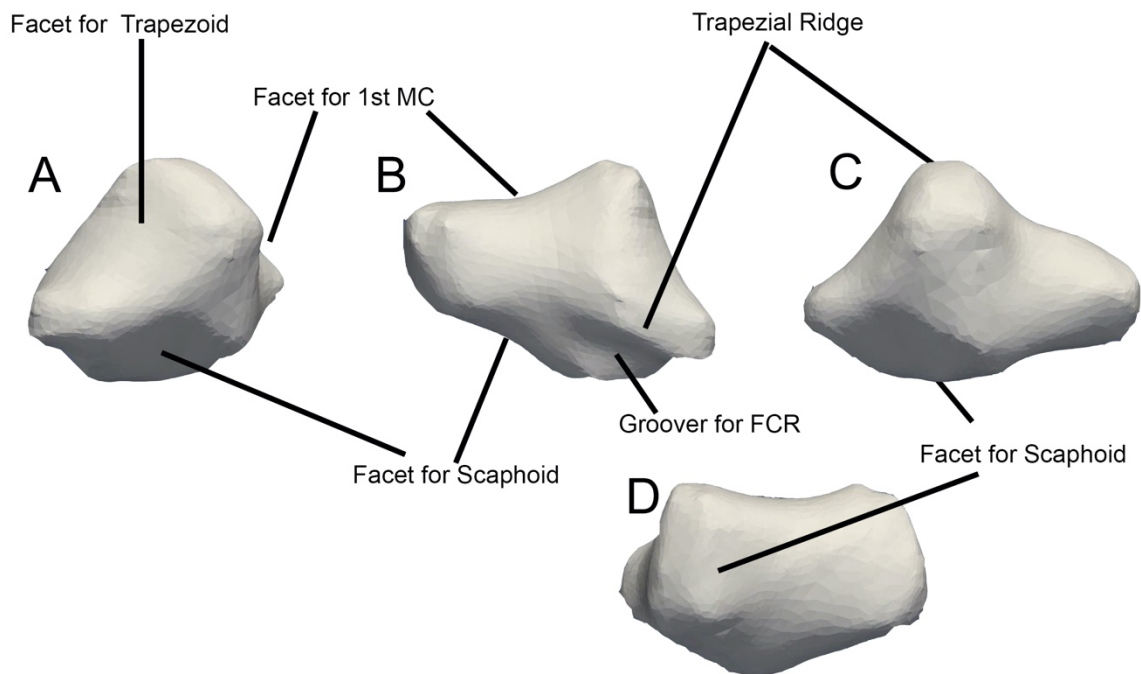


**Figure 1.6: Osseous Features of the Trapezium.** Osseous anatomy of the trapezium is depicted with relevant landmarks. (A) Ulnar View, (B) Volar View, (C) Radial View, (D) Proximal Articular Surface.

### 1.1.2.5 Trapezoid

The trapezoid is described as irregular wedge-shaped bone, and is the least mobile carpal bone <sup>1</sup> (**Figure 1.7**). It is narrower volar, non-articular surface, and a broader dorsal surface. Both are ligamentous insertion sites. Distally there is a facet for the base of the 2<sup>nd</sup> metacarpal and in 35% of individuals, also an additional articulation with the 3<sup>rd</sup> metacarpal <sup>1</sup>. It has a somewhat concave ulnar facet to articulate with the capitate, and a radial facet that articulates with the trapezium. Proximally it has a concave articulation with the scaphoid.

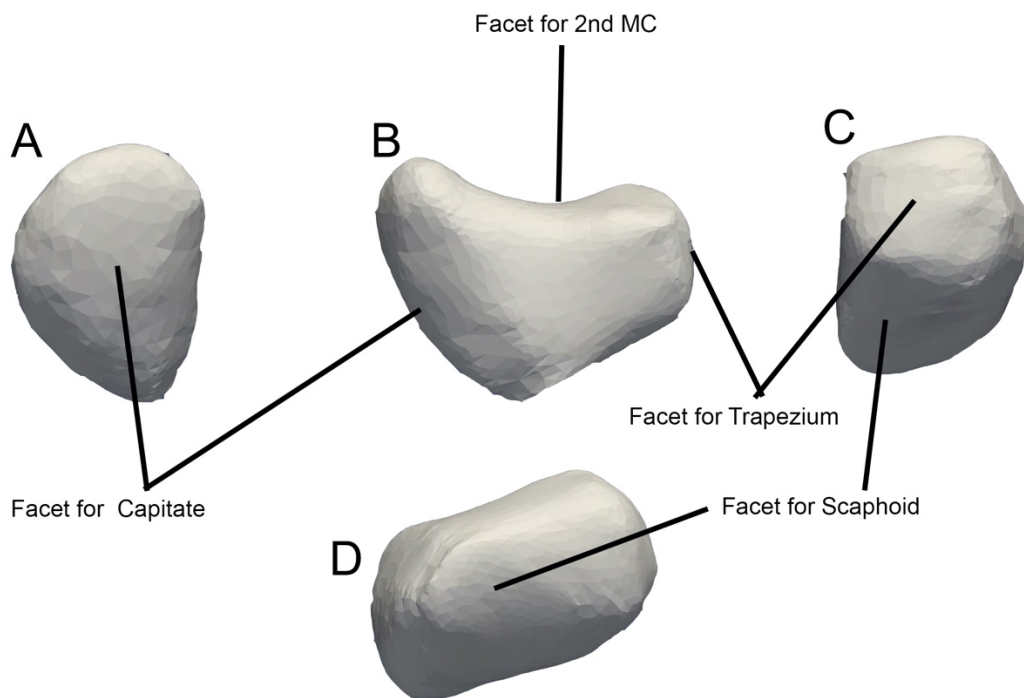


**Figure 1.7: Osseous Features of the Trapezium.** Osseous anatomy of the trapezium is depicted with relevant landmarks. (A) Ulnar View, (B) Volar View, (C) Radial View, (D) Proximal Articular Surface.

### 1.1.2.6 Capitate

The capitate is the largest carpal bone, and the most central bone of the distal carpal row (**Figure 1.8**). Non-articular regions include a dorso-ulnar region for insertion of the ulnar collateral ligament of the wrist, and direct volar and dorsal surfaces for insertion of carpal ligaments. Proximally, the large smooth articular surface is known as the head of the capitate, and articulates with the scaphoid radially, lunate centrally and triquetrum ulnarly. The distal articular surface is almost flat, and articulates with the 3<sup>rd</sup> metacarpal (3MC) at the 3<sup>rd</sup> CMC joint. Radially it has a distal facet for the 2<sup>nd</sup> metacarpal, and a more proximal facet to articulate with the trapezoid. Ulnarly it has a large facet for the hamate <sup>1,3</sup>.

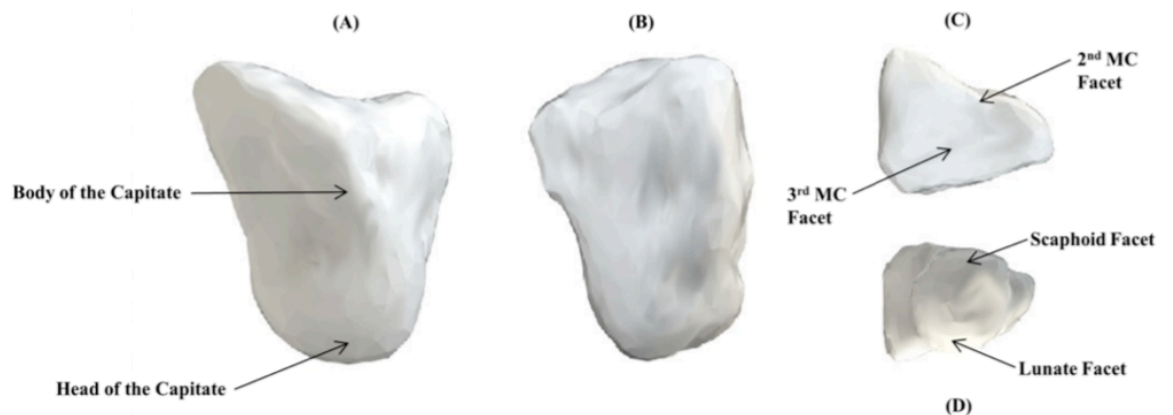


**Figure 1.8: Osseous Features of the Capitate.** Osseous anatomy of the capitate is depicted with relevant landmarks. (A) Radial View, (B) Volar View, (C) Distal Articular Surface, (D) Proximal Articular Surface. (Reused with permission from Chambers SB. *The Impact of scaphoid malunion on wrist kinematics & kinetics: a biomechanical investigation*. The University of Western Ontario; 2019. <https://ir.lib.uwo.ca/etd/6707>).

### 1.1.2.7 Hamate

The hamate is wedge-shaped, or *cuneiform* in shape and lays ulnar to the capitate in the distal carpal row (**Figure 1.9**). Its most notable feature is a large unciform hamulus or “*hook of hamate*”, projecting volarly and pointing radially, originating from its distal ulnar surface. The concavity of the hook forms the ulnar boarder of the carpal tunnel, and its tip provides attachment for the transverse carpal ligament. It has a large volar and dorsal surface for ligamentous and capsular attachment <sup>1</sup>. Radially it articulates with the capitate and proximally with the triquetrum at the TH joint. As discussed in **Section 1.1.2.3** the unique shape allows corkscrew motion between the hamate and triquetrum. In some individuals there may be a proximal and radial articulation with the lunate. Distally, the articular surface is divided into a radial and ulnar facet by a small ridge. These facets articulate with the base of the 4<sup>th</sup> and 5<sup>th</sup> metacarpals respectively <sup>3</sup>.



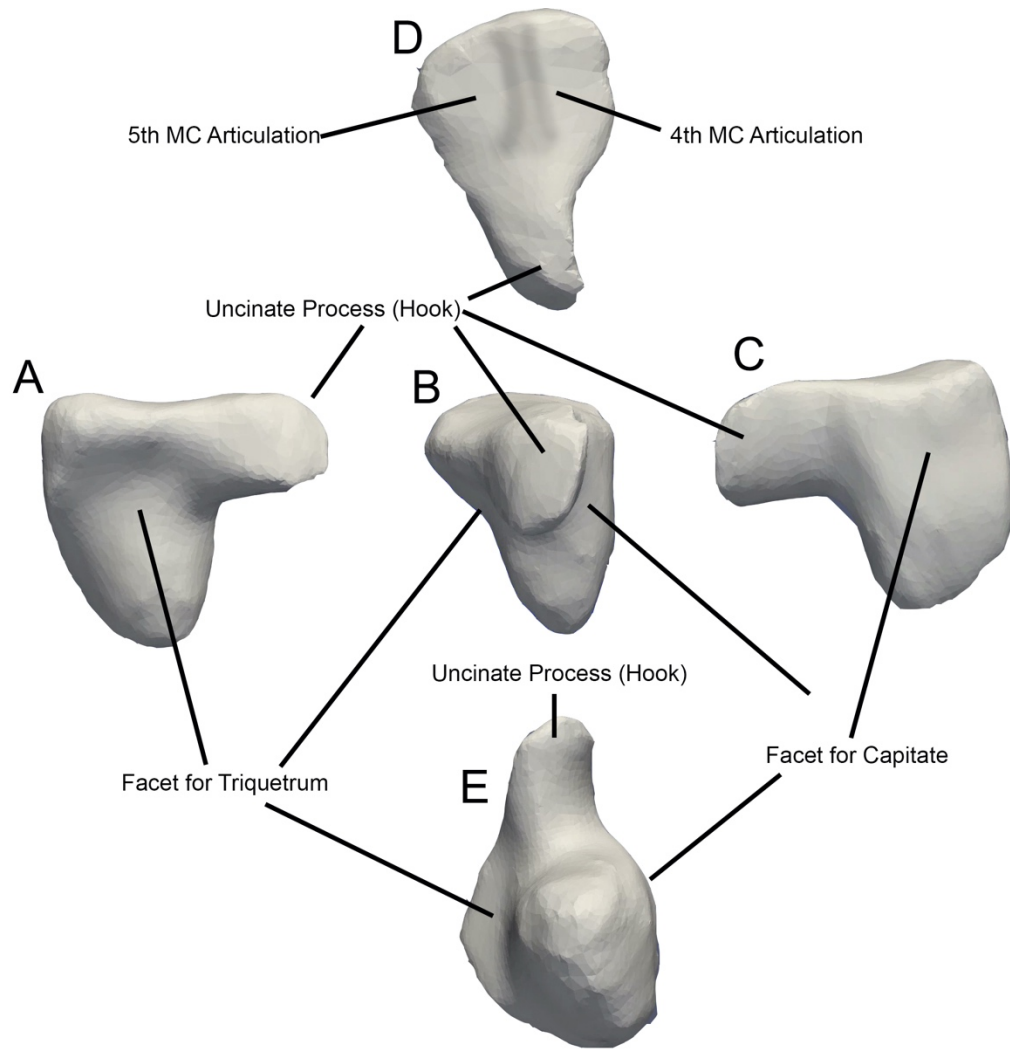


**Figure 1.9: Osseous Features of the Hamate.** Osseous anatomy of the hamate is depicted with relevant landmarks. (A) Ulnar View, (B) Volar View, (C) Radial View, (D) Distal Articular Surface, (E) Proximal Articular Surface.

### 1.1.2.8 Distal Radius

The distal radius forms the proximal platform for the carpus and articulates with the carpus at the radiocarpal joint (**Figure 1.10**). It features a radial styloid as an origin for the radial collateral ligament of the wrist, and projects as a bony stabilizer to radial deviation. Distally it has an ellipsoid articular surface comprised of a large scaphoid facet radially and square-shaped lunate facet ulnarly. On the distal aspect of the ulnar surface, there is a concave ulnar notch for articulation with the ulnar head at the DRUJ. Lister's tubercle is a sessile projection in the dorsal and radial surface of the distal radius, around which the extensor pollicis longus (EPL) tendon pivots as it radiates from its longitudinal alignment in the forearm towards the 1<sup>st</sup> ray.

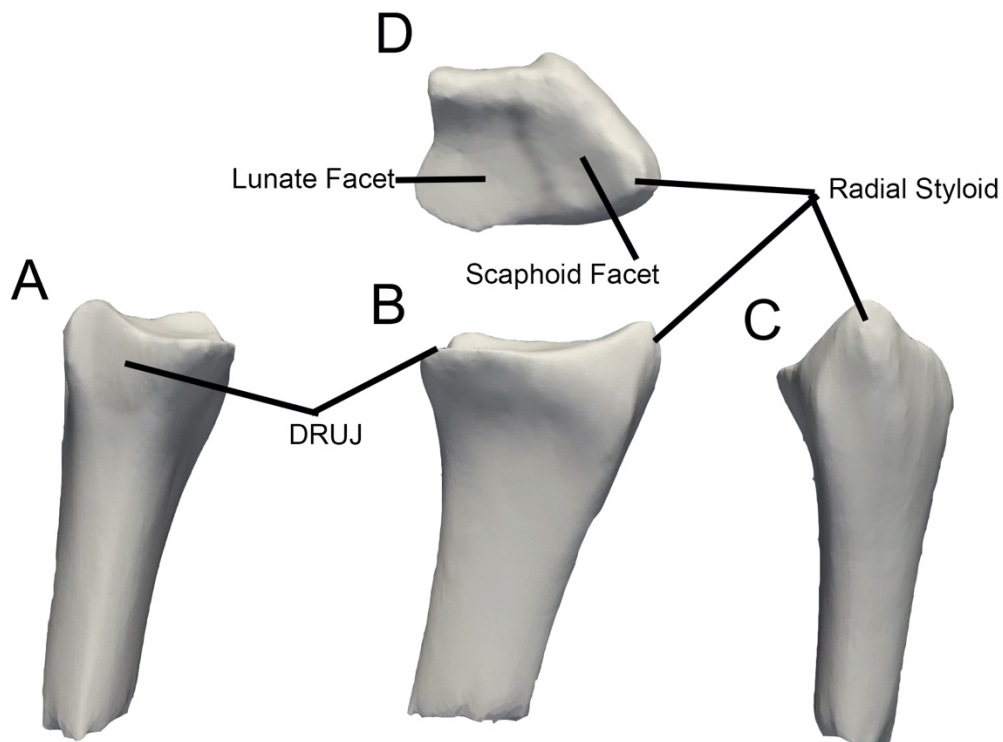


**Figure 1.10: Figure 1.6: Osseous Features of the Distal Radius.** Osseous anatomy of the distal radius is depicted with relevant landmarks. (A) Ulnar View, (B) Volar View, (C) Radial View, (D) Distal Articular Surface.

### 1.1.3 Soft Tissue Stabilizers of the Carpus

The carpus is enacted on and stabilized by multiple ligaments and muscles. Along with the osteology, these structures influence, to varying degrees, the kinematic motion of the carpus. Intrinsic and extrinsic ligaments comprise the static stabilizers while muscles are the dynamic stabilizers.

#### 1.1.3.1 Static Stabilizers

##### 1.1.3.1.1 Extrinsic Carpal Ligaments

Extrinsic carpal ligaments connect the distal radius and ulna to the carpal bones. These can be divided into volar radiocarpal, volar ulnocarpal and dorsal carpal ligaments. Additionally, the radial collateral ligament of the wrist runs directly radial, originating on the radial styloid and inserting on the radial aspect of the scaphoid and triquetrum. Similarly, there is an ulnar collateral ligament of the wrist, originating from the ulnar styloid and inserting on the triquetrum, hamate and base of the 5<sup>th</sup> metacarpal.

##### 1.1.3.1.1.1 Volar Radiocarpal Ligaments

The radiocarpal ligaments originate from the volar aspect of the distal radius and styloid and insert onto the trapezium, scaphoid, lunate and capitate bones. There are 4 true ligaments (**Figure 1.11**). Most radial lies the radial collateral ligament of the wrist, arising deep on the radial styloid with attachments to the radial aspect of the scaphoid and trapezium. From radial to ulnar runs the radioscapohcapitate ligament (RSCL) and the long radiolunate ligament (LRLL) superficially. The RSCL is especially important in carpal stability, and acts as a fulcrum on which the scaphoid rotates <sup>1</sup>. The most ulnar of the radiocarpal ligaments is the short radiolunate ligaments (SRLL) directly from the medial volar lip of the distal radius to the lunate. It is the deepest of the volar radiocarpal ligaments. Of note, the radioscapohlunate ligament (RSLL), also known as the Ligament of Testut, is a misnomer. In actuality, it is a neurovascular bundle opposed to a ligament and runs between the LRLL and SRLL.

### 1.1.3.1.1.2 Volar Ulnocarpal Ligaments

Although variations on the ulnocarpal stabilizers exist, there are three main stabilizers on the volar ulnar side which form the ulnocarpal ligamentous complex<sup>4</sup> (**Figure 1.11**). These include the ulnocapitate ligament (UCL) which runs from the superficial volar surface of the ulnar to the capitate. This forms an inverted “v” shape with the RSL, with its apex at the capitate. It acts to stabilize the capitate and decelerate the scaphoid<sup>1</sup>. More deeply lies the ulnolunate ligament (ULL) and the ulnotriquetral ligament (UTL) which originate from the TFCC and attach to the lunate and triquetrum respectively. These together form a proximal “v” shape with the apex meeting at the volar aspect of the distal ulna and TFCC. These ligaments transmit force between the ulnar and the proximal carpal row, and help to prevent radial translation of the carpus throughout motion<sup>1</sup>. It is important to note there are no dorsal ulnocarpal ligaments as the TFCC ligaments are situated in this region.

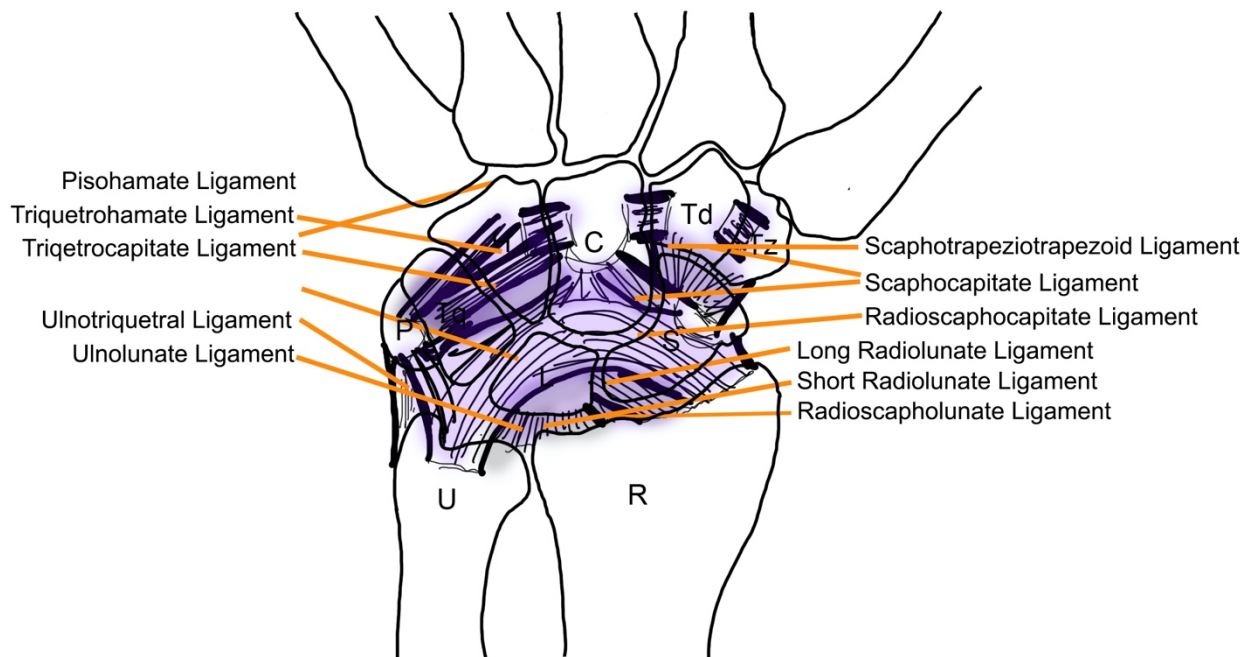


**Figure 1.11: Volar Intrinsic and Extrinsic Ligaments.** Anatomic depiction of the volar wrist ligaments. Major volar extrinsic and intrinsic ligaments are highlighted. (C) Capitate, (U) Ulna, (R) Radius, (Td) Trapezoid, (Tz) Trapezium, (P) Pisiform, (S) Scaphoid.

### 1.1.3.1.1.3 Dorsal Radiocarpal Ligaments

The dorsal radiocarpal ligament (DRCL) is the sole extrinsic ligament found on the dorsal side of the wrist (**Figure 1.12**). It originates from the dorsal surface of the distal radius, approximately halfway between Lister's Tubercle and the DRUJ and broadly inserts along the lunate on its way to terminating at the triquetrum.

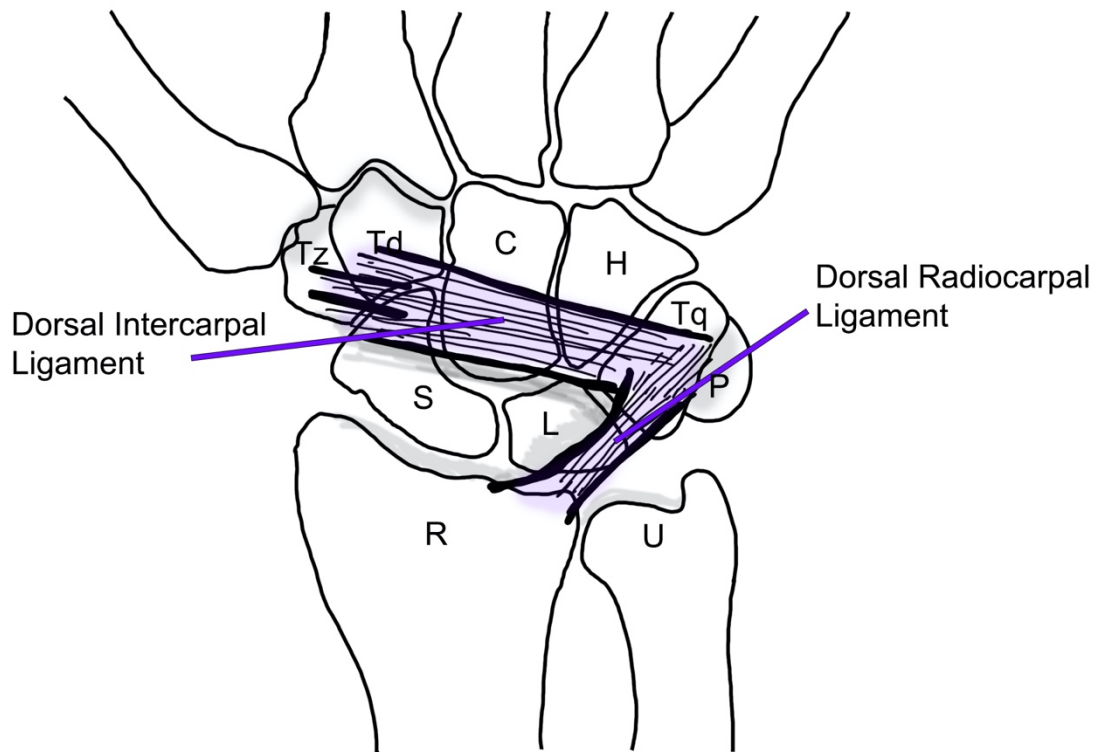


**Figure 1.12: Major Dorsal Wrist Ligaments.** Relevant dorsal wrist ligaments are depicted including the dorsal intercarpal ligament (DIC) and dorsal radiocarpal ligament (DRC). (Tz) Trapezium, (Td) Trapezoid, (C) Capitate, (H) Hamate, (S) Scaphoid, (L) Lunate, (Tq) Triquetrum, (P) Pisiform, (R) Radius, (U) Ulna.

### 1.1.3.1.2 Intrinsic Carpal Ligaments

There are numerous short, stout ligaments directly connecting adjacent carpal bones. These intrinsic ligaments connect directly to the cartilage, and some additionally expand beyond the articular surface also connect directly to bone via Sharpey's fibers <sup>1</sup>. The majority of these ligaments act to stabilize between bones of the same row, be it the distal or row. An in-depth discussion of each of these ligaments is beyond the scope of this work. The two most important intrinsic carpal ligaments are the scapholunate ligament (SLL) and lunotriquetral ligament (LTL). Both serve to stabilize the lunate, and disruption of either can result in altered alignment and instability of the proximal carpal row <sup>5</sup>. Anatomically they are very similar, with c-shaped morphology, comprised of membranous volar and dorsal components, and a fibrous proximal interosseous component. They differ in that the dorsal portion of the SLL has been shown to be the strongest, whereas the LTL is strongest in the volar portion <sup>6</sup>.

There are considerably less intercarpal ligaments stabilizing between the distal and carpal row, which contributes to the decreased constraint and increased mobility at the midcarpal joint <sup>1</sup>. The main volar stabilizing ligaments include the scaphocapitate ligament (SCL), and scaphotrapezotrapezoid ligament (STTL). The dorsal intercarpal ligament (DICL) is the only dorsal intrinsic ligament traversing the distal and proximal carpal rows (**Figure 1.12**). It spans from the triquetrum, inserting along the lunate, capitate and distal scaphoid, before terminating at the STT joint.

### 1.1.3.2 Dynamic Stabilizers

#### 1.1.3.2.1 Volar Muscles

The volar musculature is subdivided into superficial, intermediate and deep layers. These act as flexors of the wrist and fingers and are summarized in **Table 1.1** and shown in **Figure 1.13**<sup>3</sup>.

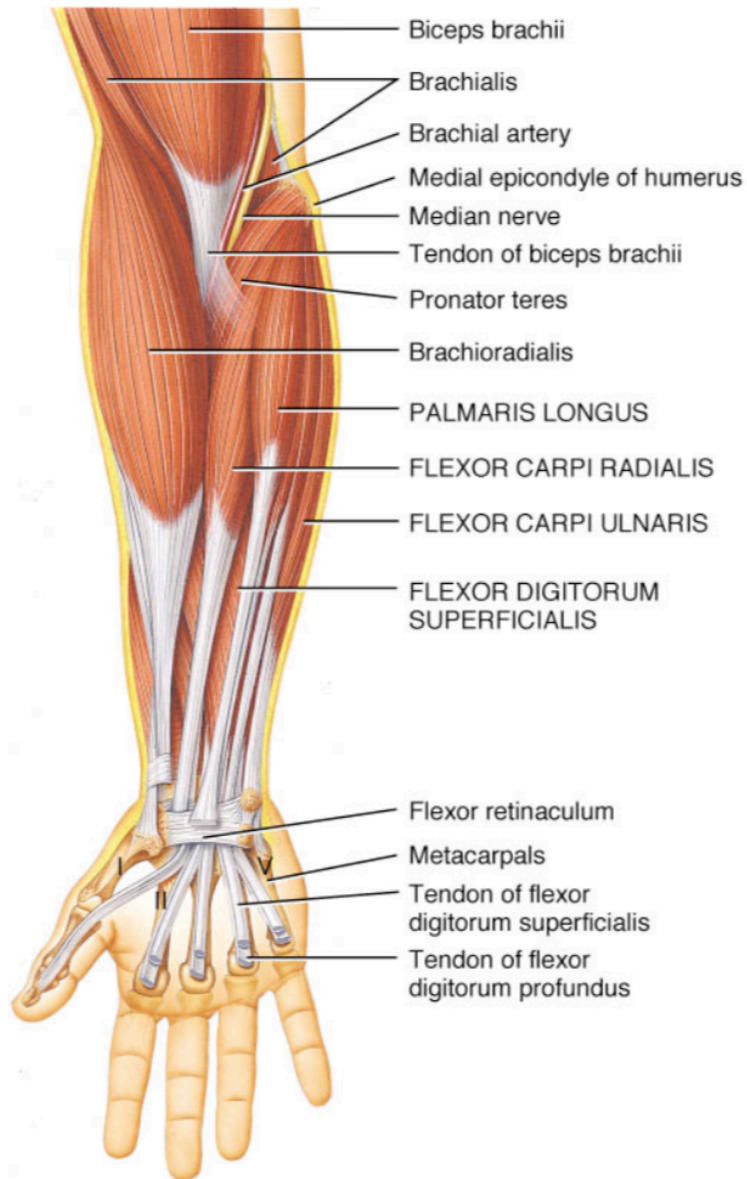


**Figure 1.13: Volar Extrinsic Muscles of the Wrist and Forearm.** A selective depiction of volar extrinsic forearm and wrist musculature is shown with pertinent anatomy highlighted. A complete list is presented in **Table 1**. (Reused with permission from Chambers SB. *The Impact of scaphoid malunion on wrist kinematics & kinetics: a biomechanical investigation*. The University of Western Ontario; 2019. <https://ir.lib.uwo.ca/etd/6707>).

**Table 1.1: Volar Musculature Imparting Dynamic Stabilization of the Carpus.** The volar carpal dynamic stabilizers are divided into three anatomic layers: superficial, intermediate and deep. These muscles act to dynamically stabilize the carpus, and also generate flexion of the wrist, fingers and thumb. They also antagonistically stabilize the carpus during wrist, finger and thumb extension.

Layer	Muscle	Origin	Insertion	Function
Superficial	Flexor Carpi Radialis (FCR)	Medial Epicondyle of the Humerus	Base of 2 <sup>nd</sup> and 3 <sup>rd</sup> Metacarpals	1. Wrist Flexion 2. Wrist Radial Deviation
	Palmaris Longus (PL)		Palmar Aponeurosis	1. Weak Wrist Flexor 2. Tension Palmar Skin
	Flexor Carpi Ulnaris		Base of 5 <sup>th</sup> Metacarpal, Pisiform, Hook of Hamate	1. Wrist Flexion 2. Ulnar Deviation of the Wrist
Intermediate	Flexor Digitorum Superficialis (FDS)		Base of Middle Phalanx of Digits 2-5	Finger Flexion at PIP Joints
Deep	Flexor Digitorum Profundus (FDP)	Volar and Medial Surface of the Ulnar Diaphysis	Base of Distal Phalanx of Digits 2-5	Finger Flexion at DIP Joints
	Flexor Pollicis Longus (FPL)	Medial Aspect of the Radius	Base of Distal Phalanx of 1 <sup>st</sup> Digit	Thumb Flexion
	Pronator Quadratus	Volar Medial Surface of the Distal Ulna	Volar Lateral Surface of the Distal Radius	Forearm Pronation



### 1.1.3.2.2 Dorsal Muscles

The dorsal musculature is subdivided into superficial and deep layers. These act as extensors of the wrist and fingers and are summarized in **Table 1.2**, and shown in **Figure 1.14**<sup>3</sup>

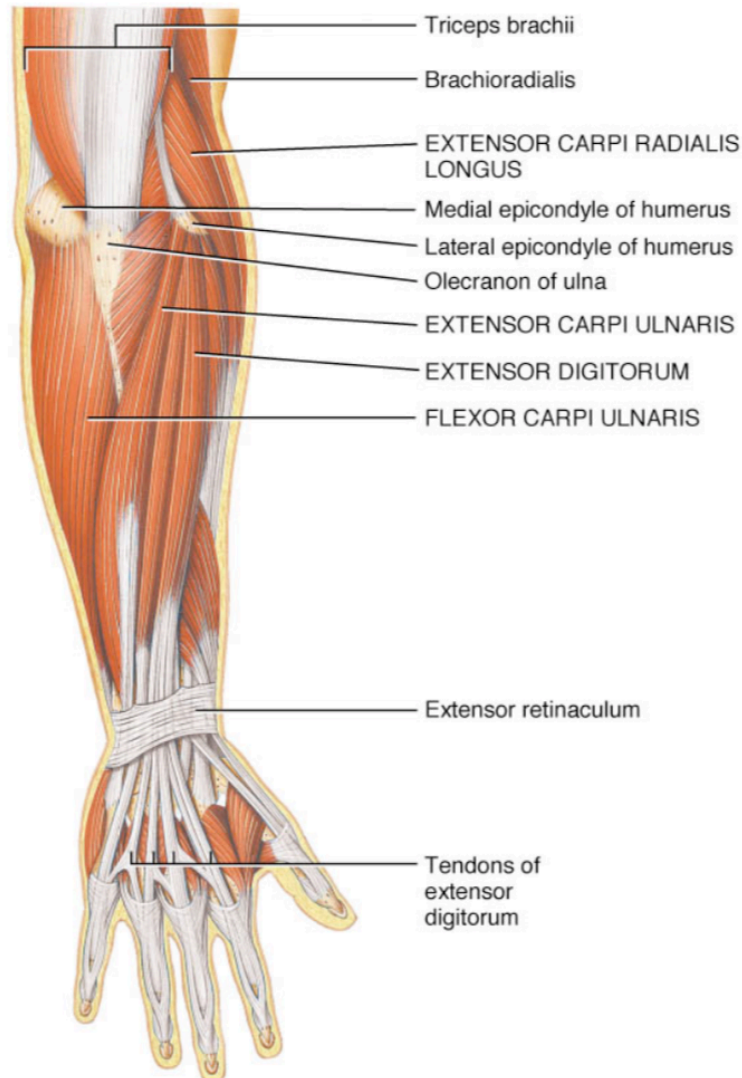


**Figure 1.14: Dorsal Extrinsic Muscles of the Wrist and Forearm.** A selective depiction of dorsal extrinsic forearm and wrist musculature is shown with pertinent anatomy highlighted. A complete list is presented in **Table 2**. (Reused with permission from Chambers SB. *The Impact of scaphoid malunion on wrist kinematics & kinetics: a biomechanical investigation*. The University of Western Ontario; 2019. <https://ir.lib.uwo.ca/etd/6707>).

**Table 1.2: Dorsal Musculature Imparting Dynamic Stabilization of the Carpus.** The dorsal carpal dynamic stabilizers are divided into two anatomic layers: superficial and deep. These muscles act to dynamically stabilize the carpus and also generate extension of the wrist, fingers and thumb. They also antagonistically stabilize the carpus during wrist, finger and thumb flexion.

Layer	Muscle	Origin	Insertion	Function
Superficial	Extensor Carpi Radialis Brevis (ECRB)	Lateral Epicondyle of the Humerus	Base of 3 <sup>rd</sup> Metacarpal	1. Wrist Extension 2. Wrist Ulnar Deviation
	Extensor Carpi Radialis Longus (ECRL)		Base of 2 <sup>nd</sup> Metacarpal	
	Extensor Digitorum Communis (EDC)		Base of Distal Phalanx of Digits 2-5, Extensor Hood	Finger Extension
	Extensor Digiti Quinti (EDQ)		Base of Distal Phalanx of 5 <sup>th</sup> Digit, Extensor Hood	Small Finger Extension
	Extensor Carpi Ulnaris (ECU)		Base of 5 <sup>th</sup> Metacarpal	1. Wrist Extension 2. Wrist Ulnar Deviation
Deep	Abductor Pollicis Longus (APL)	Medial Aspect of the Dorsal Radius and Ulnar Shaft	Base of 1 <sup>st</sup> Metacarpal	1. Thumb Abduction 2. Thumb Extension
	Extensor Pollicis Longus (EPL)	Dorsal Surface of the Proximal Ulna	Base of Distal Phalanx of Thumb	Thumb Extension at IP Joint
	Extensor Pollicis Brevis (EPB)	Radius and Interosseus Membrane	Base of Proximal Phalanx of Thumb	Thumb Extension at MCP Joint
	Extensor Indicis Proprius (EIP)	Distal Third of Dorsal Ulna	Base of Distal Phalanx of 2 <sup>nd</sup> Digit, Extensor Hood	Index Finger Extension

## 1.2 Carpal Kinematics

Kinematics is the study of pure motion of a body or group of bodies. As it pertains to this work, carpal kinematics allow us to describe the motion of the individual wrist and carpal bones through various planes of motion. The wrist joint has the ability to move with 6 degrees-of-freedom, allowing multiplanar motion and complex spatial positioning of the hand and wrist <sup>7</sup>. In-plane motion including Flexion-Extension Motion (FEM) (**Figure 1.15**), in the sagittal plane, and Radioulnar Deviation (RUD) (**Figure 1.16**) in the coronal plane are accomplished through articulations within the bones of the carpus as well as their articulations with the distal radius and ulna <sup>1</sup>. Additionally, the distal articulation between the radius and ulna at the DRUJ provides rotation of the forearm in the axial plane producing pronation and supination. Due to the high degree-of-freedom, multiple out-of-plane motions are also possible. Dart-thrower's motion (DTM) is a path of motion from radial deviation and extension, to ulnar deviation and flexion, is the main out-of-plane motion to be characterized, and is associated with many functional tasks such as power grip and hammering <sup>7</sup> (**Figure 1.17**).

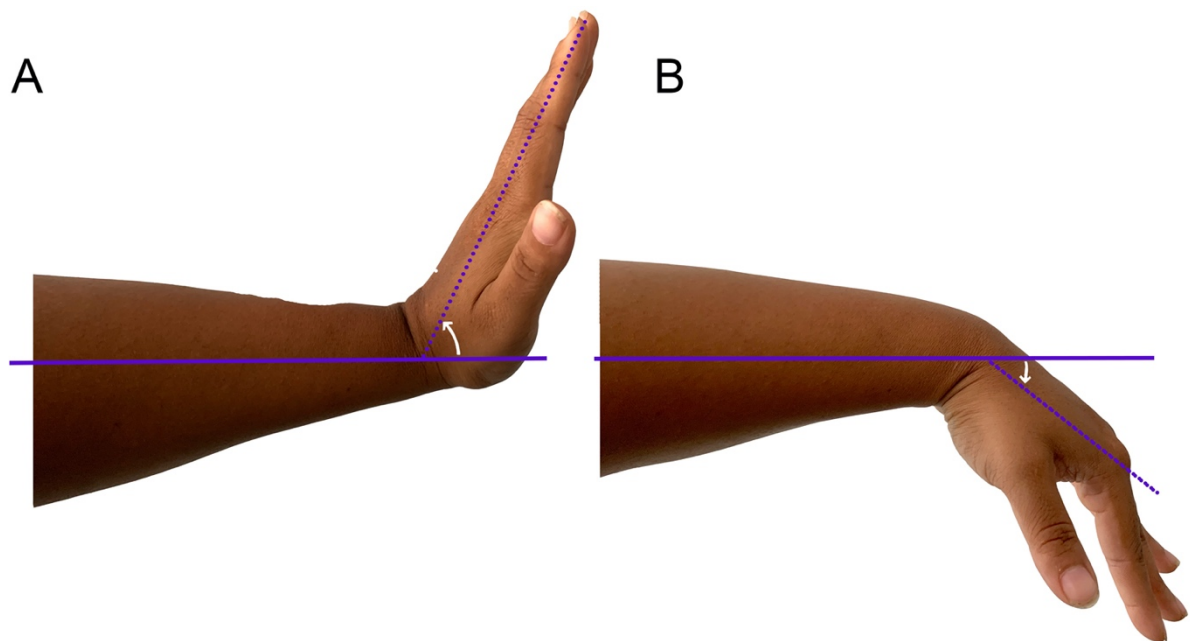


**Figure 1.15: Flexion-Extension Motion (FEM) of the Wrist.** (A) Wrist Extension, (B) Wrist Flexion.

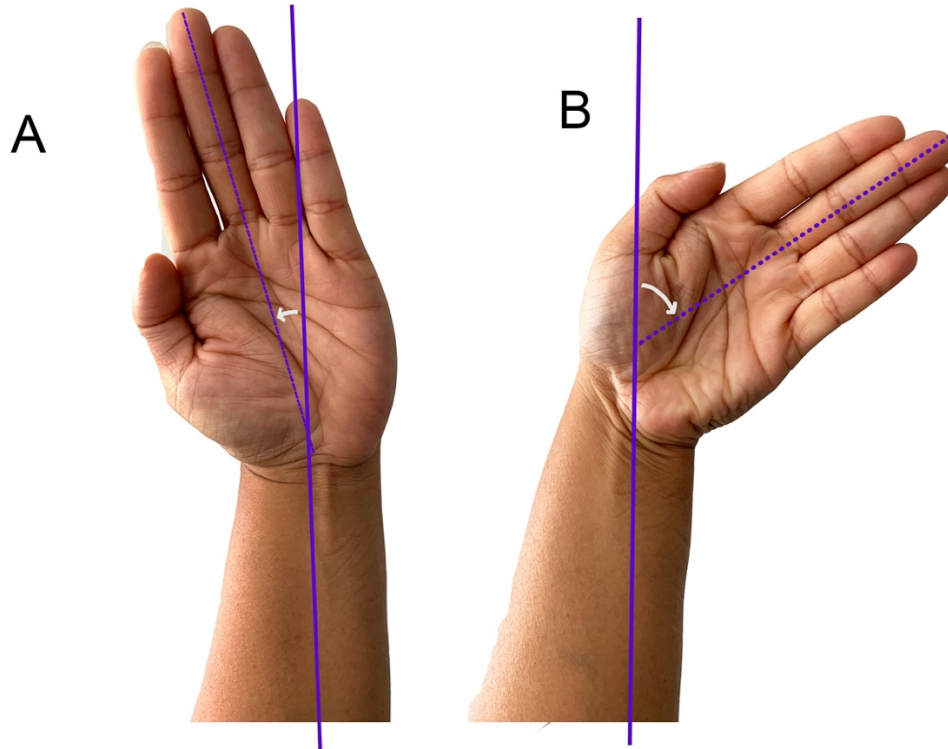


**Figure 1.16: Radioulnar Deviation (RUD) of the Wrist.** (A) Radial Deviation, (B) Ulnar Deviation.

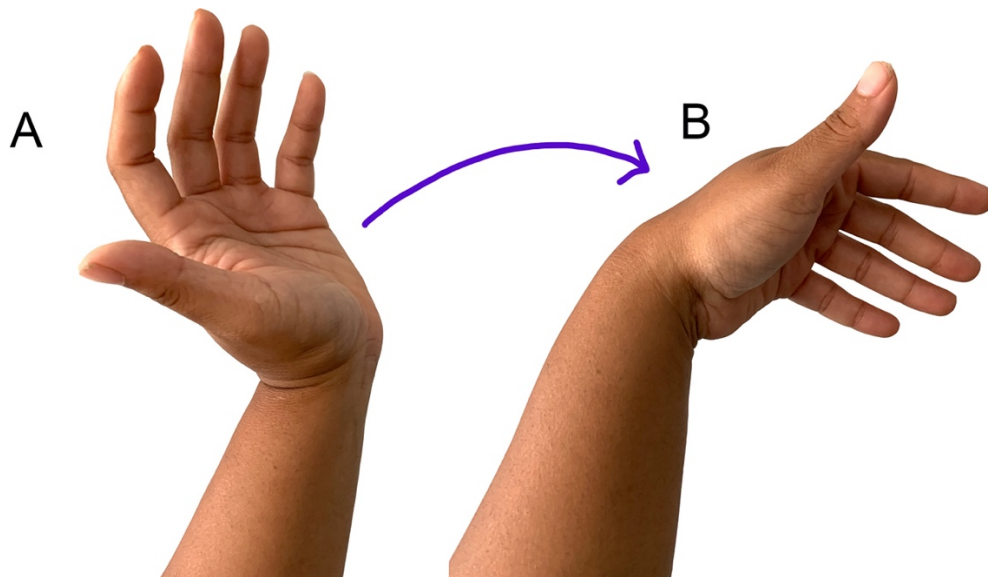


**Figure 1.17: Dart Thrower's Motion (DTM) of the Wrist.** Dart thrower's motion is an out-of-plane motion of the wrist used in many functional tasks. It is a path of motion from wrist extension and radial deviation (A), to wrist flexion and ulnar deviation (B).

## 1.2.1 Prevailing Theories of Carpal Kinematics

Although no consensus, overarching description of carpal kinematics currently exists, several theories have been proposed, subsequently refined, and accepted as leading theories. Each new theory has broadened our understanding of carpal movement as new information became available. The earliest theories of carpal kinematics were formulated at the end of the 19<sup>th</sup> century following the advent of roentgenograms, the earliest form of x-ray technology.

### 1.2.1.1 Column Theory

Bryce first described carpal normal carpal motion only a year following the debut of roentgenograms in 1896<sup>8</sup>. In 1921, the Column Theory of carpal motion was first proposed by Navarro<sup>9</sup>, and later refined by Taleisnik in the 1970s. This theory describes the carpus as three functional columns. The central column, including the lunate, capitate and hamate, is the main column responsible for flexion and extension movements. The scaphoid column is comprised of the scaphoid, trapezium and trapezoid bone and contributes to coronal plane motion of the wrist as well as rotation around the central column. Lastly, the ulnar column is comprised of the triquetrum and has contributions to rotation<sup>5,7</sup> (**Figure 1.18**).

Since its original description, the column theory has remained the basis for additional theories, which expanded upon its core principles as new information regarding kinematic movement were discovered. Kauer suggested that these columns functioned independently, with the radial and central columns being most important for most wrist movements<sup>5,10</sup>. This is based on the differential contribution to wrist flexion between the scaphoid and the lunate, with the scaphoid contributing more to wrist flexion than the wedge-shaped lunate<sup>7</sup>.

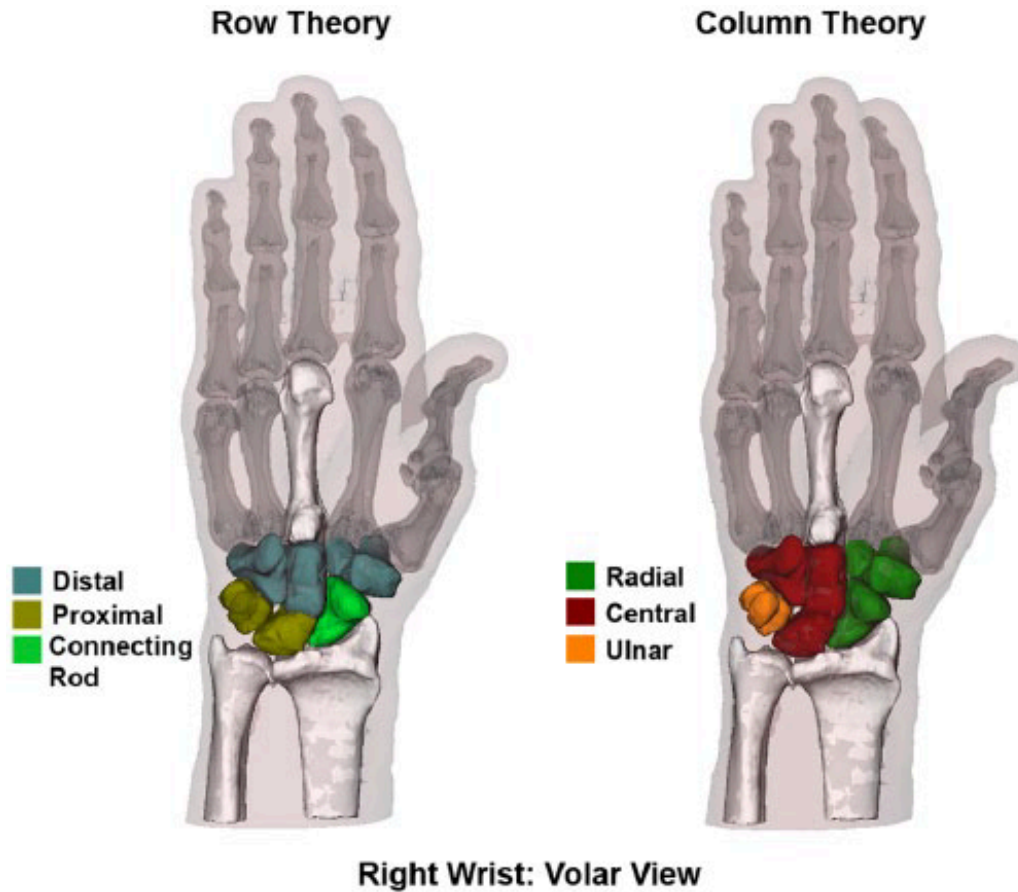


**Figure 1.18: Functional Kinematic Units as Described in Row and Column Theory.** The differences in kinematic groupings between the row and column theories of carpal kinematics are shown. The row theory divides the wrist into distal and proximal rows with the scaphoid acting as a linkage. The column theory has three divisions including the central, radial and ulnar column. (Reused with permission by Rainbow MJ, Wolff AL, Crisco JJ, Wolfe SW. Functional kinematics of the wrist. *J Hand Surg Eur Vol.* Jan 2016;41(1):7-21. doi:10.1177/1753193415616939).

### 1.2.1.2 Row Theory

Another leading theory of carpal kinematics is the Row Theory proposed by Destot in 1926<sup>11</sup>. Using roentgenograms in various positions, he postulated that the carpus divides itself into two main functional rows, a distal row comprising of the hamate, capitate trapezoid and trapezium, as well as a proximal row comprised of the lunate, triquetrum and pisiform. The scaphoid is classified as a separate entity and acts to link the motions of the distal and proximal carpal rows (**Figure 1.18**). The head of the capitate was described to be the center of wrist motion<sup>5,7,11</sup>. Landsmeer then suggested the idea of intercalated segments with a relatively fixed distal row, and movement guided by the bones of the proximal carpal row<sup>7</sup>, which was corroborated with observations of volar and dorsal intercalated segmental instability (VISI and DISI) generated from disruption of the proximal intercarpal ligaments<sup>7,12</sup>.

### 1.2.1.3 Oval Ring Theory

Although row and column theories remained the leading theories of carpal kinematics, they, along with other theories, are found to be insufficient to fully explain carpal kinematics. Litchman proposed the Oval Ring Theory of carpal kinematics in 1981, which described movements of the carpus akin to a ring, with two mobile links at the STT joints and the TH articulation<sup>13</sup> (**Figure 1.19**). Radial disruption of the ring leads to disruption of the scapho-lunate-capitate articulations, and ulnar disruption creates midcarpal instability. This model accounts for the tendency of the proximal row to rotate together, and the minimal differences seen between scaphoid and lunate motion. Additionally, it outlined the role of intercarpal ligaments in stabilizing the STT joints as well as in generating DISI and VISI deformities<sup>13</sup>.

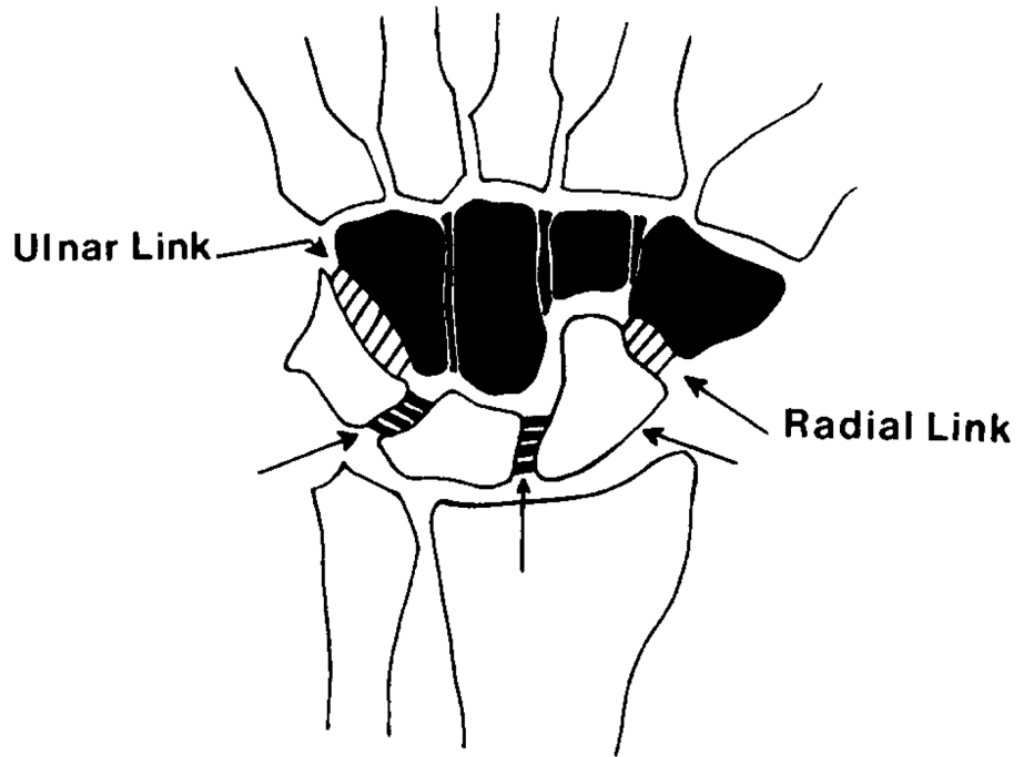


**Figure 1.19: Oval Ring Theory as Described by Litchman et al.** The main links of the oval ring theory are shown here, with the distal carpal row acting as one unit (black). It was proposed to be linked to the proximal row at two main points, the TH joint ulnarly and the scaphotrapezium joint radially. (Reused with permission from Lichtman DM, Schneider JR, Swafford AR, Mack GR. Ulnar midcarpal instability—Clinical and laboratory analysis. *The Journal of Hand Surgery*. 1981;6(5):515-523. doi:10.1016/s0363-5023(81)80115-3).



#### 1.2.1.4 Applied Forces to a Balanced Lunate

With further study using cadaveric studies as well as with the use of CT technology, Garcia-Elias then went on to expand these theories. He suggests a hybrid model in which there are 4 mechanisms of carpal stabilization that all balance to act on the lunate during motion. This includes proximal row, distal row, midcarpal and radiocarpal stabilization, with positioning of the lunate held in balance by a variety of ligaments including the intercarpal ligaments such as the SLL, and LTL, as well as extracarpal ligaments including the ulnocarpal and radiocarpal ligaments. Detailed overview of these ligaments is presented in **Section 1.1.3.1**. Anatomic shape of the carpal bones were also thought to contribute to stability.<sup>14,15</sup> (**Figure 1.20**).

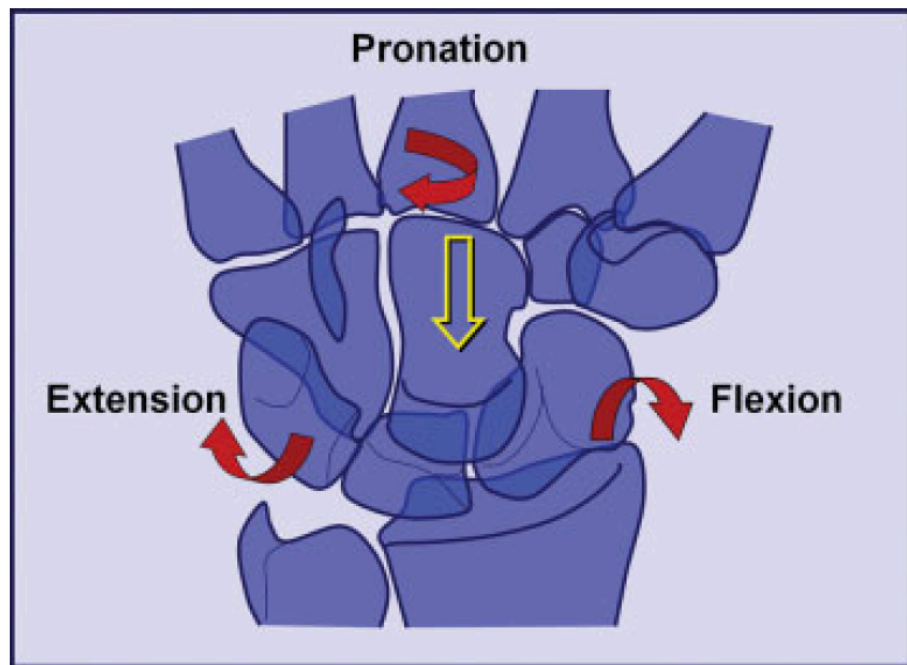


**Figure 1.20: Forces Applied to a Balanced Lunate as Described by Garcia-Elias et al.**

In this theory the lunate, on which the carpus sits, is stabilized by its morphology and surrounding ligamentous restraints in order to balance the forces imparted by the adjacent bones. The capitate imparts axial load, the triquetrum has a tendency to extend and the scaphoid flexes. (Reused with permission from Garcia-Elias M. Understanding wrist mechanics: a long and winding road. *J Wrist Surg.* Feb 2013;2(1):5-12. doi:10.1055/s-0032-1333429).

### 1.2.1.5 Central Column Theory

Although multiple theories had been proposed, it was felt by Sandow and colleagues that theories to date had been mostly observational, and had low predictive value<sup>16</sup>. In 2014, Sandow and colleagues used 3-dimensional CT (3DCT) technology to propose a central column theory of kinematics, in which there is a central column to link the forearm to the hand comprised of the lunate, capitate, hamate, trapezoid and trapezium<sup>5,16</sup>(**Figure 1.21**). The scaphoid then provides a lateral column, acting to support the central column as a “two-gear, four-bar linkage”, and the trapezoid acts to rotate the axis of the central column<sup>16</sup> (**Figure 1.22**). This rotation allows for out-of-plane movements such as DTM. They suggest the value is their model used synthesis kinematics, and can be used to anticipate and predict motion patterns at each of the joints involved in the model<sup>16</sup>

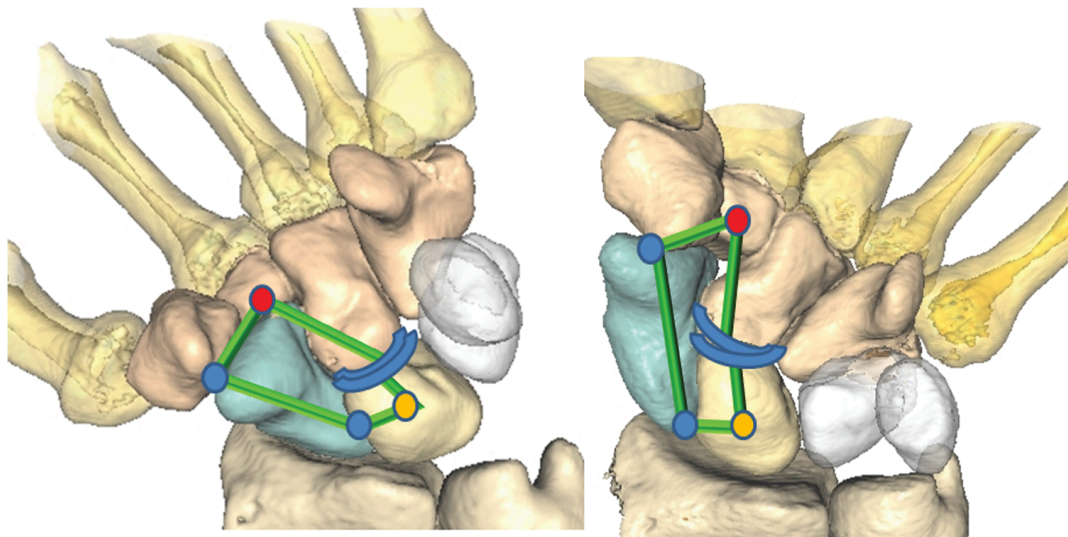


**Figure 1.21: Four-Gear, Two-Bar Linkage Concept of Central Column Theory.** Blue dots represent the connection of the scaphoid to the distal and proximal carpal rows, with connection by green bars. The red dot represents the centroid of the distal row and the yellow the centroid of the proximal row. (Reused with permission from Sandow MJ, Fisher TJ, Howard CQ, Papas S. Unifying model of carpal mechanics based on computationally derived isometric constraints and rules-based motion - the stable central column theory. *J Hand Surg Eur Vol.* May 2014;39(4):353-63. doi:10.1177/1753193413505407).

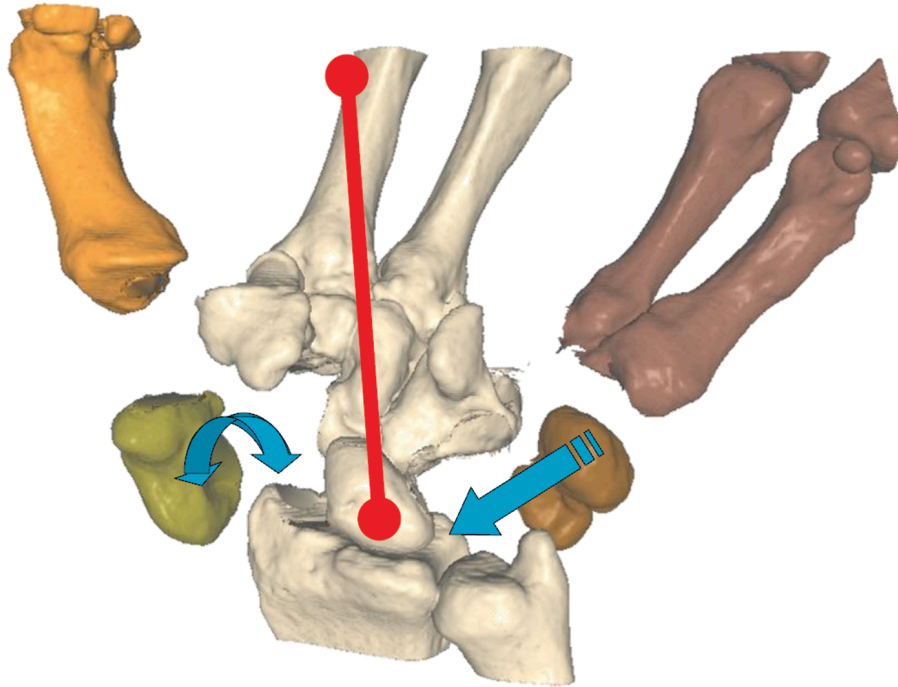


**Figure 1.22: Central Column Theory as Described by Sandow et al.** The central column is composed of the distal carpal row acting as articulating with the lunate (white). There is a separate ulnar restraint articulating with the triquetrum (brown), and an independent scaphoid on the radial side (green), and independent 1<sup>st</sup> ray (orange). (Reused with permission from Sandow MJ, Fisher TJ, Howard CQ, Papas S. Unifying model of carpal mechanics based on computationally derived isometric constraints and rules-based motion - the stable central column theory. *J Hand Surg Eur Vol.* May 2014;39(4):353-63. doi:10.1177/1753193413505407).

## 1.2.2 Challenges and Controversies in the Study and Characterization of Carpal Kinematics

There are several factors that contribute to the difficulties encountered in the study of carpal kinematics. Firstly, unlike the hip or the knee which comprise of one to three articulations, the wrist is comprised of eight bones divided into a proximal carpal row (scaphoid, lunate, triquetrum and pisiform) and a distal carpal row (trapezium, trapezoid, capitate and hamate). Each bone articulates with multiple adjacent bones, as well as the distal radius and ulna of the forearm proximally, and the metacarpals of the hand distally<sup>7,12</sup>. The sheer number of articulations is a hint towards the complexity in degree and direction of movement that can be generated by the wrist. Additionally, intercarpal and extracarpal ligaments as well as numerous volar and dorsal tendons and muscles play a role in the functional capabilities of the carpus<sup>17</sup>. This complex anatomic design, and involvement of multiple bony, soft tissue and muscular structures makes it challenging to parse out the contributions to cumulative motion of each bone and its individual articulations from the surrounding soft tissue and musculature<sup>18</sup>.

Next, the wrist joint has the ability to move, unconstrained in 6 degrees-of-freedom. This ranges from wide circumduction maneuvers to smaller intricate movements of the carpus. Although the wrist can generate movements along the traditional 6 planes (abduction and adduction, flexion and extension, pronation and supination), many functional tasks, including hammering, writing and swinging are composite motions, that are performed out-of-plane<sup>7,17,19,20</sup>. This makes easily accessible 2-dimensional techniques such as x-ray, cineradiography and fluoroscopy prone to error in the study of carpal kinematics, as they cannot accurately capture the 3-dimensional motion and non-planar motion patterns of the wrist that frequently comprise functional carpal motion. The advent and increased accessibility of 3-dimensional modalities such stereotactic trackers and 3-dimensional imaging including computed tomography (CT), and magnetic resonance imaging (MRI) have allowed more detailed and accurate studies of carpal kinematics through multiple motion planes<sup>21,22</sup>.

Additionally, the small size of the carpal bones, and relatively small movements between bones imposes a technical challenge regarding accurate measurement and kinematic study<sup>18,23</sup>. External sensors run the risk of increased error, as skin and soft tissue between the sensors and the bones introduce inaccuracies in measurements. There is difficulty assuring motion is attributed to a

specific bone, without contribution from the numerous other articulations in close proximity. Tracking methods involving implantation into the bone of interest, as well as CT technology have helped to mitigate that challenge, and allowed study of motion with high degrees of accuracy in multiple planes <sup>17,22</sup>.

A large degree of controversy exists when describing the true motion of the scaphoid. Cragen and Stanley show that the scaphoid has differential motion in different positions, with women more likely displaying column-type kinematics, and conversely, men having more tendency towards a row-type configuration <sup>24</sup>. At the time, the idea of a variably-moving scaphoid was also supported by findings that overall ligamentous laxity correlates to the degree of out-of-plane scaphoid motion <sup>25</sup>. Although the idea of an over-arching model of carpal kinematics is attractive, more detailed study of the carpal bones shows that these theories likely represent an over-simplified model to describe true kinematic motion at the wrist. Wolfe further elucidated the variability of the scaphoid using 3DCT *in-vivo* analysis <sup>26</sup>. Although there is a general consensus that the distal carpal row moves as a single unit, bound tightly by intercarpal ligaments <sup>16,17</sup>, the true motion of the proximal carpal row is not agreed upon and may include a high-degree of variability between individuals. Further advances in technology now allow better examination of carpal kinematics stereographically and *in-vivo* and can help to confirm these observations.

Regardless of these challenges, perseverance in truly understanding the normal kinematic motion of the wrist remains critical in our ability to understand normal anatomic function. By understanding normal, we can define targets for the treatment of injury, with the aim of restoring anatomic function and optimizing outcomes.

## 1.3 Thesis Rationale

Kinematic study has provided ample knowledge of motion and function of the various joints throughout the body. Although our understanding of wrist kinematics continues to grow, there remains no consensus understanding of normal kinematic behaviour of the carpal bones. There are several popular theories of carpal kinematics, including the Row, Column, Oval Ring, Balanced Forces Applied to the Lunate, and Central Column Theory that have been proposed, none of which has been fully confirmed or disproven. It is likely that the original column and row theories are oversimplifications, given the limited technology available at their inception to truly understand the complex 3-dimensional motions of the carpus.

The main criticism of studies to date is the lack of extreme fidelity required to characterize motion in this region without doubt or error. Four-dimensional computed tomography technology allows the most high-fidelity examination of *in-vivo* carpal kinematics without the limitations associated with cadaveric or 3-dimensional scanning protocols regarding lack of true joint reactive forces and contribution of muscle tone and soft tissue. Currently, there remains no 4DCT kinematic analysis of the entire carpus throughout flexion-extension motion (FEM) within the literature. Dart-thrower's, an enticing movement for post-operative rehabilitation protocols, has been studied by multiple authors at this time. Additionally, the wide variability and minimal movement, noted in proximal carpal row mechanics during RUD make it more challenging to draw definitive conclusions on.

Our study is the first study to analyze *in-vivo* carpal kinematics of the entire wrist using dynamic, non-invasive 4DCT technology, during unconstrained FEM. Previous *in-vivo* studies have largely focused on the scapho-lunate and capitate articulations without much attention to the remainder of the carpus. A better understanding of normal baseline wrist kinematics is required. Although numerous studies have been performed, a consensus has yet to be reached due to the challenges involved in the study of carpal kinematics, and the varying accuracy and fidelity of the techniques used to date. These are further discussed in **Chapter 2**. This knowledge has significant clinical implications. Knowing the range of normal kinematics of the entire carpus may provide a clearer picture of anatomic targets in order to refine specific repair and reconstruction techniques and allow clinicians to optimize their management techniques. This can include things such as

determining sites for partial wrist fusions, or reconstructing ligaments in order to restore normal function. Ultimately, the hope is that restoring normal will lead to increased satisfaction, functional outcomes, and longevity of implants following operative intervention. Additionally, a complete understanding of wrist kinematics would allow the optimization of rehabilitation strategies to maximize recovery. Without a true consensus and understanding of normal, these goals remain a moving target.

### 1.3.1 Objective and Hypothesis

The main objective of this study is to quantify *in-vivo* carpal kinematics during flexion-extension motion using 4DCT technology.

This is accomplished by:

- a) Quantify the degree and direction of sagittal rotation of each carpal bone during Flexion-Extension Motion (FEM) by using helical axes data.
- b) Identifying bones which move together and can be grouped into a single kinematic body and defined as “blocks”
- c) Quantifying degree of motion between blocks during FEM by using helical axes data.

The secondary objective is to use our findings to support or contradict the currently accepted theories of carpal kinematics by comparing the consistency of those theories with our kinematic findings.

We hypothesize that the currently accepted row, column and oval ring theories will be shown to be oversimplifications and will have features not consistent with our findings. We postulate that our results will largely support one of the remaining theories more strongly.

### 1.3.3 Overview

**Chapter 2:** This chapter provides a review of current literature pertaining to kinematic study of the carpus.

**Chapter 3:** This chapter details the methodology and statistics employed in this study.

**Chapter 4:** This chapter presents a detailed review of study results and statistical analysis.

**Chapter 5:** This chapter provides a discussion of results, summary and conclusion, as well as possible future directions of this work.



## Chapter 2

### **2 Review of Literature: Techniques in the Study of Carpal Kinematics & the Use of Helical Axes**

*This chapter reviews carpal kinematic study, from historical to current study techniques and technologic advances. There is a particular focus on 4-dimensional CT technology, and its use in carpal kinematic study to date, efficacy and safety profile. Elaboration into the use of helical axes in kinematic study is also provided.*

## 2.1 Earlier Modalities for the Study of Wrist Kinematics

As with many fields, the rate of progress of our knowledge regarding carpal kinematics has been paced largely by advances in technology. This section reviews historic and current technology used in the study of carpal kinematics, and reviews their associated strengths and weaknesses.

### 2.1.1 2-Dimensional Imaging Techniques

Original theories of carpal kinematics were generated from analysis of 2-dimensional (2D) imaging modalities such as x-rays, cineradiography and fluoroscopy. All three modalities can be applied to both *in-vitro* and *in-vivo* models. X-rays generate a static, projected 2D picture, and are relatively safe as they only require a single-dose of radiation for exposure. Unfortunately, static films cannot capture dynamic pathology<sup>17</sup>. Cineradiography allows analysis of dynamic motion through acquisition of multiple images. A series of x-rays are taken in sequential motion, producing a stop-frame film of multiple static images, but in 2D. The benefit is the ability to analyze static motion over time, but comes at the cost of a higher radiation exposure. Fluoroscopy generates continuous 2D x-ray images, but has the highest radiation exposure of the three, as subjects are radiated for the entire duration of exposure.

Although 2D imaging techniques were advanced for their time, these modalities remain limited in many ways. They estimate motion in 3-dimensional (3D) space by measuring changes in 2D length of bones (**Figure 2.1**). Although the estimations are good for gross analysis, and the technology is relatively inexpensive and accessible, these techniques cannot accurately capture complex morphology and spatial movement of the carpal bones. Error is generated from the overlap of multiple bones, and limited ability to capture 6-degrees-of-freedom composite motion in two dimensions<sup>17</sup>. Additionally, the majority of wrist motion does not occur in orthogonal planes, and thus it is beneficial to be able to study motion in 3D<sup>27,28</sup>.

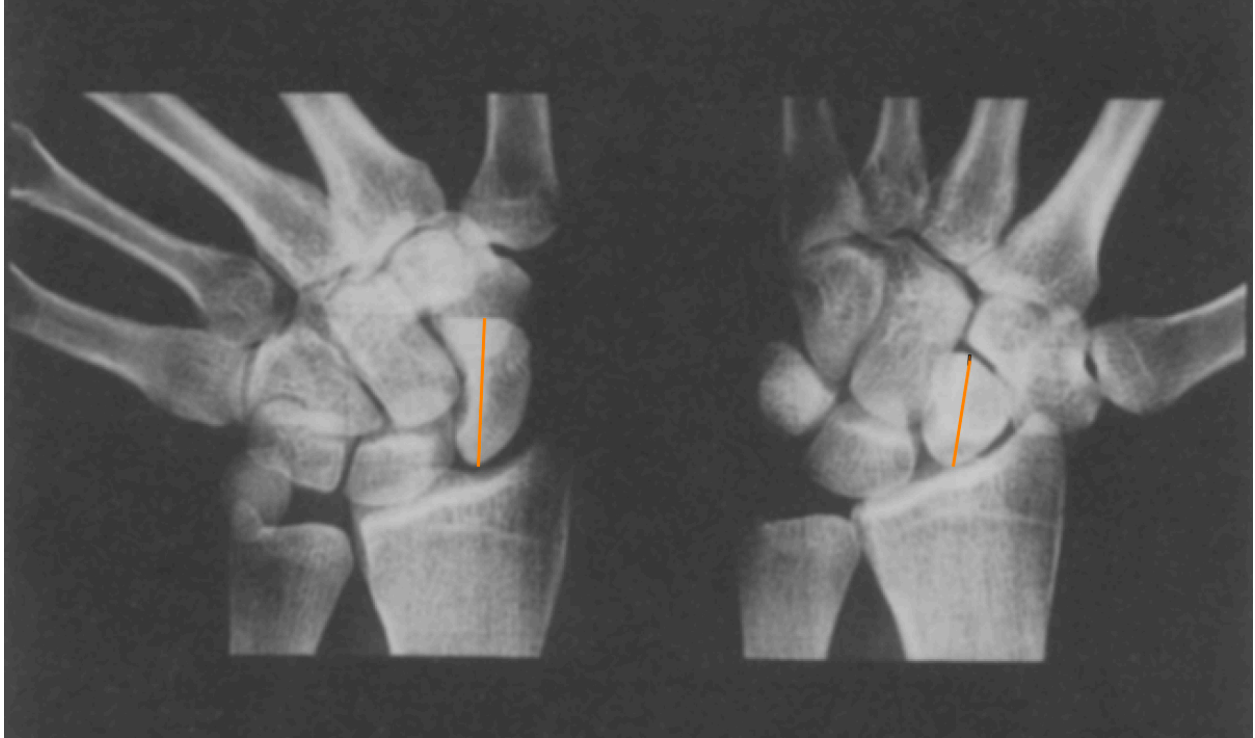


**Figure 2.1: Xray Imaging to Compare Carpal Morphology in Radioulnar Deviation.** Two separate x-rays taken of the same wrist are used to compare changes in the length of carpal bones from ulnar deviation to radial deviation. The change in length of the scaphoid is demonstrated here showing flexion as this wrist moves from ulnar to radial deviation. Multiple views would be required to infer changes in 3-dimensional space. (Adapted with permission from Garcia-Elias M, Ribe M, Rodridguez J, Cots M, Casas J. Influence of joint laxity on scaphoid kinematics. *J Hand Surg Eur Vol.* 1995;20(3)(B):379-382).

### 2.1.2 3-Dimensional Imaging with Implantable Trackers

The limitation of 2D evaluation were superseded by the advent of 3-dimensional (3D) study. Three-dimensional kinematic study was approached in one of two ways; the use of implantable trackers, and marker-less bone registration discussed in **Section 2.1.3**. Initially, the use of accurate, magnetic or optical trackers which could be implanted into the bone were implemented (**Figure 2.2**). The benefit to this modality is high accuracy and the ability to track multiplanar motion even in a small bone. Ishikawa et al. used this technique to show the influence of ligament tension on movement of the proximal carpal row in the setting of wrist distraction <sup>29</sup>. They showed that magnetic trackers could accurately track movement with 6-degrees of freedom. They also demonstrated that the percentage contribution of the radiocarpal joint to global wrist flexion-extension decreased more significantly than that of midcarpal motion in wrist distraction, demonstrating increased constraint of the proximal intercarpal ligaments. Additionally, in traction the dorsal radiocarpal ligament (DRCL) constrained radiolunate flexion more than capsular structures. Scaphocapitate (SCL) and scaphotrapezotrapezoid ligaments (STTL) were found to induce ulnar deviation of the scaphoid, which became more pronounced in traction. This highlights the importance of accounting for soft tissue structures in the study of carpal kinematics. Werner and colleagues used implantable trackers in 7 cadavers with simulated motion <sup>28</sup>. They were able to show that the scaphoid and lunate moved in the same plane of wrist movement, whether in flexion-extension motion (FEM), or radioulnar deviation (RUD), but to a lesser degree than the global composite motion.

The main limitation associated with the use of implantable trackers is the morbidity associated with them, as they require a separate procedure to implant. This largely limits their use to cadaveric study and requires a degree of violation of soft tissue to mount <sup>28</sup>. Cadaveric studies, although useful, come with their own limitations. They introduce an increased cost associated with performing these analyses, and do not allow for *in-vivo* analysis which take into account muscle tone, and soft tissue restraint, or the joint contact pressures created by them. Although *in-vitro* cadaveric study can aim to re-create these forces by retaining as much tissue as possible, and pulling force through cross-sectioned forearm tendons; they cannot completely replicate *in-vivo* conditions <sup>18,21,22</sup>. *In-vitro* studies also preclude the ability to study changes in kinematics pre- and post- injury or intervention in addition to an inability to examine functional tasks <sup>7</sup>.

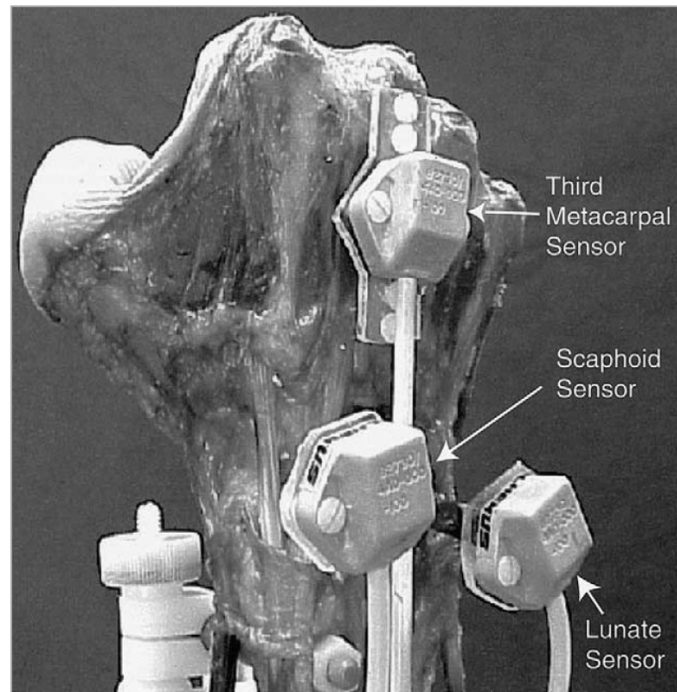


**Figure 2.2: Implantable Trackers Used to Measure Kinematic Motion in Cadaveric Study.**

Trackers are implanted into each individual bone of interest. Displacement of each bone is captured by an external sensor and displacement in 3D space is calculated. (Reused with permission by Werner FW, Green JK, Short WH, Masaoka S. Scaphoid and lunate motion during a wrist dart throw motion. *J Hand Surg Am.* May 2004;29(3):418-22. doi:10.1016/j.jhssa.2004.01.018).

### 2.1.3 Marker-less Bone Registration in 3-Dimensional Imaging Modalities

Cross-sectional imaging including both computerized tomography (CT) and magnetic resonance imaging (MRI) are non-invasive modalities to study both *in-vitro* and *in-vivo* carpal kinematics. Three-dimensional computerized tomography (3DCT) based marker-less bone registration was first described by Wolfe and Crisco, and provides a non-invasive way to assess *in-vivo* motion with the ability to detect small changes in motion between the carpal bones <sup>21,30</sup> (**Figure 2.3**). Accuracy was cited to be within error of 0.5° of rotation and 0.5 mm of translation, and has been reproduced by other investigators <sup>18,21,22</sup>. This method also allows multiple methods of kinematic analysis including the calculation of a centroid of movement and a helical axis of motion, which is further explored in detail in **Section 2.3** <sup>23</sup>. Three-dimensional CT analysis also allows for surface mapping and study of joint-contact motion and extrapolation of arthrokinematics by analysis in changes of distance between adjacent bones in motion <sup>31,32</sup>. This technique was used by Sandow et. al <sup>16</sup> to propose the Central Column Theory of wrist kinematics previously discussed in **Section 1.2.1.5**. Kamal and colleagues were also able to use 3DCT to show kinematics of the triquetrohamate (TH) joint during dart throwers motion (DTM) during a simulated hammering task. They were able to disprove previous ideas of a simple helicoid articulation, and instead follows more ellipsoid motion guided by the concave distal ride of the hamate <sup>20</sup>.

Multiple *in-vivo* 3DCT studies have shown variation in scaphoid and lunate kinematics and axis of rotation <sup>23,33,34</sup>. Variability appears to be more pronounced in RUD versus FEM <sup>18</sup>. These 3DCT studies largely point to the main motion of the scaphoid to be within the sagittal plane of flexion-extension, during all of FEM, RUD and DTM. The direction of scaphoid movement follows that of that of the global movement of the carpus <sup>23,33</sup>. Additionally, the scaphoid flexes and extends more so than the lunate in FEM <sup>18</sup>. Rainbow et. al. <sup>31</sup> examined scaphoid, lunate and capitate kinematics at the extremes of FEM using marker-less bone segmentation. They showed that at the extremes of motion, there is less contribution of the radiocarpal articulations to motion than the midcarpal joints, implying that the scaphoid and lunate are further restrained by both the volar wrist ligaments as well as impingement on the dorsal ridge of the scaphoid facet <sup>31</sup>.

Three-dimensional CT analysis is a powerful tool, allowing for both analysis of arthrokinematics and carpal kinematics *in-vivo*. Unfortunately, *in-vivo* 3D scanning still has limitations. The main

limitation is the lack of physiologic muscle loading. These studies are inert, and require shuttered, interval motion of a joint through an arc of motion. This means a static scan is performed, followed by movement to a new position and an additional static scan. This is continued until the entire desired arc of motion is captured. Marker-less bone registration with 3DCT scanning, still does not account for real-time muscle tone and inertia throughout an arc of motion, and therefore does not give the most physiologic representation of carpal kinematics. Dynamic *in-vivo* scanning addresses this limitation.

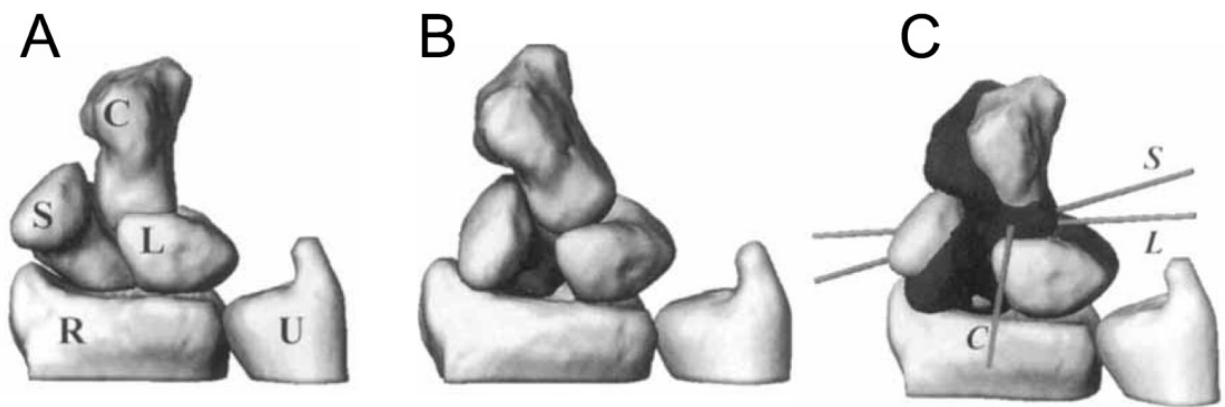


**Figure 2.3: Marker-less Bone Registration as Developed by Crisco et al.** Segmentation of each frame of a CT scan are used to create 3D meshes of each bone. Neutral models (A) are then compared to a dynamic model (B), and degree of displacement in the x, y, z axis is computed based on a coordinate system referenced to the distal radius (C). (Reused with permission by Crisco JJ, McGovern RD, Wolfe SW. Noninvasive technique for measuring in vivo three-dimensional carpal bone kinematics. *J Orthop Res.* 1999;17(1):96-100).

## 2.2 4-Dimensional CT in Carpal Kinematic Analysis

Four-dimensional computerized tomography (4DCT) is an ideal tool for *in-vivo* analysis of carpal kinematics. The fourth dimension is the addition of a real-time arc of motion in addition to the 3D information obtained in a static CT scan. This incorporates normal muscle tone and inertia throughout motion, and provides the benefit of truly being able to assess for dynamic pathology as the wrist is completing functional movements.<sup>35</sup> It may allow earlier diagnosis of truly dynamic pathology not evident on static films or scans<sup>36-39</sup>. Additionally, it can be used to monitor changes in kinematics pre- and post- injury or intervention<sup>40</sup>. This technology has become more widely available, and comes with several benefits in kinematic evaluation of the wrist. It compares directly to 3DCT analysis in terms of its accuracy in detecting small changes in motion, and capturing composite out-of-plane motion<sup>27,41</sup>. As well, helical axis data can be similarly computed. This, with the added benefit of capturing dynamic, unconstrained motion.

### 2.2.1 Accuracy & Resolution

What makes 4DCT ideal compared to MRI analysis for dynamic scanning is its temporal resolution, which decreases motion artifact and blurring. Zhao and colleagues<sup>42</sup>, demonstrated that error measurements were within  $< 1^\circ$  of rotation and  $< 0.5\text{mm}$  of translation. They concluded that 4DCT has accuracy comparable to static imaging modalities. This has been supported by several additional studies.<sup>32,43,44</sup> Although MRI offers excellent spatial resolution, its long image acquisition times is neither practical for a clinician's workflow, nor offers a high enough temporal resolution to capture motion without significant blurring<sup>35</sup>. Scans can increase temporal resolution in two ways. Firstly, by rotating the gantry during scan acquisition, a decrease in scan time and blurring is reduced. Unfortunately this method can also introduce error, especially in motions within the same plane as the gantry rotation, but rotating in the opposite direction as the rotation of the gantry<sup>22</sup>. Secondly, the use of dual gantries has been found to decrease acquisition time and temporal resolution, without introduction of similar error<sup>35</sup>. There is no definite consensus on which type of 4DCT scanner is optimal, as no study directly compares the two<sup>35</sup>.



## 2.2.2 4DCT Radiation Dose & Safety

Although concerns could be raised about the safety of prolonged CT exposure required for continuous scanning throughout an arc of motion, in reality, radiation exposure during 4DCT has been shown to be low. Four-dimensional CT scanners have integrated several technologies aimed at decreasing radiation exposure during scanning<sup>40</sup>. Studies have shown radiation to be minimal with reported average radiation exposure between 0.009 -0.07mSv<sup>32,40,43,45</sup>.. This is approximately 2-15% of normal annual background radiation, and well below the recommended annual limit of 1 Sv radiation for the general public. Overall, 4DCT has been shown to be a highly efficacious, accurate, convenient, and safe tool for analysis of *in-vivo* carpal kinematics<sup>35,42,46</sup>. For these reasons, foremost of which is its ability to give a true-to-life look at the carpus during real-time functional motion, we have chosen to use it as the primary modality to analyze carpal kinematics in our study.

## 2.2.3 Uses of 4DCT to Analyze Carpal Kinematics in Healthy Patients to Date

Four-dimensional CT is a validated tool for the evaluation of carpal kinematics in live, healthy patients, and has been increasingly applied to the study of *in-vivo* carpal kinematics<sup>43,47</sup>. Edirisinghe and colleagues (2014), used it to describe kinematics of the carpus through out-of-plane DTM in 7 healthy patients. They found that during DTM, the distal carpal row moved as a single segment and the majority of motion occurred through the midcarpal joint, with the lunate-capitate hinge acting as a pivot point<sup>27</sup>. They were also able to characterize the motion arc of the trapezium and trapezoid, as well as hamate-triquetrum as hinges, and concluded the axis of rotation for DTM was roughly 27 degrees of anteversion and 44 degrees of varus angulation<sup>27</sup>. Kelly et. al (2018), quantified normal diastasis of the scapholunate interval in both clenched fists and with RUD. They found movement between the two bones under those physiologic stresses were minimal, with 1.19mm of movement or less between the two bones<sup>48</sup>.

Scapholunate (SL) rotation axis is also of great interest as a target for anatomic repair or reconstruction. 4DCT studies have shown that there is minimal motion between the scaphoid and lunate in RUD (approximately 8°), but in FEM, the scaphoid rotates approximately 38° relative to the lunate, with its axis of rotation along the dorsal ridge<sup>44</sup>. This confirms a dorsal reconstruction

would be anatomic. In the same study by de Roo et. al. (2019), there was found to be higher degrees of variability of rotation RUD, and thus they could not comment on a definitive rotational axis. Radio-ulnar deviation of the carpus in patients with suspected scapholunate ligament (SLL) injury was further assessed by Rauch and colleagues (2018) by analyzing total arc of motion of the radioscaphoid and lunocapitate (LC) articulations. They found reduced LC motion decreased by 13-44% in patients with SLL injuries <sup>41</sup>. They suggest that the decreased motion has a high sensitivity (93%) and lower specificity (65%) for detecting SLL injury, and has a synergistic function with radioscaphoid motion <sup>41</sup>.

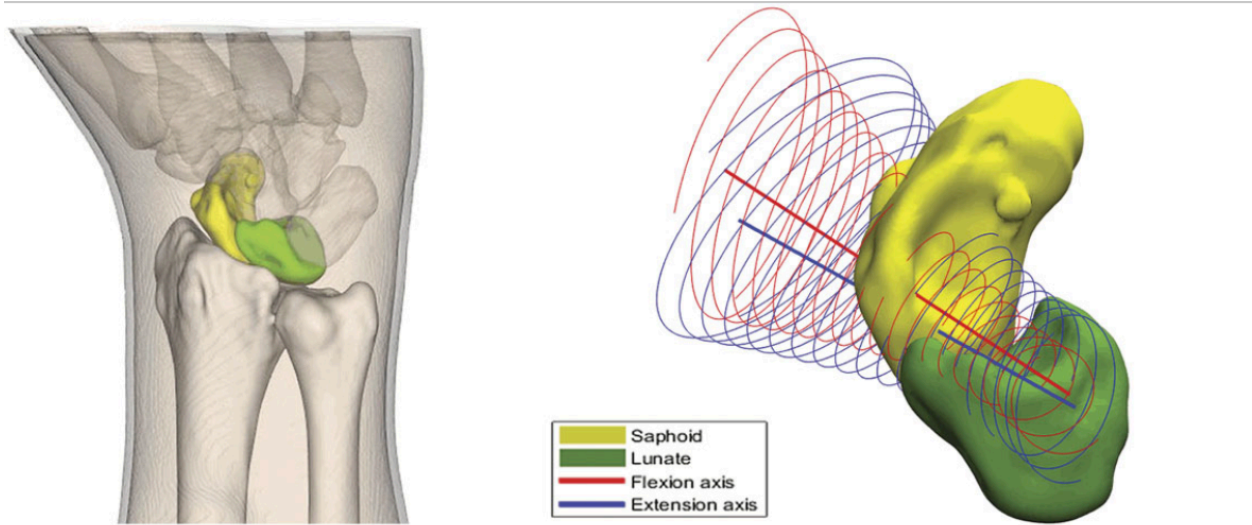
Most recently, scaphoid, lunate and capitate kinematics were assessed using 4DCT scan by Brinkhorst and colleagues (2021). They analyzed 20 healthy patients in FEM and RUD and were able to confirm findings of scaphoid and lunate flexion with wrist flexion, and conversely, extension when the wrist extends. All three of the lunate, scaphoid and capitate deviate ulnarly during flexion of the wrist, and radially during extension. During RUD, the scaphoid and lunate extend when the wrist is ulnarly deviated and flex when the wrist is radially deviated <sup>49</sup>. This study focused only on the three bones and does not give insight as to the possible hinge or guiding mechanisms that may be present at the STT joint or the triquetrohamate articulation. This would be better elucidated by quantifying the axis of rotation between bones, to see movement of one bone relative to another at each articulation, and where within each bone, those axes cross. To our knowledge, our study is the first to describe *in-vivo* kinematics in terms of individual carpal motion in 6-degrees of freedom, and axis of rotation of bones in both carpal rows throughout FEM.

## 2.3 The Use of Helical Axis in Kinematic Study

### 2.3.1 Helical Axis to Describe Kinematic Motion

The helical axis, originally described as the rotation axis, is the unique axis on which a body in motion translates on and rotates around for a given path of motion<sup>50,51</sup>. Helical axis motion (HAM) is a method of describing multiplanar motion compared to a previous time point opposed to a reference marker, and is comprised of the rotation axis, angle of rotation, translation of an object along an axis of rotation and the location of rotation axis in 3-dimensional space<sup>34,52</sup> (**Figure 2.4**). This is in contrast to a 6 degree-of-freedom analysis which decomposes motion into three separate translations corresponding to the Cartesian axes, as well as three separate rotation angles around said axes<sup>53</sup>. Although ultimately both methods can be used to quantify kinematic motion, HAM has the advantage of being easier to communicate as it is independent of the Cartesian plane and requires fewer values in its description. This is advantageous while studying carpal kinematics as it provides a visual representation of motion that can be used to compare the numerous small bodies moving along their own unique axes. Intersection points between axes can also be used to see how bodies move in relation to each other, independent of a standard reference body.

There are two main types of helical axes described: finite and instantaneous. For finite helical axis (FHA), movements are analyzed in discrete steps and the axis of rotation is generated between two time points. Instantaneous helical axis (IHA) instead describes the rotation of one body in respect to another<sup>52</sup>. Although IHA is associated with a physical meaning whereas FHA is a theoretical axis, both can be used to determine the center of a body in motion and its axis position. Both methods have been found to be mathematically equivalent<sup>54</sup>. HAM is a powerful tool that provides a robust and detailed method of quantifying kinematic motion and allows standardized quantification and description of motion across several 3D modalities.



Position of the rotation axis (right) from an ulnodorsal view of the wrist (left)

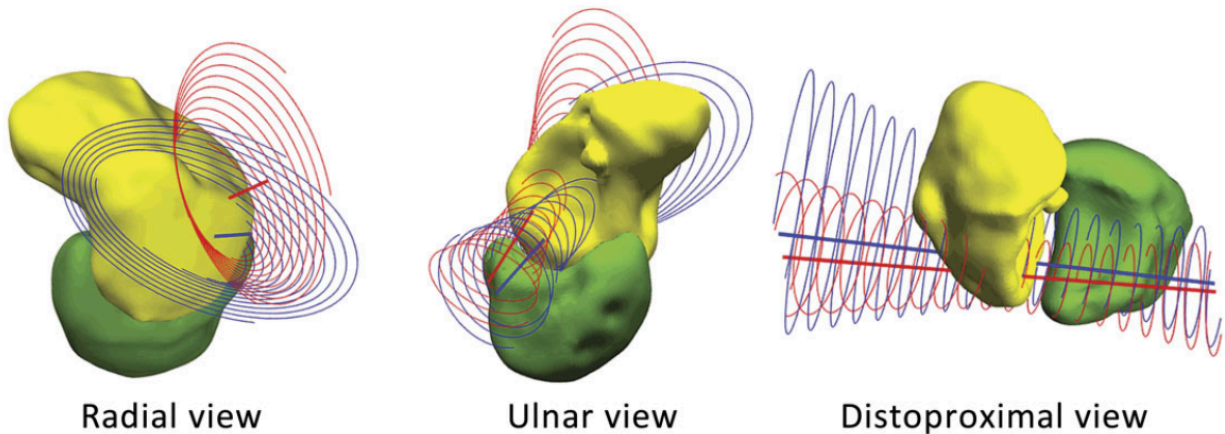


**Figure 2.4: Depiction of Helical Axis of Rotation of the Scaphoid as Demonstrated by deRoo et al.** Marker-less bone registration and 4DCT were used to determine helical axis of the scaphoid during wrist FEM and RUD. The axis represents the line on which the scaphoid rotates and translates on as it moves through 3D space. (Reused with permission by de Roo MGA, Muurling M, Dobbe JGG, Brinkhorst ME, Streekstra GJ, Strackee SD. A four-dimensional-CT study of in vivo scapholunate rotation axes: possible implications for scapholunate ligament reconstruction. *J Hand Surg Eur Vol.* Jun 2019;44(5):479-487. doi:10.1177/1753193419830924).

### 2.3.2 Helical Axis in Joint Kinematics

HAM has been used to reliably describe kinematic motion in the shoulder, spine, ankle, and knee <sup>45,55,56</sup>. Although the use of HAM to describe kinematic motion in the body was first applied in the 1980s <sup>50</sup>, dynamic kinematic analysis using sequential CT scans was first performed by Patterson et. al. in 1998 on cadavers with the use of implantable trackers in the wrist <sup>57</sup>. Subsequently in 1999, the first use of marker-less bone registration was performed using 3DCT scans of the carpus *in-vivo* and provided a non-invasive method of obtaining HAM <sup>21</sup>. Although these original studies provide a representation of kinematics in motion, they are not truly dynamic, as they were obtained with a series of static scans in different positions of motion. Regardless, they showed that the HAM could be reliably obtained and used to describe sub-millimetre, multiplanar motion <sup>21,50</sup>.

To date, there have been two *in-vivo* applications of helical axis data being used to quantify carpal kinematics via dynamic 4DCT scans. We have previously discussed Brinkhorst and colleagues' work characterizing scaphoid and lunate kinematics during wrist FEM and RUD in Section 2.2.3. The second study was performed by de Roo et al, in their investigation of kinematic motion between the scaphoid and lunate through FEM and RUD <sup>44</sup>, They compared not only degree of rotation between the two bones, but use the helical axes data to determine where the rotation axis intersected each bone. De Roo et al, found that the helical axis between the scaphoid and the lunate intersects dorsally, and thus concluded that it was important to reconstruct the SLL in a way as to reconstruct that dorsal rotation axes of the SL interval (**Figure 2.4**)<sup>44</sup>. Their group suggested that any reconstruction that alters the normal kinematic rotation axis between the two bones has the potential to limit natural motion of the SL complex and result in worse surgical outcomes. This is an important example of how helical axes data can be used to compare kinematic motion at a specific articulation, not just in regards to degrees of motion, but also to determine key pivot points between two bodies.

To expand on previous work performed using 4DCT to assess kinematics, our work uses helical axis to analyze motion beyond the SL interval, and specifically looks at the carpus in its entirety. It includes rotation of all 7 carpal bones contributing to FEM, and allows comparison of movement at each articulation. This allows quantification of the magnitude of rotation between bones and determination of which bones may act as a single group or kinematic unit.

## 2.4 Summary

This chapter demonstrates the current technology available for kinematic study and reviews its pros and cons. 4DCT analysis provides a dynamic, safe, non-invasive and accurate method of kinematic study of the carpus. Additionally, data obtained from 4DCT scans can be quantified by allowing calculation of helical axes in order to describe kinematic motion. This allows analysis and comparison between bones of the wrist. In **Chapter 3**, we discuss the methodology employed in this work. We elaborate on using 4DCT data to model each carpal bone, generate their helical axis of motion, and analyze kinematic motion of each bone throughout an arc of FEM.

## Chapter 3

### **3 Methodology for *in-Vivo* Carpal Kinematic Analysis using 4-Dimensional CT Acquisition**

*This chapter presents the methodology used to conduct kinematic analysis of in-vivo carpal motion through a wrist flexion-extension arc of motion. Detailed description of participant recruitment, CT image acquisition protocol, and creation of 3D carpal bone reconstructions is provided. Additionally, this chapter elaborates on the generation of instantaneous helical axes to quantify rotation for each carpal bone throughout flexion-extension motion- the output variable for overall carpal bone kinematic analysis in this study.*

## **3.1 Image Acquisition and Scanning Protocol**

Western University Research Ethics Board (REB) approval was obtained for participant recruitment and experimental protocol (REB 111702) and complied with the Declaration of Helsinki of 1975, revised 2000. Healthy participants were recruited on a volunteer basis from the local population via newspaper advertisement. Participant recruitment was performed on a prospective basis, to allow the creation of a database of volunteer scans. Inclusion criteria included participants 18 years of age or older with no previous history of wrist injury or surgical interventions. Written and informed consent was obtained from all participants undergoing the scanning protocol. Participants were retrospectively excluded from analysis for this study if there was radiographic evidence of carpal arthritis or previous injury to the distal radius, carpal bones or carpal ligaments.

### **3.1.1 Pre-Scanning Protocol**

Participants were donned with appropriate radiation safety equipment including lead apron, thyroid shields and lead eyeglasses. Patients were positioned prone with their dominant arm outstretched overhead so that only the wrist of interest was within the scanning field. This allowed freedom of wrist motion while decreasing radiation exposure to the thorax and abdomen. Neutral alignment was chosen as the starting position prior to any motion, and physical starting position in three-dimensional space was standardized for all participants.

### **3.1.2 4DCT Image Acquisition and Scanning Protocol**

Unilateral, dynamic 4-dimensional computed tomography (4DCT) imaging was performed of the dominant wrist of each participant using a Computerized Tomography (CT) scanner (Revolution CT Scanner, General Electric Healthcare, Waukesha, Wisconsin, USA). The scanning protocol used in this study has been previously developed and routinely used for 4DCT image acquisition<sup>46</sup>. Scanning was performed at 80kV, 125 effective mA, axial scans and 0.35 s rotation time. Effective scanning volume for our scanner was 16cm<sup>3</sup>. This area was configured as 128, 1.25mm thick slices, repeatedly scanned at 0.35 s intervals over 24.5 second duration for a total of 70 volumes at 2.86 Hz. This produced a voxel size of 0.625 x 0.625 x 1.25mm. This resolution was sufficient for capture of the anatomic area of interest without significant noise. The scanning area



was able to capture the carpal bones, proximal metacarpals, distal radius and distal ulna. Initial localizing scan was performed to ensure that the carpus was captured and centered within the effective scanning area prior commencement.

Participants underwent an initial static CT scan with the wrist in neutral alignment. This was followed by three kinematic scans, each capturing a single pass of wrist motion. The first pass scanned the wrist from full extension to full flexion, encompassing the extremes of possible wrist motion for each individual participant. The second pass captured the return pass from full wrist flexion to full wrist extension. The wrist was once again brought from full extension back to full flexion to complete the final pass. The duration of each pass lasted 8.75 seconds, and produced 25 stop frames of motion for analysis. A video demonstration the desired flexion-extension motion (FEM) arc was played to participants throughout scanning, with the goal of demonstrating the desired wrist motion, as well offering a target tempo of 22°/second for participants to mimic. This ensured that participants completed motion cycles at a similar rate throughout scanning.

### 3.1.3 Radiation Exposure

Total exposure time for the three kinematic passes was 24.5 s total for all three passes. This resulted in a dose length product (DLP) of 713.64 [mGY-cm]. This is equivalent to a total skin dose of 0.067 Gy; less than 10x lower than the threshold for skin erythema from radiation exposure (2 Gy). Additionally, scatter radiation dose measured under the patient's lead apron was 0.013 mSv, and is used as a surrogate marker for total body radiation received by the patient during the study. Scatter dose radiation was deemed to be negligible as the annual background radiation received by an average person is 3mSv, a value 231 times higher than their exposure in this study.

## 3.2 Scan Processing and Data Analysis

Scans were preliminarily reviewed to determine appropriateness for reconstruction and further analysis. Participant scans were excluded if there was any radiographic evidence of prior injury or surgery within the wrist and carpus. Younger participant scans were preferentially selected for analysis to mitigate the chance of unidentified arthritis or injury. Ten participants were included in the analysis.

### 3.2.1 3D Image Reconstruction and Modelling

Volumetric images were visualized in 3D Slicer (open-source software version 4.11.0; <https://www.slicer.org>). This allowed visualization of the entire 3D carpus over 25 frames of motion for each pass. Global Carpal Flexion Angle (GCFA) was defined as the angle subtended a line through the longitudinal axis of the capitate, and a line through the longitudinal axis of the distal radius on the midsagittal CT cut (**Figure 3.1**). It represents the degree of flexion or extension of the carpus, compared to a stationary radius during FEM and allows definition of the total amount of wrist flexion or extension at any position. Using this angle, frames of interest were identified for reconstruction and registration. Initially, the neutral frame was identified, in which the longitudinal axes of the capitate and distal radius were parallel. Frames of interest were chosen at 10° increments between 40° of wrist extension to 40° of composite wrist flexion. Degrees of wrist extension were represented by negative angles, and conversely, positive angles represented degrees of wrist flexion. Two complete passes were included in analysis, completing a full motion from full wrist extension to full wrist flexion and back to full extension.

Three-dimensional modelling was then generated for each the capitate, hamate, trapezoid, triquetrum, scaphoid, lunate, triquetrum, 3<sup>rd</sup> metacarpal (3MC) and distal radius for each of the identified frames of interest. Using Mimics software (Version 22.0, Materialise NV, Leuven, Belgium) bones were segmented using a semi-automated segmentation method, in which a threshold value was manually selected in order to differentiate bone from the surrounding cartilage and soft tissue. Subsequently, each bone underwent refinement using manual segmentation to optimize accuracy of modelling. Finally, a median smoothing filter was applied with a kernel size

of 3mm, to filter rough edges and fill small gaps generated by the semi-automated and manual segmentation.

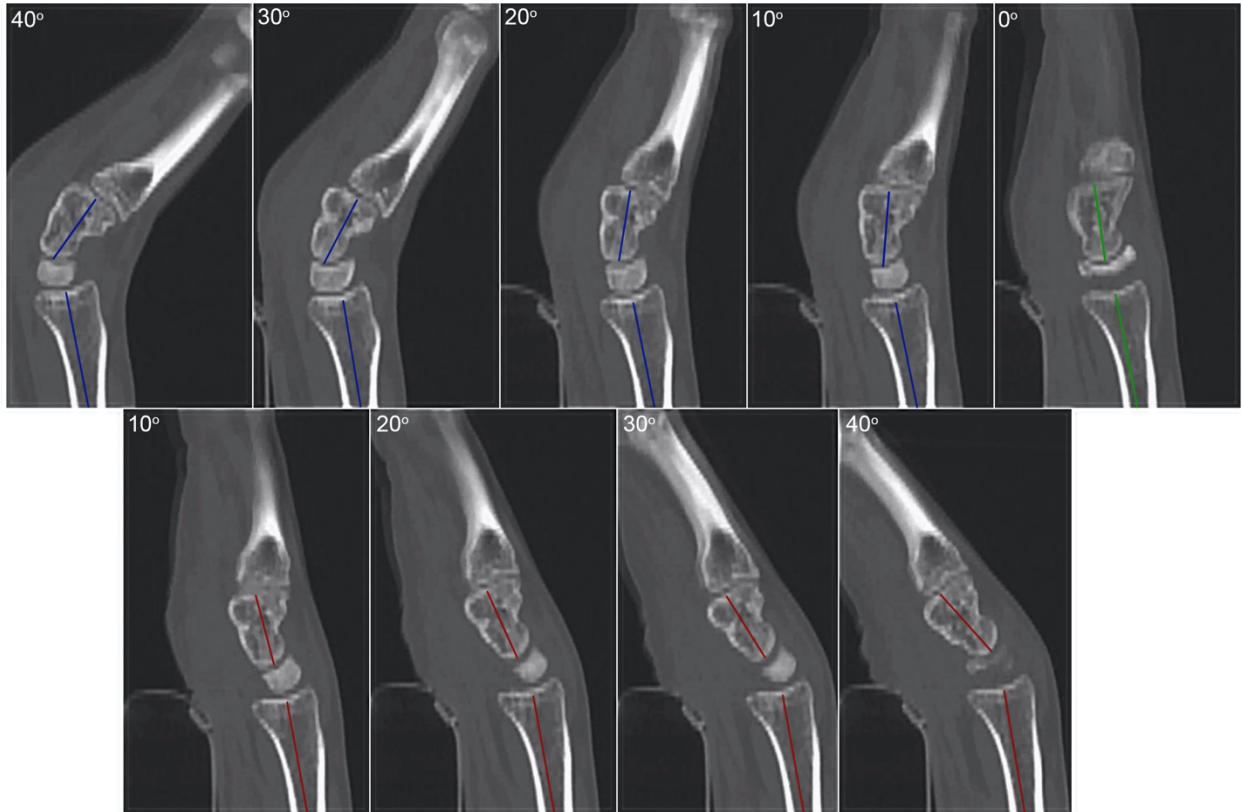


**Figure 3.1: Identifying Global Carpal Motion and Frames of Interest During Wrist FEM.**

Global Carpal Flexion Angle (GCFA), defined as the angle subtended by a line bisecting the capitate and a line bisecting the distal radius on a mid-sagittal CT cut, are demonstrated for frames of interest. The neutral frame (0°, green line), where the GCFA = 0, was identified first. Frames of interest were identified in 10 degree increments from 40 degrees of extension to 40 degrees of flexion. Extension angles are represented in blue, and flexion angles in red.

### 3.2.2 Registration and Helical Axes

Three-dimensionally reconstructed bones (scaphoid, lunate, triquetrum, trapezium, trapezoid, hamate, capitate, distal radius and 3MC) were registered in 3D Slicer using Besl and Mackay surface-based registration, in which an iterative closest point (ICP) algorithm is used to identify correlation of surfaces of best-fit <sup>58</sup>. Static models for each bone were registered to their corresponding kinematic models. In cases where surface-based registration generated inadequate registration, a previously developed python code with a two-step registration process using landmark plus ICP. Registration output produced resultant transformation matrices representative of the 3D displacement of the bone from its neutral position to its position at each kinematic model. Of note, a significant proportion of third metacarpals could not be reliably registered secondary to motion artifact, and were excluded from registration.

The helical axis of motion (HAM) of a body in motion is the axis on which that body translates and rotates on between two points in time. It allows characterization of kinematic motion without definition according to a traditional x, y, z coordinate system <sup>52</sup>. A detailed description of HAM is provided in **Section 2.3.1**. The instantaneous helical axis (IHA) describes the rotation of a body in relation to another body <sup>52</sup>. In this study, IHA was used and carpal bones were compared to the stationary radius. Transformation matrices were inputted into an adapted MATLAB (Version 2020a, The MathWorks Inc., Natick, Massachusetts, USA) code. The resultant output was the degree of rotation of given carpal bone, in the sagittal plane of the distal radius at each point in motion. In order to standardize outputs between participants, a global coordinate system within the radius was employed in accordance with the International Society of Biomechanics (ISB) standards <sup>59</sup>. Neutral alignment was assigned as 0 degrees of rotation referenced in relation to a coordinate system generated from the neutral position of the corresponding participant's distal radius. Degrees of sagittal rotation in extension were assigned a negative value, whereas degrees of sagittal rotation in flexion were assigned a positive value. **Figure 3.2** provides an example of computation of a helical axis of the scaphoid and lunate bones, with red shading representing the neutral position of the bone, and the blue shading showing the position of a single participant at 40° of wrist extension (**Figure 3.2**).

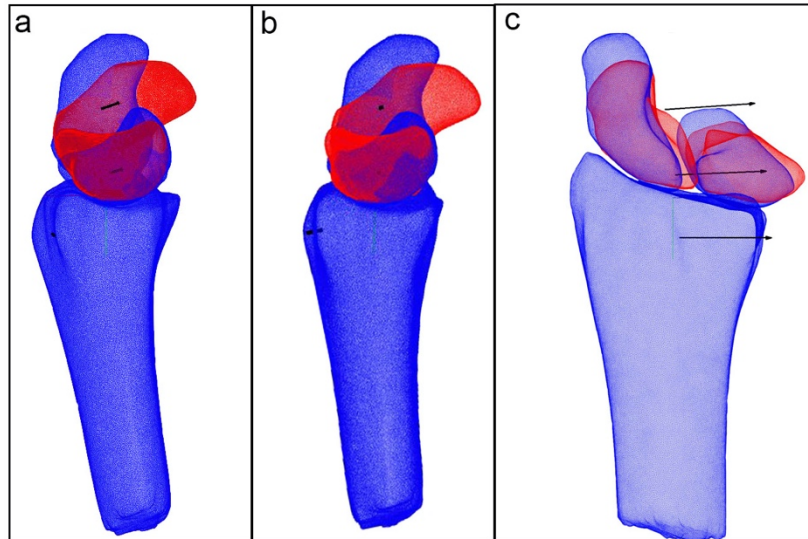


**Figure 3.2: Visual Representation of Helical Axis of the Scaphoid, Lunate and Distal Radius from Neutral to 40 Degrees of Wrist Extension.** The helical axis of rotation of the scaphoid and lunate as they move from neutral (red shading), to 40° of wrist extension (blue shading), is represented by the black line vectors, crossing through each bone. This is the line on which each bone rotates around in space. The most superior line is the helical axis of the scaphoid, the middle line corresponds to the lunate and a third, most inferior line corresponds to the distal radius. The trajectory of these helical axes run in 3D space, and is shown in the sagittal (a), oblique (b), and coronal (c) planes.

### 3.2.3 Statistical Analysis

Sagittal rotation of each carpal bone from neutral alignment was expressed in degrees ( $^{\circ}$ ). Mean values and variability was calculated for each bone of study ( $n=10$ ). A two-way, repeated-measures ANOVA was first used to identify differences in mean displacement through FEM for each bone at each position. Dunnett T3 test was used for post-hoc comparison of each bone by wrist position throughout FEM. Statistical significance was set at  $p < 0.05$ , 95% CI.

Bones with statistically similar rotation were organized into a single kinematic block. This resulted in four separate kinematic blocks, of which the bones within each block had no significant difference in their displacement at each wrist position through FEM. Mean displacement of each bone within a block was averaged, producing a composite mean displacement of the entire block. This was performed for each position of motion in the FEM arc. For example, the lunate and triquetrum had no statistical difference in displacement at any point in motion and were aggregated to form a single group, exclusive of the remaining carpal bones. The mean displacement of the lunate and triquetrum was averaged at each position in motion, to generate the composite displacement of the entire block. A subsequent two-way repeated measures ANOVA was performed on the composite means for each block, in order to analyze the difference in mean displacement between the defined blocks throughout FEM. Once again, a Dunnett T3 test was used for post-hoc comparison of mean bone position by wrist position throughout FEM. Statistical significance was set at  $p < 0.05$ , 95% CI.

### 3.2.4 Inter-Joint Distance Analysis

A subsequent joint contact analysis of the trapeziotrapezoid joint and the scaphotrapezoid joints were performed based on the results of our statistical analysis. The methods are consistent with and have been previously described in detail, and validated by Lalone et al<sup>60</sup>. Surface maps previously generated by ICP registration as described in **Section 3.2.2**, were used, and distances between bones at individual joints were quantified using a mean measurement of the closest surface points between the articulating surfaces of the two joints of interest. Distance measurements were converted to colour maps for qualitative visual analysis of motion at each joint of interest.

# Chapter 4

## **4 Results**

*This section provides a detailed description of the results of this work and associated tables and figures.*

## 4.1 Participant Demographics

Demographic details of participants are summarized in **Table 4.1**. A total of 10 participants, 3 male and 7 female, were included with a mean age of 24. All patients were right-hand dominant, and had their right hand scanned for this investigation. All patients were healthy with no previous hand or wrist injury, surgical intervention, or identifiable degenerative arthritis on review of scans.

**Table 4.1: Demographic Summary of Participants.** Demographic information by participant. A total of 10 participants were included for study with a mean age of 24. There were 3 males and 7 females. All participants were right-hand dominant and had their right wrist scanned and analyzed.

<b>Participant ID</b>	<b>Age</b>	<b>Sex</b>	<b>Scanned (Dominant) Hand</b>
13	23	Female	Right
28	24	Female	Right
29	25	Female	Right
41	24	Male	Right
44	27	Male	Right
51	22	Male	Right
52	35	Female	Right
53	18	Female	Right
54	22	Female	Right
58	22	Female	Right
	<b>Mean: 24.2</b>		



## 4.2 Degree of Flexion-Extension Around Carpal Bone Through FEM

Mean sagittal rotation (flexion/extension) of each carpal bone through each position in FEM is detailed in **Table 4.2.1** and **4.2.2**. Rotation is represented in degrees of flexion compared to the radius with positive numbers representing bone flexion, and negative numbers representing bone extension. The capitate rotation with respect to the radius was used to define the Global Composite Flexion Angle (GCFA) representing global wrist flexion and as a result, its motion is equivalent to global wrist position at 100% (SD = 2.4°). Of the remaining bones in the distal carpal row, the Hamate and the Trapezoid moved with the capitate, and rotated 99% (SD = 3.9°), and 102% (SD = 3.7°) respectively. The trapezium moved slightly less at 95% of global wrist motion (SD = 2.9°). The scaphoid rotates 87% of global wrist motion, with an average SD between participants of 2.8°. This is compared to the lunate and the triquetrum which rotate 63% (SD = 4.9°), and 70% (SD = 4.4°) of global wrist motion respectively. Comparisons of degree of rotation of each bone by wrist position is shown in **Figures 4.1.1 and 4.1.2**.

**Table 4.2.1: Rotation in Degrees of Carpal Bones from Wrist Extension to Flexion.** Mean sagittal rotation (flexion/extension) of each bone is expressed in degrees  $\pm$  SD in relation to the stationary radius (n =10). Rotation is presented in 10-degree intervals of wrist motion from 40 degrees of wrist flexion to 40 degrees of wrist flexion. Negative values represent rotation in extension, and positive values rotation in flexion.

<b>Global Wrist Position in Degrees</b>									
	-40	-30	-20	-10	0	10	20	30	40
<b>Carpal Bone</b>	<b>Mean Flexion Around Helical Axis <math>\pm</math> SD (Degrees)</b>								
Scaphoid	-35.7 $\pm$ 3.5	-26.0 $\pm$ 3.2	-16.2 $\pm$ 3.1	-8.8 $\pm$ 3.5	0.0 $\pm$ 0.0	8.0 $\pm$ 2.18	17.8 $\pm$ 2.5	25.8 $\pm$ 3.4	33.7 $\pm$ 3.6
Lunate	-22.9 $\pm$ 9.8	-17.5 $\pm$ 7.6	-11.4 $\pm$ 4.9	-7.1 $\pm$ 3.8	0.0 $\pm$ 0.0	6.3 $\pm$ 2.4	10.5 $\pm$ 3.7	16.0 $\pm$ 5.1	20.9 $\pm$ 6.6
Capitate	-39.9 $\pm$ 2.1	-28.71 $\pm$ 1.8	-18.21 $\pm$ 1.4	-9.1 $\pm$ 2.2	0.0 $\pm$ 0.0	8.8 $\pm$ 2.6	20.3 $\pm$ 2.8	30.2 $\pm$ 3.1	40.0 $\pm$ 3.5
Hamate	-40.0 $\pm$ 2.5	-29.3 $\pm$ 3.8	-17.9 $\pm$ 3.1	-9.5 $\pm$ 3.8	0.0 $\pm$ 0.0	9.1 $\pm$ 3.3	20.2 $\pm$ 4.2	29.0 $\pm$ 4.7	39.6 $\pm$ 4.3
Triquetrum	-27.4 $\pm$ 7.5	-20.0 $\pm$ 6.4	-12.9 $\pm$ 4.6	-7.7 $\pm$ 4.6	0.0 $\pm$ 0.0	6.6 $\pm$ 2.7	12.3 $\pm$ 4.7	19.0 $\pm$ 6.4	22.3 $\pm$ 6.7
Trapezium	-40.6 $\pm$ 3.4	-28.6 $\pm$ 1.9	-18.3 $\pm$ 3.3	-10.3 $\pm$ 4.8	0.0 $\pm$ 0.0	8.3 $\pm$ 2.8	18.2 $\pm$ 3.0	26.8 $\pm$ 2.4	34.6 $\pm$ 2.9
Trapezoid	-40.8 $\pm$ 3.1	-28.0 $\pm$ 2.0	-18.6 $\pm$ 3.4	-10.9 $\pm$ 4.1	0.0 $\pm$ 0.0	9.3 $\pm$ 3.7	19.0 $\pm$ 5.9	30.0 $\pm$ 3.9	37.5 $\pm$ 5.7

**Table 4.2.2: Rotation in Degrees of Carpal Bones from Wrist Flexion to Extension.** Mean sagittal rotation (flexion/extension) of each bone is expressed in degrees  $\pm$  SD in relation to the stationary radius (n=10). Rotation is presented in 10-degree intervals of wrist motion from 40 degrees of wrist flexion to 40 degrees of wrist extension. Negative values represent rotation in extension, and positive values rotation in flexion.

<b>Global Wrist Position in Degrees</b>									
	40	30	20	10	0	-10	-20	-30	-40
<b>Carpal Bone</b>	<b>Mean Flexion Around Helical Axis (Degrees) +/- SD</b>								
Scaphoid	31.2 $\pm$ 5.3	23.2 $\pm$ 2.9	16.1 $\pm$ 4.5	9.0 $\pm$ 2.9	0.0 $\pm$ 0.0	-9.1 $\pm$ 2.8	-17.2 $\pm$ 4.1	-28.5 $\pm$ 4.0	-36.8 $\pm$ 2.8
Lunate	20.4 $\pm$ 7.3	15.0 $\pm$ 5.7	10.5 $\pm$ 5.8	6.4 $\pm$ 2.9	0.0 $\pm$ 0.0	-6.4 $\pm$ 2.6	-12.2 $\pm$ 4.2	-18.7 $\pm$ 6.9	-24.0 $\pm$ 7.2
Capitate	40.3 $\pm$ 2.7	29. $\pm$ 2.53	19.4 $\pm$ 3.8	9.8 $\pm$ 2.2	0.0 $\pm$ 0.0	-10.9 $\pm$ 3.3	-19.8 $\pm$ 2.8	-30.6 $\pm$ 3.2	-40.6 $\pm$ 3.3
Hamate	39.5 $\pm$ 5.0	29.0 $\pm$ 3.1	18.9 $\pm$ 5.4	10.2 $\pm$ 3.4	0.0 $\pm$ 0.0	-11.1 $\pm$ 3.7	-20.3 $\pm$ 3.8	-31.6 $\pm$ 4.9	-40.5 $\pm$ 3.3
Triquetrum	21.1 $\pm$ 7.1	16.7 $\pm$ 5.9	12.1 $\pm$ 4.7	6.76 $\pm$ 2.7	0.0 $\pm$ 0.0	-8.6 $\pm$ 2.0	-14.8 $\pm$ 2.4	-21.5 $\pm$ 4.7	-28.8 $\pm$ 5.5
Trapezium	34.9 $\pm$ 2.9	26.9 $\pm$ 2.8	17.6 $\pm$ 3.9	9.3 $\pm$ 1.7	0.0 $\pm$ 0.0	-11.0 $\pm$ 4.4	-20.1 $\pm$ 3.8	-31.5 $\pm$ 4.2	-41.2 $\pm$ 3.1
Trapezoid	40.2 $\pm$ 2.8	31.7 $\pm$ 3.8	20.8 $\pm$ 3.9	13.1 $\pm$ 4.3	0.0 $\pm$ 0.0	-10.7 $\pm$ 4.1	-19.3 $\pm$ 5.1	-31.5 $\pm$ 6.6	-39.5 $\pm$ 4.1

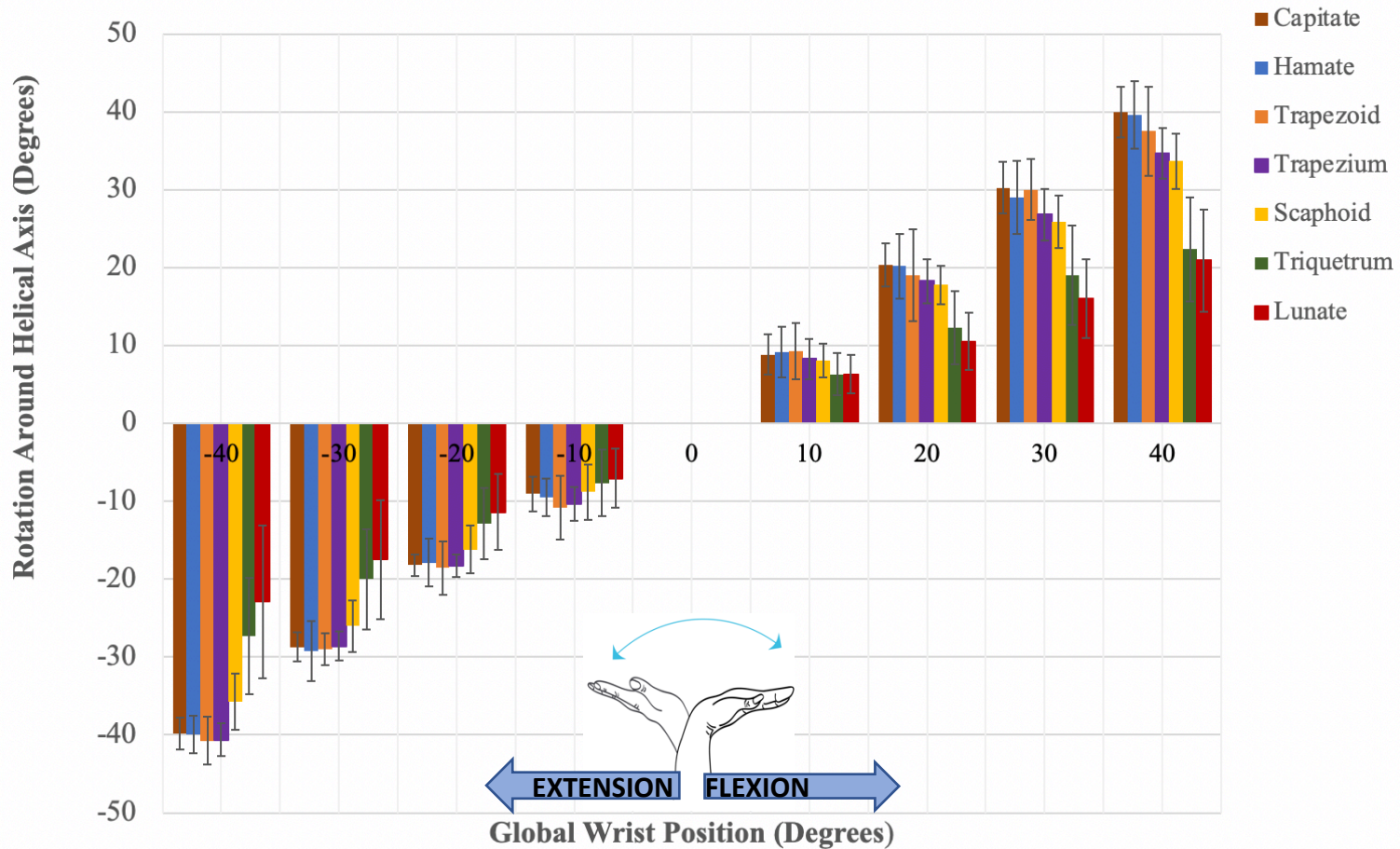


**Figure 4.1.1: Rotation of Each Carpal Bone from Wrist Extension to Flexion.** Comparison of mean sagittal rotation (degrees) by carpal bone at each position from 40 degrees of wrist extension to 40 degrees of wrist flexion (n=10). Capitate motion represents global wrist motion with negative values representing extension positioning, and positive values representing flexion positioning. Error bars depicted represent standard deviation (degrees). Three distal carpal row bones (Capitate, Hamate and Trapezoid) mirror displacement consistent with global wrist and move together at each position throughout FEM.

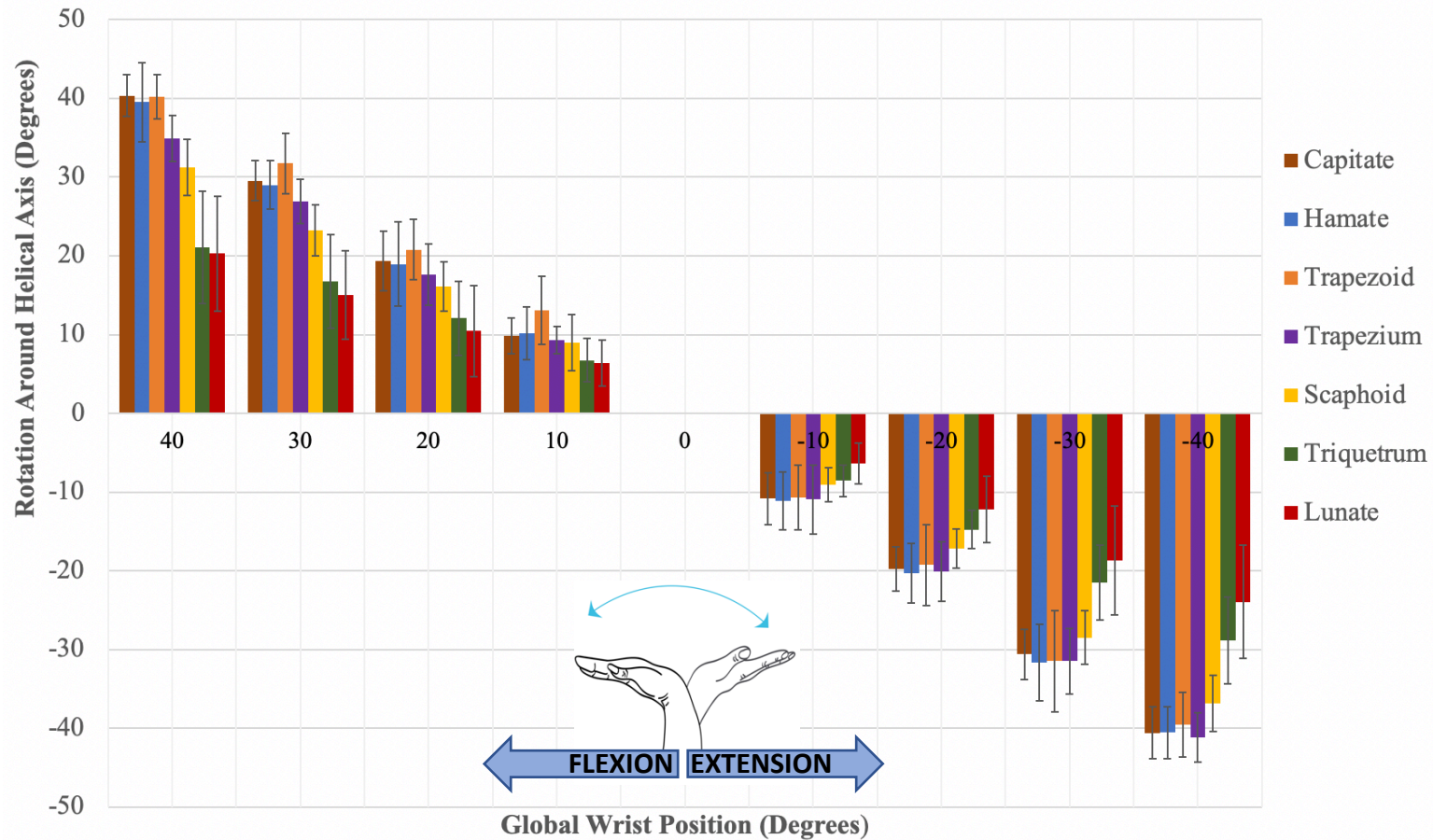


**Figure 4.1.2: Rotation of Each Carpal Bone from Flexion to Extension.** Comparison of mean sagittal rotation (degrees) by carpal bone at each position from 40 degrees of wrist flexion to 40 degrees of wrist extension (n=10). Capitate motion represents global wrist motion with negative values representing extension positioning, and positive values representing flexion positioning. Error bars depicted represent standard deviation (degrees). Bones rotate to similar degree and rate as the pass of motion from wrist extension to flexion (Figure 4.1.1).

### 4.3 Grouping of Carpal Bones by Kinematic Blocks Based on Degree of Rotation Through FEM

Sagittal rotation motion (flexion/extension) of each bone was plotted by global wrist position and compared to each other through each of the two passes (**Figures 4.2.1, 4.2.2, 4.2.3, 4.3.4**) in order to visualize rotation over motion. In the first pass from wrist extension to flexion, the capitate, hamate and trapezoid move together and contribute rotation, equivalent to global wrist motion (**Figure 4.2.1**). Mean rotation in degrees  $\pm$  SD overlapped at every position in motion and thus they were deemed to rotate together through the entire arc of motion, this is also seen in the second pass from wrist flexion to extension (**Figure 4.2.2**). Additionally, the lunate and the triquetrum move together throughout the arc of motion (**Figures 4.2.3 & 4.2.4**). The scaphoid rotates to a lesser degree than the distal carpal bones, but more than the lunate and triquetrum. The motion of the trapezium is unique throughout the full arc of motion. In extension, the trapezium moves with the bones of the distal carpal row. Interestingly, in flexion, it diverges from the distal carpal row, and appears to follow the rate of flexion seen in the scaphoid. Similarly in the second pass of motion from wrist flexion to wrist extension, it moves with the scaphoid in flexion but differs in extension where it travels with the other bones of the distal carpal row (**Figure 4.2.1, Figure 4.2.3**). The same trend is seen in the second pass of motion from wrist flexion to wrist extension (**Figure 4.2.2, Figure 4.3.4**). These plots allowed division of carpal bones into 4 main kinematic units in FEM: the distal block (capitate, hamate, trapezoid), the proximal block (lunate and triquetrum), the scaphoid block, and the trapezium block (**Figure 4.3**).

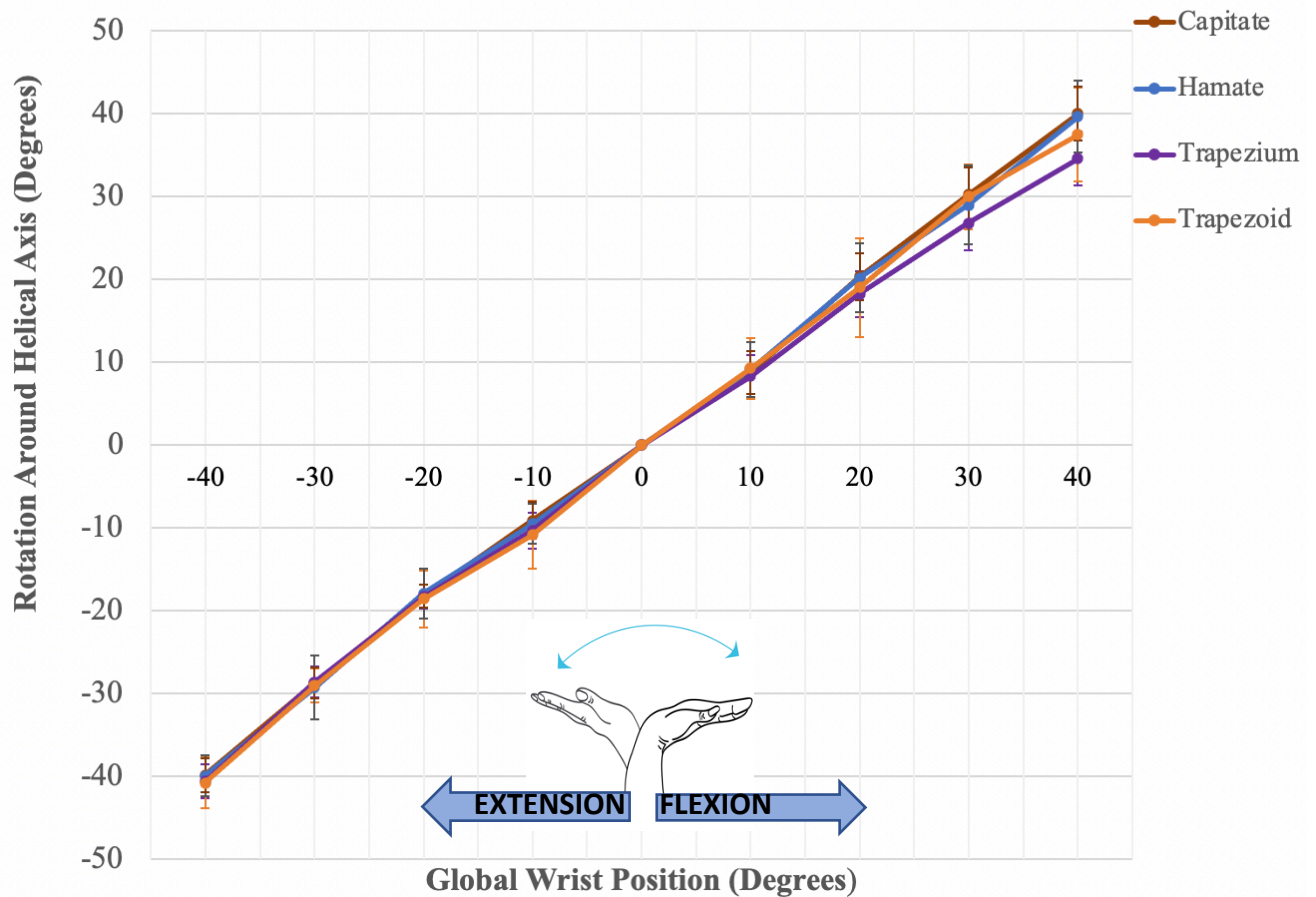


**Figure 4.2.1: Rotation of the Distal Carpal Row Bones from Wrist Extension to Flexion.** Mean sagittal rotation (flexion/extension) of the distal carpal row bones in degrees during the first pass of wrist motion is shown (n=10). Negative values represent extension positions, and positive values flexion positions. At the beginning of motion, the trapezium moves with the remainder of the distal carpal row (capitate, hamate and trapezoid). It deviates from the remainder of the row in higher degrees of flexion. Error bars represent standard deviation in degrees.

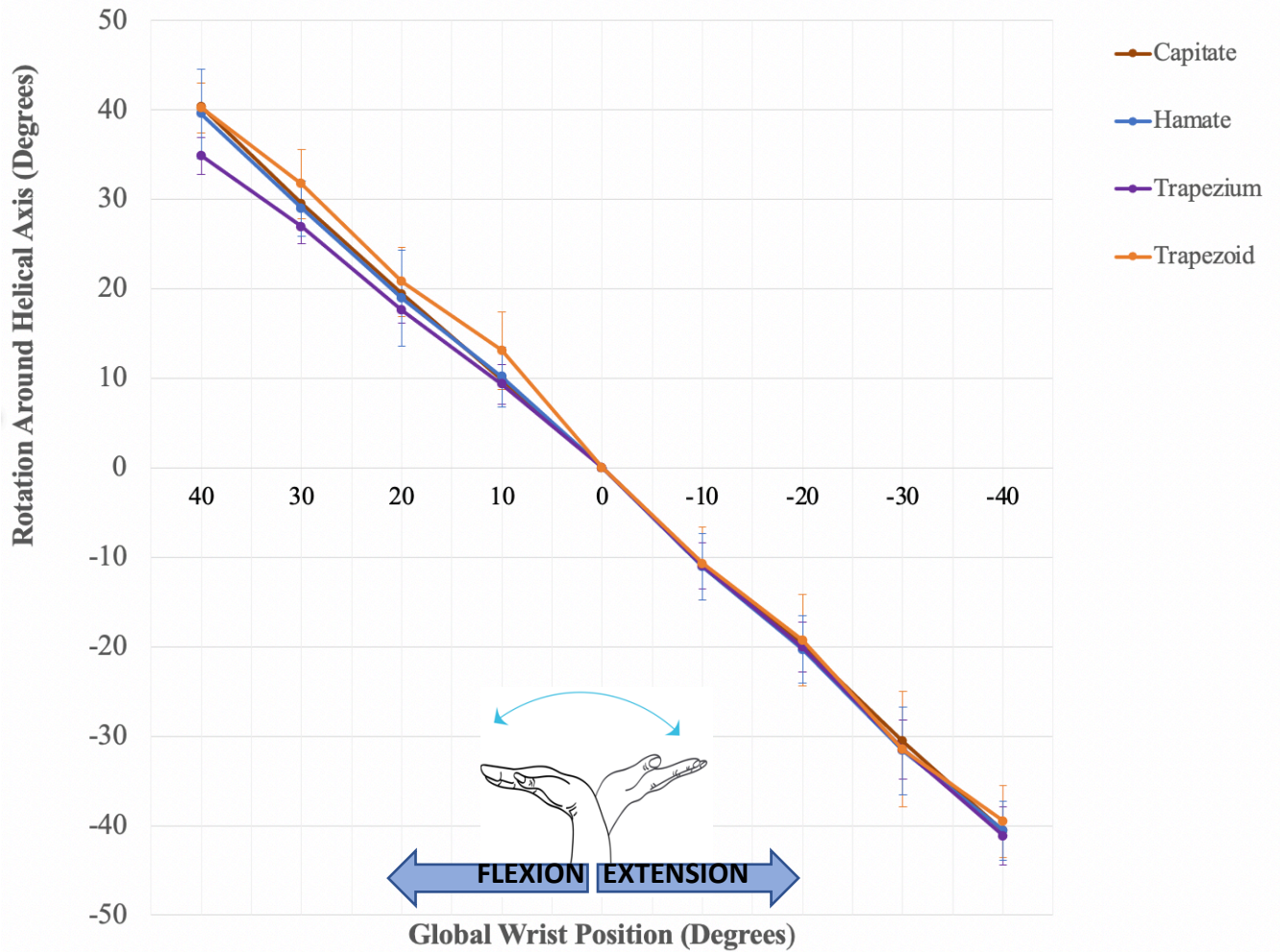


**Figure 4.2.2: Rotation of the Distal Carpal Row Bones from Wrist Flexion to Extension.** Mean sagittal rotation (flexion/extension) of the distal carpal row bones in degrees during the second pass of wrist motion is shown (n=10). Negative values represent extension positions, and positive values flexion positions. The trapezium (purple) starts at a lesser degree of flexion the remainder of the row (capitate, hamate and trapezoid). Their degree of flexion converges as the wrist moves from flexion to extension. Error bars represent standard deviation in degrees.



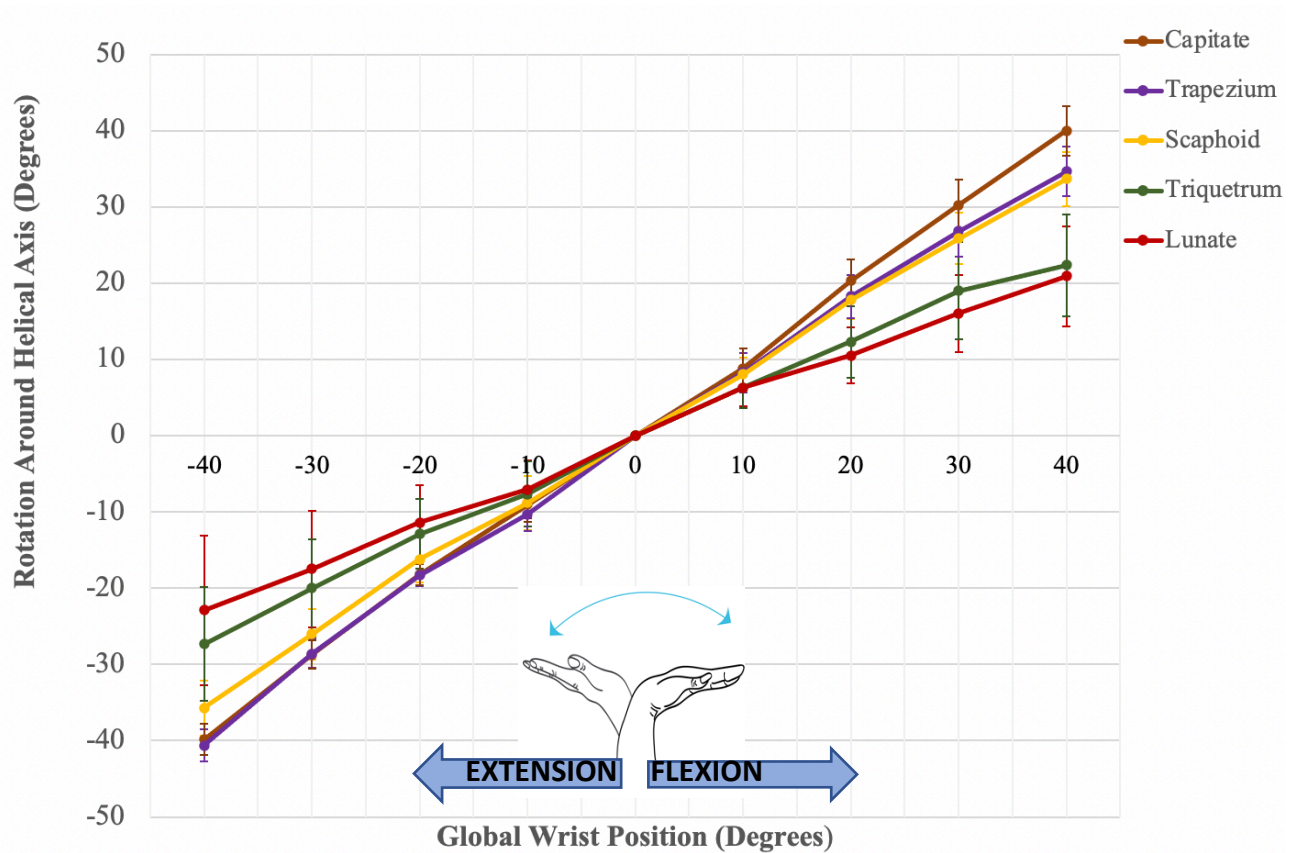


**Figure 4.2.3: Rotation of Each Carpal Bone from Wrist Extension to Flexion.** This graph depicts the mean sagittal rotation (flexion/extension) in degrees, and the rate of flexion-extension rotation of the trapezium, scaphoid, triquetrum and lunate from wrist extension to wrist flexion (n=10). Negative values represent extension positions, and positive values flexion positions. Capitate motion represents global wrist position. The trapezium (purple), follows the capitate in wrist extension and the scaphoid in wrist flexion. Error bars represent standard deviation in degrees.

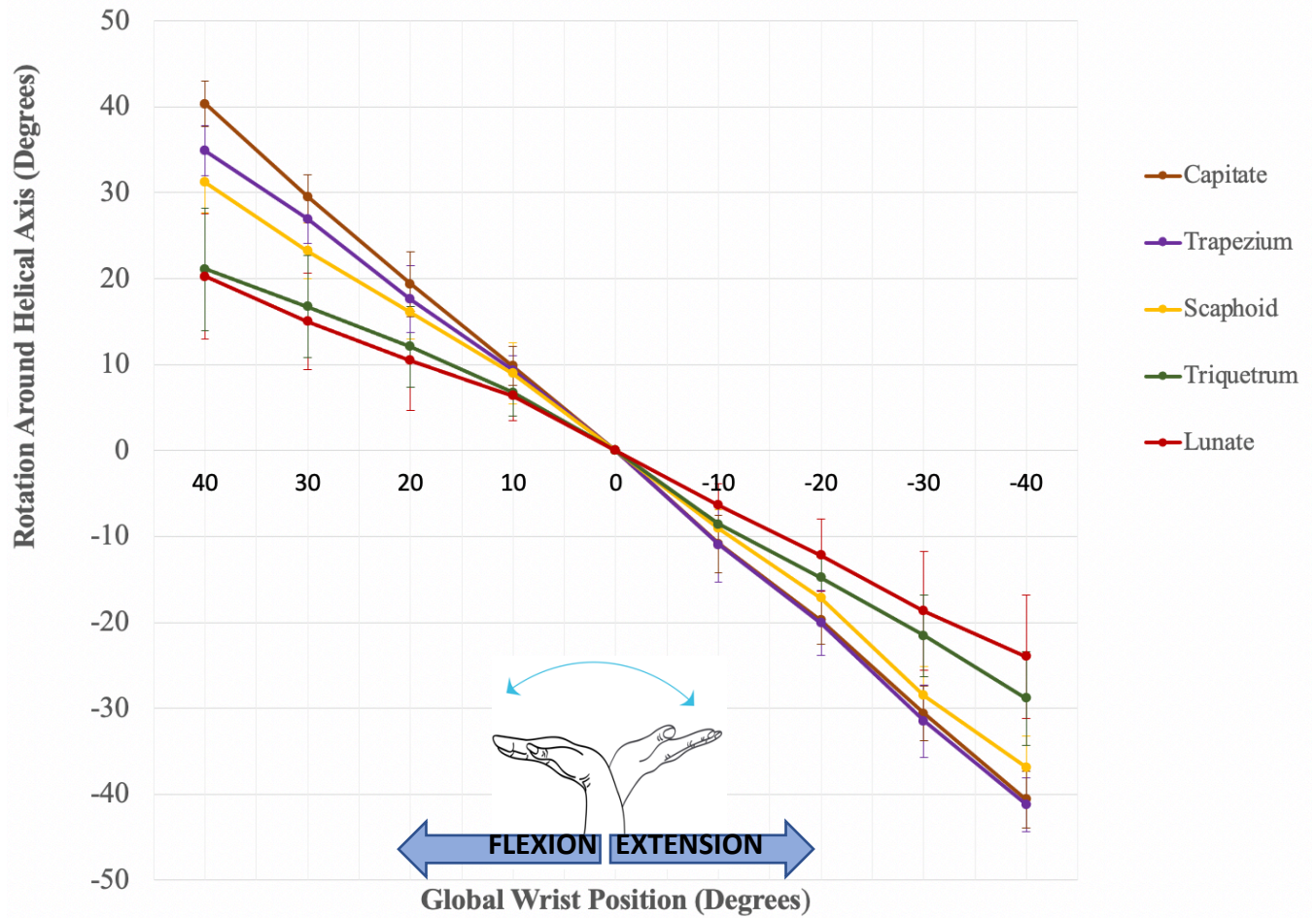


**Figure 4.2.4: Rotation of Each Carpal Bone from Wrist Flexion to Extension.** This graph depicts the mean sagittal rotation (flexion/extension) in degrees, and rate of flexion-extension rotation of the trapezium, scaphoid, triquetrum and lunate from wrist flexion to wrist extension (n=10). Negative values represent extension positions, and positive values flexion positions. Capitate motion represents global wrist position. As in the first pass of wrist motion from extension to flexion, the trapezium (purple), follows the scaphoid in flexion, and the capitate in extension. Error bars represent standard deviation in degrees.



**Figure 4.3: Division of Carpal Kinematic Blocks:** This figure depicts the distal radius and the 7 carpal bones analyzed. Carpal bones are divided into four kinematic blocks with bones within the same block displaying the same kinematics of rotation around their helical axes during FEM. The blocks are: the distal block (blue) comprised of the capitate, hamate and trapezoid, the proximal block (green) comprised of the lunate and triquetrum, the scaphoid block (red) and the trapezial block (yellow).

## 4.4 Analysis of Kinematic Blocks

Sagittal rotation (flexion/extension) of bones within each block were averaged to determine the mean rotation of each block. Mean rotation of each block for each pass is presented in detail in **Tables 4.3.1** and **4.3.2**. Repeated-measures ANOVA showed significant difference in kinematic motion between the distal block, proximal block, and scaphoid block (95% confidence interval) (**Table 4.4**). Pair-wise comparisons between blocks confirm statistically individual blocks of motion ( $p < 0.05$ ) (**Appendix 3**). Confidence intervals show the trapezial block is not statistically different than the scaphoid block or the distal block, despite the distal and scaphoid block being statistically different from each other. Kinematic motion of each block, from extension to flexion is depicted in **Figures 4.4.1, 4.4.2** and **4.4.3**.

**Table 4.3.1: Mean Sagittal Rotation in Degrees of Each Kinematic Block from Wrist Extension to Flexion (n=10).** Negative values represent rotation in extension, and positive values rotation in flexion.

Global Wrist Position in Degrees									
	40	30	20	10	0	-10	-20	-30	-40
<b>Kinematic Block</b>	Mean Flexion Around Helical Axis (Degrees) +/- SD								
Distal	-40.0 ± 2.4	-28.87 ± 2.7	-18.3 ± 2.7	-9.7 ± 2.9	0.0 ± 0.0	9.0 ± 3.2	20.1 ± 4.4	29.9 ± 3.9	39.2 ± 4.3
Proximal	-25.1 ± 8.8	-18.8 ± 6.8	-12.2 ± 4.7	-7.4 ± 3.9	0.0 ± 0.0	6.3 ± 2.5	11.4 ± 4.2	17.5 ± 5.8	21.6 ± 6.5
Scaphoid	-35.7 ± 3.6	-26.0 ± 3.3	-16.2 ± 3.1	-8.8 ± 3.5	0.0 ± 0.0	8.0 ± 2.2	17.8 ± 2.5	25.8 ± 3.4	33.7 ± 3.6
Trapezial	-40.62 ± 3.4	-28.6 ± 1.9	-18.3 ± 3.3	-10.3 ± 4.8	0.0 ± 0.0	8.3 ± 2.8	18.2 ± 3.0	26.8 ± 2.4	34.6 ± 2.9

**Table 4.3.2: Mean Sagittal Rotation in Degrees of Each Kinematic Block from Wrist Flexion to Extension (n=10).** Negative values represent rotation in extension, and positive values rotation in flexion.

Global Wrist Position in Degrees									
	40	30	20	10	0	-10	-20	-30	-40
<b>Kinematic Block</b>	Mean Flexion Around Helical Axis (Degrees) +/- SD								
Distal	39.7 ± 3.7	30.0 ± 3.3	19.9 ± 4.3	11.0 ± 3.4	0.0 ± 0.0	-10.9 ± 3.8	-19.8 ± 3.8	-31.4 ± 4.6	-40.3 ± 3.3
Proximal	20.7 ± 7.0	15.9 ± 5.7	11.3 ± 5.2	6.6 ± 2.8	0.0 ± 0.0	-7.5 ± 2.5	-13.5 ± 3.6	-20.1 ± 6.0	-26.4 ± 6.7
Scaphoid	31.2 ± 5.4	23.2 ± 2.9	16.1 ± 4.3	9.0 ± 2.9	0.0 ± 0.0	-9.1 ± 2.8	-17.2 ± 4.1	-28.5 ± 4.0	-36.8 ± 2.8
Trapezial	34.9 ± 2.9	26.9 ± 2.8	17.6 ± 3.9	9.33 ± 1.7	0.0 ± 0.0	-11.0 ± 4.4	-20.1 ± 3.8	-31.5 ± 4.2	-41.2 ± 3.1

**Table 4.4: Repeated-Measures ANOVA for Differences in Mean Rotation (Degrees) Between Kinematic Blocks.** Statistical analysis of difference between mean motion of each kinematic block reveals three main distinct blocks (distal, proximal and scaphoid). All values shown are in degrees. The trapezium block is statistically similar to the distal and scaphoid blocks ( $p < 0.05$ ), with overlapping confidence intervals, despite those blocks being significantly different from each other. This is seen in both passes of motion.

<b>Kinematic Block</b>	<b>Mean</b>	<b>Standard Error</b>	<b>95% Confidence Interval</b>
<b>Pass 1</b>			
Distal	21.7	0.3	21.0 – 22.3
Proximal	13.4	0.4	12.6 – 14.2
Scaphoid	19.5	0.6	18.3 – 20.6
Trapezium	20.8	0.6	19.6 – 21.9
<b>Pass 2</b>			
Distal	22.616	0.366	21.9 – 23.4
Proximal	13.844	0.436	13.0 – 14.7
Scaphoid	19.039	0.634	17.8 – 20.3
Trapezium	21.114	0.776	19.6 – 22.7

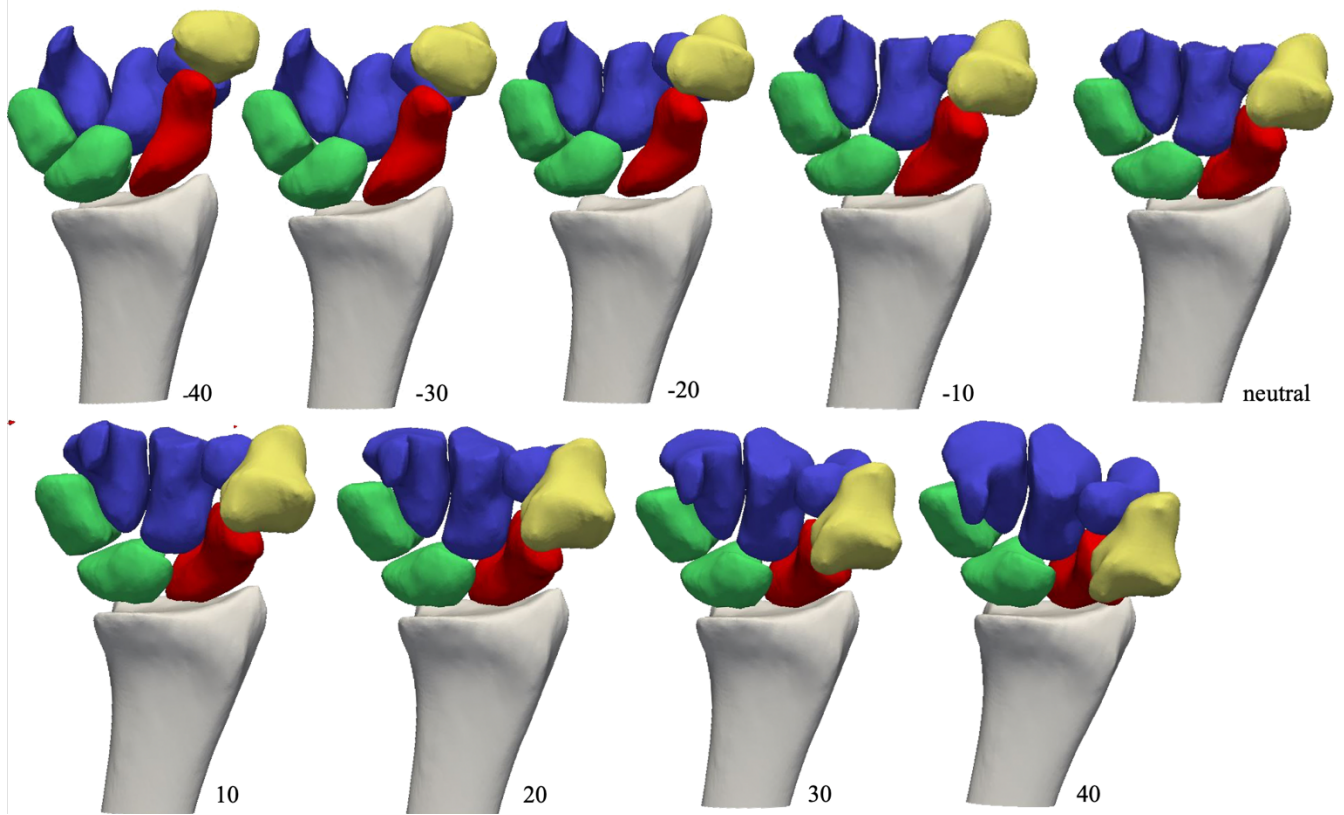


**Figure 4.4.1: Coronal Visualization of Kinematic Blocks During FEM.** 3D reconstruction of carpal motion during FEM from 40 degrees of extension to 40 degrees of flexion is shown for a single representative participant. The carpus is divided by kinematic blocks including the distal block (blue), proximal block (green), scaphoid block (red), and trapezial block (yellow).



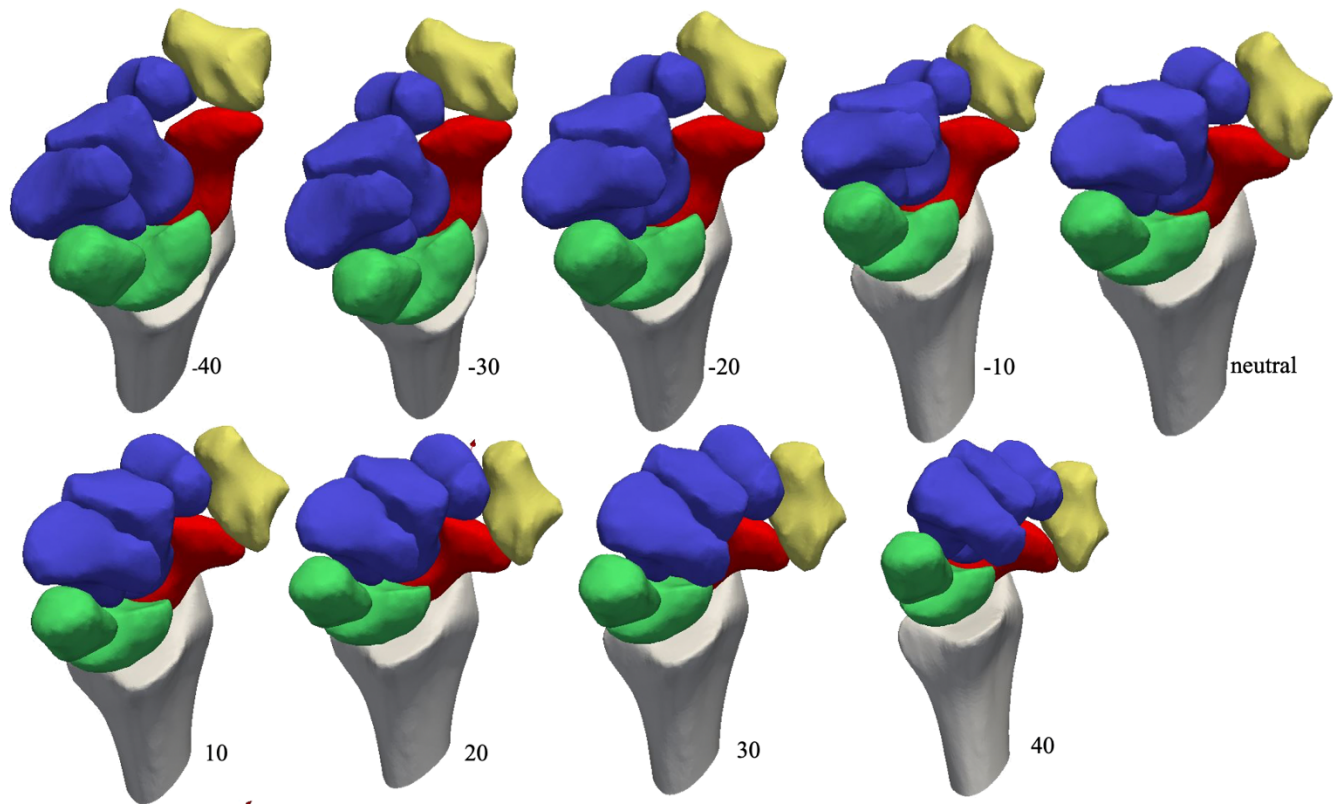


**Figure 4.4.2: Superior-Oblique Visualization of Kinematic Blocks During FEM.** 3D reconstruction of carpal motion during FEM from 40 degrees of extension to 40 degrees of flexion is shown for a single representative participant. The carpus is divided by kinematic blocks including the distal block (blue), proximal block (green), scaphoid block (red), and trapezial block (yellow).



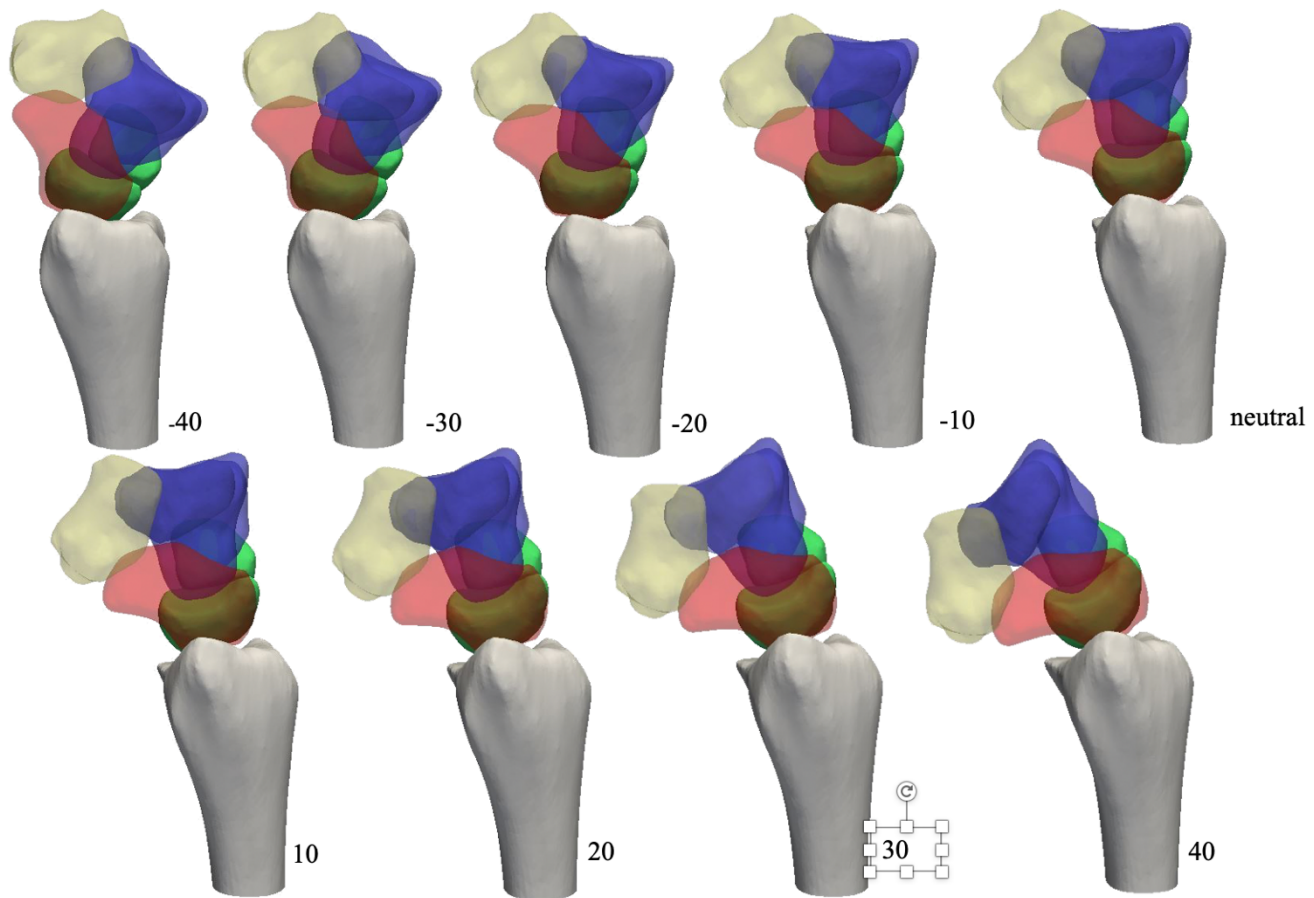


**Figure 4.4.3: Coronal Visualization of Kinematic Blocks During FEM.** 3D reconstruction of carpal motion during FEM from 40 degrees of extension to 40 degrees of flexion is shown for a single representative participant. The carpus is divided by kinematic blocks including the distal block (blue), proximal block (green), scaphoid block (red), and trapezial block (yellow).

## 4.5 Joint Distances Around the Trapezial Block

Statistical analysis showed differential motion of the trapezial block, which followed the distal block in extension and the scaphoid block in flexion. To better understand the kinematic motion around the trapezium, colour maps of inter-joint distances between adjacent articulating bones were created using the surface reconstructions of the bones. The area of contact between the trapezium and trapezoid is relatively stable through a single pass of motion, with minimal increase or decrease in contact distance. This shows there is no distraction or compression in the joint. The area of contact does translate slightly on the trapezoid, showing there is differential rotation between the two bones (**Figure 4.5.1**). The same analysis at the scaphotrapezial joint shows a progressive decrease in inter-joint distance with progressive wrist flexion, as the trapezium moves closer to the scaphoid (**Figure 4.5.2**). The contact proximity increases more volarly at the articulation, indicating flexion at the joint as the wrist moves into flexion.

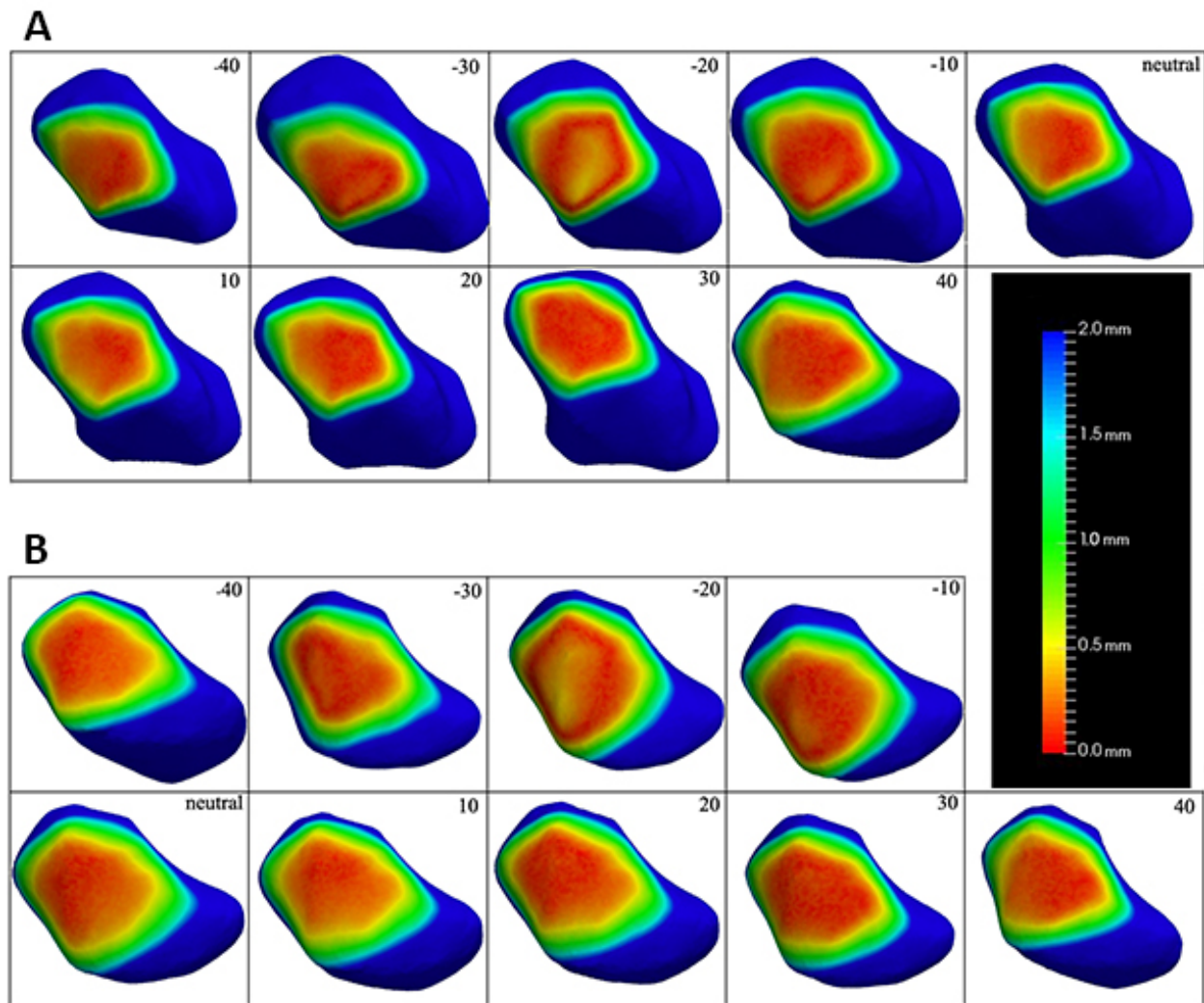


**Figure 4.5.1: Inter-Joint Distance at the Trapeziotrapezoid Joint Through FEM.** Colour maps display distance (mm) between bones at the trapeziotrapezoid joint in a single pass FEM motion from 40 degrees of wrist extension to 40 degrees of wrist flexion. These maps are generated from a single representative participant. Both sides of the joint are shown including the trapezoid facet of the trapezium (A), and the trapezoidal facet of the trapezoid (B). Values in each box represent wrist position, with negative values representing extension positions and positive values representing flexion positions. Inter-joint distance remains relatively consistent throughout the entire arc of motion showing only rotational motion between the bones. Movement in the area of contact between the two bones throughout motion, confirm subtle, but differential rotation.

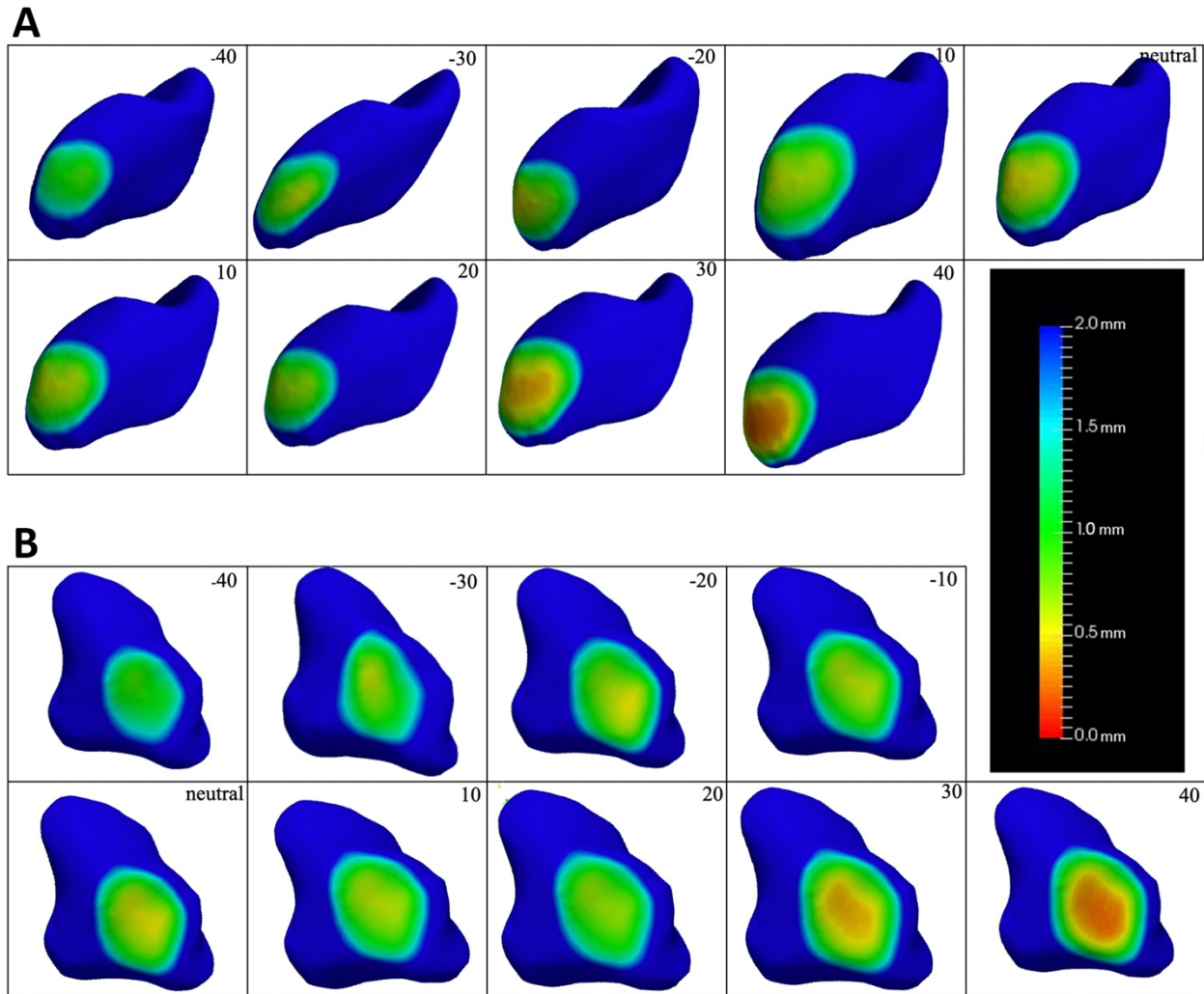


**Figure 4.5.1: Inter-Joint Distance at the Scaphotrapezium Joint Through FEM.** Colour maps display distance (mm) between bones at the scaphotrapezium joint in a single pass FEM motion from 40 degrees of wrist extension to 40 degrees of wrist flexion. These maps are generated from a single representative participant. Both sides of the joint are shown including the distal articulating facet of the scaphoid (A), and the scaphoid facet on the trapezium (B). Values in each box represent wrist position, with negative values representing extension positions and positive values representing flexion positions. Inter-joint distance progressively decreases between the two bones as the wrist is brought from extension to flexion. This is seen more volarly at the scaphoid articulation (B) representing flexion between the two bones.

# Chapter 5

## **5 General Discussion & Conclusions**

*In this final chapter, we will review the objectives and hypothesis of this study and summarize our results. A comparison to current carpal kinematic understanding in the literature is set forth, and conclusions of this work are presented. Strengths, weaknesses and implications of this work are discussed in addition to future directions of study.*

## 5.1 Overview and Discussion of Results

The primary objectives of this work were to:

- a) Quantify the degree and direction of sagittal rotation of each carpal bone during Flexion-Extension Motion (FEM) by using helical axes data.
- b) Identifying bones which move together and can be grouped into a single kinematic body and defined as “blocks”.
- c) Quantify degree of motion between blocks during FEM by using helical axes data.

Within our study, we were able to quantify wrist kinematics for the entirety of the carpus during FEM and identify functional kinematic blocks. Firstly, we were able to quantify the degree and direction of flexion-extension motion during FEM using helical axis data. Our data was consistent with previous data regarding flexion movement of the carpal bones. As the wrist flexed, each bone flexed, and as the wrist extended, each bone extended. The hamate, capitate and trapezoid were each found on average to flex approximately 100% of the Global Composite Flexion Angle (GCFA) when compared at each wrist position.. As the capitate was the marker for measurement of the GCFA its flexion angle was used to calculate the GFCFA at each position as highlighted in **Section 3.2.1 (Figure 3.1)**, and constituted 100% of GFCFA (SD = 2.4°). The hamate flexed 99% (SD = 3.4°), and the trapezoid 102% (SD = 3.7°). Studies have shown that there is minimal motion between the capitate and the 3<sup>rd</sup> metacarpal (3MC), allowing the capitate to be used a surrogate for GCFA<sup>61</sup>. We found that the lunate flexed on average 63% (SD = 4.9°) the amount of the capitate, higher than observed in previous studies that reported a range from 45 to 70 percent<sup>17,31,33</sup>. These studies found a greater amount of lunate rotation in extension (65% of GCFA) and a lesser degree of lunate rotation in flexion (45% of GCFA)<sup>17</sup>. We did note a similar trend with flexion angles being slightly lower in the lunate, but it was within the range of standard error (**Tables 4.2.1 & 4.2.2**). Similarly, the scaphoid was found to rotate 87% (SD = 2.8°) of GCFA, which has also been cited in the current body of literature between 70-100%<sup>26,31</sup>. It has been highlighted that the scaphoid has variable kinematic motion between individuals<sup>18,25</sup>. Our findings did not see this variability between participants, with a mean SD of 2.79°. This is likely due to the fact that scaphoid variability was largely noted in radioulnar deviation (RUD) motions, and this study

looked exclusively at FEM in which scaphoid motion has been shown in the literature to be more predictable<sup>18,26</sup>.

Our findings differ from the literature to date in regards to the separation of the trapezium from the distal carpal row. Previously it has been thought that the trapezium is a rigid body with the hamate, capitate and trapezoid in the distal carpal row<sup>17,62,63</sup>. In full flexion, the trapezium on average flexed 95% (SD = 2.85°) of the GCFA, which suggests some modulation effect from the dorsal scaphotrapeziotrapezoid (STT), ligaments and differential motion between the trapezium and the trapezoid in flexion. In extension, we found that the trapezium had the same degree of rotation as the remainder of the distal carpal row, implying some degree of increased laxity of the volar STT ligaments compared to the dorsal side. Although subtle, motion was present between the trapezoid and trapezium during FEM. This motion was found to be entirely rotational with no observable change in the inter-joint distance through the complete arc of motion (**Figure 4.5.1**). The separation of the trapezial block from the distal carpal row may also be related to the independent mobility of the 1<sup>st</sup> ray and thumb compared to the adjacent rays regardless of the position of the wrist. For example, even in a flexed grip position, the thumb and 1<sup>st</sup> metacarpal are able to flex and extend and independently posture from the remainder of the metacarpals, which may not be exclusively derived from the 1<sup>st</sup> carpometacarpal (CMC) joint. Clinically the differential motion of the trapezial block supports selective fusion of not only the scaphotrapezoid and scaphotrapezial joints in isolated STT joint arthritis, but also fusion of the trapeziotrapezoid (TT) joint as we've demonstrated subtle but significant differential motion at that joint. Failure to address all three articulations may result in residual pain following STT fusion surgery.

Based on our analysis of which bones moved as a unit through FEM, we were able to divide the carpus into 4 distinct blocks: distal, proximal, scaphoid and trapezial (**Figure 4.3, Table 4.4**). Each of the distal (trapezoid, capitate, hamate), proximal (lunate, triquetrum) and scaphoid blocks were found to be statistically different from each other, with non-overlapping confidence intervals (**Table 4.4**). Degrees of motion of each of the blocks were quantified and can be reviewed in **Tables 4.3.1 & 4.3.2**. The trapezial block was distinct as it was influenced by both the distal carpal block as well as the scaphoid block. Its confidence interval overlapped with both the scaphoid and the distal blocks, but the scaphoid and distal blocks remain distinct from each other with non-overlapping confidence intervals (**Table 4.4**). This also supports the paring of a 3-corner fusion,

with scaphoidectomy and triquetrectomy, in order to fuse moving articulations, and remove the triquetrohamate (TH) articulation. Short and mid-term results of a scaphoidectomy and bicolumnar fusion and 3-corner fusion with scaphoidectomy and triquetrectomy have been similar<sup>64,65</sup>. Our data suggests this is likely because both address all movement between kinematic blocks via either excision or fusion.

Our secondary objective was to compare our kinematic findings to currently accepted theories of carpal kinematics, to offer support or rebut these theories. We were able to partition the carpus into kinematic blocks with articulations between blocks being the primary sites of motion through FEM. The prevalent theories of carpal kinematics may be reviewed in **Section 1.2.1**. Our findings are not consistent with the column theory as our kinematic blocks do not follow a column-like pattern that suggests motion between the capitate and trapezoid as well as a distinct triquetral block<sup>5,7,9</sup>. Additionally, our findings contradict the row theory as our results demonstrate differential motion between the trapezium and the remainder of the distal carpal row. The oval ring theory states the two main mobile articulations in the wrist to be at the TH and the STT joints<sup>13</sup>. Our findings suggest that there are additional mobile articulations between the SL joint and TT joints. The oval ring theory also fails to address the independent motion between the scaphoid which has been repeatedly observed in previous studies<sup>18,24,26</sup>, as well as our own. The column, row and oval ring theories may be oversimplified theories for the more nuanced and complex realities of carpal motion.

Garcia-Elias' theory of balanced forces applied to the lunate proposed the idea of a variety of intrinsic forces being applied to the central lunate with the tendency for a specific bone to flex or extend based on bone morphology. The tendency for the lunate to extend with load due to its lower curvature dorsally compared to volarly is balanced by forces imparted by the adjacent scaphoid and triquetrum through ligamentous connections. We did observe more mobility between the bones of the proximal carpal row than the distal carpal row in terms of movement between the scaphoid and the lunate, and to a lesser degree between the triquetrum and the lunate, which were not found to be statistically significant in our study. Additionally, we observed a lesser range of motion arc of the proximal carpal block compared to the other blocks, implying more restraint from the radiocarpal ligaments across the radiocarpal joint, compared to the more lax ligamentous attachments allowing continuation of flexion and extension through the midcarpal joint.



Our study would support the idea of the lunate as part of the proximal block articulating with a distal carpal block and a scaphoid block as well as the radiocarpal joint. There is less variation between the lunate and triquetrum flexion in FEM which infers a tightly bound ligamentous stabilizers between the two causing them to move as a single kinematic unit through FEM. We are unable to fully corroborate the effect each block has on the lunate, which would require scanning in patients with injury to the stabilizing structures and comparing how those mechanics differ from what is observed in this study. Although our study differs from the descriptions of Garcia-Elias' original theory in that we see a separate trapezoidal block vs a tightly bound distal row, the trapezium does not articulate with the lunate or the proximal carpal block. This suggests some balanced motion between the scaphoid, first ray, and the distal carpal row in addition to forces imparted on the lunate.

Lastly, our findings share many similarities to Sandow's central column theory. Sandow et al. suggest a "2-gear, 4-bar linkage" system with articulations between the lunate and the capitate, the lunate and the scaphoid, and the scaphoid and the trapezoid and trapezium<sup>16</sup> (**Figure 1.21**). They also depict a stable central column with independent movement of the thenar and hypothenar rays. These articulations are generally consistent with the allocation of our carpal blocks. The main difference is that the central column theory groups the trapezium with the distal carpal row and found minimal motion between the two. It also partitions the lunate from the triquetrum. The central column theory appropriately, but simply captures the complexity in interactions between multiple kinematic blocks in the carpus during motion. It is important to note that Sandow's study looked at purely *in-vivo* radioulnar deviation (RUD) motion in the wrist using static 3-dimensional CT and marker-less bone registration. This may be the reason that they saw greater differential motion between the lunate and the triquetrum, and less differential motion between the trapezium and the distal carpal row than we observed in our study restricted to FEM. It also highlights the importance of analyzing carpal kinematics in all motion planes prior to confirming a comprehensive and uniting theory.

## 5.2 Strengths and Limitations

There are multiple strengths to our analysis. First and foremost, this is the first study to our knowledge to characterize in-vivo carpal kinematics in the entire carpus using four-dimensional computerized tomography (4DCT) scanning. Several studies to date have characterized the kinematics of the scaphoid, lunate and capitate using this technique, but not the entire carpus. By characterizing all seven bones, we were able to get a complete picture of motion of each bone and group according to kinematic motion. 4DCT protocols have been shown to be highly accurate with an average of approximately 0.5mm translational error and 0.5° rotational error using the same technique<sup>22,32,42</sup>. This accuracy allows capture of the small and subtle motion changes at each carpal articulation. This study is also *in-vivo* with data acquired during dynamic motion opposed to multiple static scans. This captures the dynamic forces and stabilization imparted by muscles, as well as the constraining effects of ligaments throughout motion. This more closely represents forces acting upon the carpus in clinical scenarios. Finally, participants were radiographically and clinically confirmed to have no evidence of previous injury or arthritis prior to analysis, which decreases the possibility of confounding pathology.

Our investigation also has limitations. Firstly, range of motion analysis was limited to FEM. We looked specifically at a motion arc between 40 degrees of wrist extension to 40° motion, despite the ability for many individuals to achieve greater range. We chose to focus on functional mid-range of FEM to allow a standard, achievable range of motion between participants, and decrease the chance of individual variability. Next, the motion was unconstrained, and therefore there was no control for out of plane motion generated by each participant. Analysis of unconstrained motion has the benefit of being more physiologic, but can introduce variability between participants. In addition, FEM motion analyzed in this study was unloaded which does not take into account the effect of load on carpal kinematics. These loads are commonly imparted with day-to-day tasks including tool use, as well as lifting, pushing, pulling and carrying actions of the hand and wrist. The rate of motion our participants were guided to complete their motion arc at was approximately 22°/sec. This again is artificial, and was chosen to decrease blurring artifact in our scans. Vocational tasks have been shown to be performed on average at a higher speed of approximately 30°/second for the dominant hand<sup>66</sup>.

This study also did not take into account variation in patient morphology or ligamentous laxity, which has been shown to have some influence on variability of individual carpal kinematics<sup>5,17,25,67</sup>, although again, this has largely been seen in RUD motion opposed to more consistent FEM kinematics. Further protocols with inclusion of RUD should identify participants with clinical hyperlaxity in an attempt to correlate its effects. Carpal bone morphology was not delineated due to the small sample size and gross variability in morphology that can be seen across individuals<sup>68</sup>. Variation in lunate morphology has been shown to affect translation kinematics of the scaphoid during RUD, but it has not been shown in FEM<sup>67</sup>.

Regarding our sample size, we had a small sample of 10 participants. We were powered sufficiently to capture differences in motion between bones as found in our results. A higher sample size would serve to decrease the effect of unidentified bias and variability between participants. Finally, we used convenience sampling via volunteer recruitment. Of patients meeting inclusion criteria, younger patients selected for analysis in order to decrease the probability of concurrent unidentified carpal pathology or subtle arthritic changes. The convenience sampling and narrow demographic range of the participants decreases the overall generalizability of the results.

## 5.3 Current and Future Directions

This current work opens the door for further applications of 4DCT in the study of carpal kinematics. We are compelled to complete our kinematic analysis by investigating both RUD and DTM to add to the findings of this study. Currently, our group has shown kinematics of the scaphoid and lunate through RUD using the same protocol showing translation consistent with previous literature of both bones<sup>46</sup>. Regarding DTM, Edirisinghe et al. used changes in distance between surface points of each carpal bone analyzed, to delineate an axis of rotation of during unrestricted DTM<sup>27</sup>. They found this axis to be  $-27^\circ$  anteverted and 44 degrees varus angulation, with the majority of movement through the midcarpal joint, and some variability noted between patients<sup>27</sup>. Expansion to include the carpus in its entirety would allow kinematic characterization in all planes and a complete picture of interactions at each articulation of interest. The effects of carpal bone size and ligamentous laxity and possibly sex may be better delineated with increased sample sizes and a comprehensive study of all wrist motions.

It would also be of value to investigate the effect of 1<sup>st</sup> ray and thumb motion on the trapezial block and conversely, the effect of wrist position on 1<sup>st</sup> ray motion. This has clinical implications on thumb movement after procedures such as trapeziectomy and ligament reconstruction and tendon interposition (LRTI), and STT fusions commonly performed for peritrapezial arthritis. Dedicated study on the mechanics of the 1<sup>st</sup> ray and radial column of the wrist are required.

With the establishment of baseline normal range of carpal kinematics, future work can analyze pathologic scenarios. This would include alterations to kinematic function post injury or in the setting of degenerative changes. These studies could identify discrepancies from normal kinematics associated with common traumatic pathologies such as scaphoid fracture, scaphoid malunion, distal radius fracture, intercarpal ligament injury (scapholunate ligament, lunotriquetral ligament) and common degenerative wrist pathology such as scapholunate advanced collapse (SLAC), and scaphoid nonunion advanced collapse (SNAC) wrist. Some work has been done diagnostically to date in this regard. For example, Dehemri et al., showed a mild to moderate correlation between increased SL intervals and symptoms in patients with suspected SL ligament injury<sup>69</sup> Meanwhile, a small study by Troupis and Amis<sup>38</sup> showed kinematics in patients with trigger lunate, and similarly work has been done looking at altered kinematics in both midcarpal

instability<sup>39</sup> and pisotriquetral instability<sup>70</sup>. These were performed in a diagnostic sense, in patients with clinical symptoms, but normal static and loaded radiographs, as well as normal MRI. These studies not only have diagnostic value, but also provide potential anatomic targets and benchmarks for intervention.

This work has implications beyond diagnosis. It lays the foundation to be able to assess if interventions are able to restore normal kinematic motion, and if so, whether restoration of normal kinematics correlates to improved clinical outcomes. Additionally, the effects of specific surgical interventions, including partial wrist fusions, on the alteration of carpal kinematics can be characterized. The benefit to the non-invasive, *in-vivo* characteristics of the 4DCT modality in the study of wrist kinematics, is that participants can be studied both pre- and post-intervention, providing insight if restoration of normal kinematics can be achieved and what effect it has on the clinical function and outcomes for the patient. To date, we identified one study which used 4DCT to compare kinematics pre and post SL ligament repair, showing a persistence of diastasis between the scaphoid and lunate post repair, with no evidence of dynamic instability<sup>40</sup>. They did find initiation of flexion to be at the radiocarpal joint in patients post-repair, opposed to at the midcarpal joint in normal patients. Ideally, future surgical implants, repair and reconstruction techniques would be tailored to optimize restoration of normal kinematics. Future studies can help confirm the clinical effect.

## 5.4 Significance and Conclusion

A detailed understanding of carpal kinematics is vital to being able to identify pathology and help identify targets to optimize treatment. Despite many decades of study into carpal kinematics, we have yet to come to a consensus regarding how the carpal bones move with wrist motion due to challenges in kinematic study in this anatomic region. Highly accurate, non-invasive, *in-vivo* study with 4DCT scan technology allows the most representative study of carpal kinematics through live functional motion to date, and mitigates the challenges of previous forms of low-resolution, static and invasive study. This study serves to delineate the kinematic motion of the entire carpus through FEM, and offers a baseline “normal” motion pattern to which pathologic states can be compared for diagnostic purposes, and interventions can be benchmarked against.

We conclude that through FEM, the carpal bones move as four separate kinematic bodies that can be organized into blocks. These include a distal, proximal, scaphoid and trapezoidal block. We also show that the trapezium is not rigidly associated with the remainder of the distal carpal row, but the implications of its subtle independent mobility compared to the distal carpal row is still not completely understood. Our findings suggest that the previously suggested row, column and oval-ring theories are incomplete models of carpal kinematics, and the most recently proposed central column theory most consistently agrees with our findings. Further 4DCT analysis is required in RUD and DTM before we are able to comprehensively define baseline carpal kinematics. This is required before we can confirm or debunk any theory in its entirety or determine if a cohesive description of carpal kinematics truly exists. Kinematics in the wrist may be extremely individualized. Specific patterns of kinematics could display varying prevalence depending on several patient factors, and likely exists as a spectrum of normal. Regardless, this work lays the foundation for characterizing *in-vivo* FEM kinematics on the way to comprehensive characterization of carpal motion in all planes. It progresses our understanding of wrist mechanics and links to future study of the clinical implications of pathological deviation from baseline kinematics, and whether restoration of that baseline can serve to optimize clinical outcomes following intervention.

## References

1. Hirt B, Seyhan H, Wagner M, Zumhasch R. *Hand and Wrist Anatomy and Biomechanics: A Comprehensive Guide*. Thieme Publishers Struttgart; 2017.
2. Lam KS, Woodbridge S, Burke FD. Wrist function after excision of the pisiform. *J Hand Surg Eur Vol*. 2003;28(1)(B):69-72.
3. Standring S, ed. *Gray's Anatomy*. Churchill Livingstone Elsevier; 2008.
4. Feipel V, Rooze M. The capsular ligaments of the wrist: morphology, mophometry and clinical applications. *Surg Radiol Anat*. 1999;21:175-180.
5. Rainbow MJ, Wolff AL, Crisco JJ, Wolfe SW. Functional kinematics of the wrist. *J Hand Surg Eur Vol*. Jan 2016;41(1):7-21. doi:10.1177/1753193415616939
6. Shin AY, Battaglia MJ, Bishop AT. Lunotriquetral instability: diagnosis and treatment. *J Am Acad Orthop Surg*. 2000;8(3):170-179.
7. Rohde RS, Crisco JJ, Wolfe SW. The advantage of throwing the first stone how understanding the evolutionary demands of homo sapiens is helping us understand carpal motion. *J Am Acad Orthop Surg*. 2010;18(1):51-58.
8. Bryce TH. Certain points in the anatomy and mechanism of the wrist-joint reviewed in the light of a series of rontgen ray photographs of the living hand. *J Anat Physiol*. 1986;31:59-79.
9. Navarro A. Luxaciones del carpo. *Alanes De La Facultad De Medicina*. 1921;6:113-141.
10. Kauer JMG, Savelberg HHCM, Huiskes R, Kooloos JGM. Role of the wrist ligaments with respect to carpal kinematics adn carpal mechanisms. *NATO ASI Series: Series A: Life Sciences*. 1994;256:271-280.
11. Destot E. Injuries of the wrist: a radiological study. *Clin Orthop Relat Res*. 1926;202:3-8. New York, Paul B. Hoeber. English translation by F.R.B. Atkinson.
12. Linscheid MD. Kinematic considerations of the wrist. *Clin Orthop Relat Res*. 1985;202:27-39.
13. Lichtman DM, Schneider JR, Swafford AR, Mack GR. Ulnar midcarpal instability—Clinical and laboratory analysis. *The Journal of Hand Surgery*. 1981;6(5):515-523. doi:10.1016/s0363-5023(81)80115-3
14. Garcia-Elias M. Kinetic analysis of carpal stability during grip. *Hand Clinics*. 1997;13(1):151-158.
15. Garcia-Elias M. The treatment of wrist instability. *J Bone Joint Surg Am*. 1997;79-B(4):684-690.
16. Sandow MJ, Fisher TJ, Howard CQ, Papas S. Unifying model of carpal mechanics based on computationally derived isometric constraints and rules-based motion - the stable central column theory. *J Hand Surg Eur Vol*. May 2014;39(4):353-63. doi:10.1177/1753193413505407

17. Kamal RN, Starr A, Akelman E. Carpal Kinematics and Kinetics. *J Hand Surg Am.* Oct 2016;41(10):1011-1018. doi:10.1016/j.jhsa.2016.07.105
18. Moojen TM, Snel JG, Ritt MJ, Venema HW, Kauer JM, Bos KE. Scaphoid kinematics in vivo. *J Hand Surg Am.* Nov 2002;27(6):1003-10. doi:10.1053/jhsu.2002.36519
19. Wolfe SW, Crisco JJ, Orr CM, Marzke MW. The dart-throwing motion of the wrist: is it unique to humans? *J Hand Surg Am.* Nov 2006;31(9):1429-37. doi:10.1016/j.jhsa.2006.08.010
20. Kamal RN, Rainbow MJ, Akelman E, Crisco JJ. In vivo triquetrum-hamate kinematics through a simulated hammering task wrist motion. *J Bone Joint Surg Am.* Jun 20 2012;94(12):e85. doi:10.2106/JBJS.J.01644
21. Crisco JJ, McGovern RD, Wolfe SW. Noninvasive technique for measuring in vivo three-dimensional carpal bone kinematics. *J Orthop Res.* 1999;17(1):96-100.
22. Dobbe JGG, de Roo MGA, Visschers JC, Strackee SD, Streekstra GJ. Evaluation of a Quantitative Method for Carpal Motion Analysis Using Clinical 3-D and 4-D CT Protocols. *IEEE Trans Med Imaging.* Apr 2019;38(4):1048-1057. doi:10.1109/TMI.2018.2877503
23. Feipel V, Rooze M. Three-dimensional motion patterns of the carpal bones - an in vivo study using three-dimensional computed tomography and clinical applications. *Surg Radiol Anat.* 1999;21(2):125-131.
24. Cragen MAC, Stanley JK. Wrist kinematics: row, column or both? *J Hand Surg Br.* 1995;20(2):165-170.
25. Garcia-Elias M, Ribe M, Rodriguez J, Cots M, Casas J. Influence of joint laxity on scaphoid kinematics. *J Hand Surg Eur Vol.* 1995;20(3)(B):379-382.
26. Wolfe SW, Neu C, Crisco JJ. In vivo scaphoid, lunate, and capitate kinematics in flexion and in extension. *J Hand Surg Am.* Sep 2000;25(5):860-9. doi:10.1053/jhsu.2000.9423
27. Edirisinghe Y, Troupis JM, Patel M, Smith J, Crossett M. Dynamic motion analysis of dart throwers motion visualized through computerized tomography and calculation of the axis of rotation. *J Hand Surg Eur Vol.* May 2014;39(4):364-72. doi:10.1177/1753193413508709
28. Werner FW, Green JK, Short WH, Masaoka S. Scaphoid and lunate motion during a wrist dart throw motion. *J Hand Surg Am.* May 2004;29(3):418-22. doi:10.1016/j.jhsa.2004.01.018
29. Ishikawa JI, Cooney WP, 3rd, Niebur G, An KN, Minami A, Kaneda K. The effect of wrist distraction on carpal kinematics. *J Hand Surg Am.* 1999;24(1):113-120.
30. Wolfe SW, Crisco JJ, Katz LD. A non-invasive method for studying in vivo carpal kinematics. *J Hand Surg Am.* 1997;22(2)(B):147-152.
31. Rainbow MJ, Kamal RN, Leventhal E, et al. In vivo kinematics of the scaphoid, lunate, capitate, and third metacarpal in extreme wrist flexion and extension. *J Hand Surg Am.* Feb 2013;38(2):278-88. doi:10.1016/j.jhsa.2012.10.035



32. Goto A, Leng S, Sugamoto K, Cooney WP, 3rd, Kakar S, Zhao K. In vivo pilot study evaluating the thumb carpometacarpal joint during circumduction. *Clin Orthop Relat Res.* Apr 2014;472(4):1106-13. doi:10.1007/s11999-013-3066-8
33. Stoesser H, Padmore CE, Nishiwaki M, Gammon B, Langohr GDG, Johnson JA. Biomechanical Evaluation of Carpal Kinematics during Simulated Wrist Motion. *J Wrist Surg.* May 2017;6(2):113-119. doi:10.1055/s-0036-1588025
34. Best GM, Mack ZE, Pichora DR, Crisco JJ, Kamal RN, Rainbow MJ. Differences in the Rotation Axes of the Scapholunate Joint During Flexion-Extension and Radial-Ulnar Deviation Motions. *J Hand Surg Am.* Sep 2019;44(9):772-778. doi:10.1016/j.jhsa.2019.05.001
35. White J, Couzens G, Jeffery C. The use of 4D-CT in assessing wrist kinematics and pathology. *Bone Joint J.* 2019;101(11)(B):1325-1330. doi:10.1302/0301-620X.101B11
36. Halpenny D, Courtney K, Torreggiani WC. Dynamic four-dimensional 320 section CT and carpal bone injury - a description of a novel technique to diagnose scapholunate instability. *Clin Radiol.* Feb 2012;67(2):185-7. doi:10.1016/j.crad.2011.10.002
37. Kakar S, Breighner RE, Leng S, et al. The Role of Dynamic (4D) CT in the Detection of Scapholunate Ligament Injury. *J Wrist Surg.* Nov 2016;5(4):306-310. doi:10.1055/s-0035-1570463
38. Troupis JM, Amis B. Four-dimensional computed tomography and trigger lunate syndrome. *J Comput Assist Tomogr.* 2013;37(4):639-643.
39. Repse SE, Koulouris G, Troupis JM. Wide field of view computed tomography and mid-carpal instability: the value of the sagittal radius-lunate-capitate axis--preliminary experience. *Eur J Radiol.* May 2015;84(5):908-14. doi:10.1016/j.ejrad.2015.01.020
40. Shores JT, Demehri S, Chhabra A. Kinematic 4 dimensional CT imaging in the assesment of wrist biomechanics before and after surgical repair. Epub. *Eplasty.* 2013;
41. Rauch A, Arab WA, Dap F, Dautel G, Blum A, Gondim Teixeira PA. Four-dimensional CT Analysis of Wrist Kinematics during Radioulnar Deviation. *Radiology.* Dec 2018;289(3):750-758. doi:10.1148/radiol.2018180640
42. Zhao K, Breighner R, Holmes D, 3rd, Leng S, McCollough C, An KN. A technique for quantifying wrist motion using four-dimensional computed tomography: approach and validation. *J Biomech Eng.* Jul 2015;137(7)doi:10.1115/1.4030405
43. Choi YS, Lee YH, Kim S, Cho HW, Song HT, Suh JS. Four-dimensional real-time cine images of wrist joint kinematics using dual source CT with minimal time increment scanning. *Yonsei Med J.* Jul 2013;54(4):1026-32. doi:10.3349/ymj.2013.54.4.1026
44. de Roo MGA, Muurling M, Dobbe JGG, Brinkhorst ME, Streekstra GJ, Strackee SD. A four-dimensional-CT study of in vivo scapholunate rotation axes: possible implications for scapholunate ligament reconstruction. *J Hand Surg Eur Vol.* Jun 2019;44(5):479-487. doi:10.1177/1753193419830924
45. Buzzatti L, Keelson B, Apperloo J, et al. Four-dimensional CT as a valid approach to detect and quantify kinematic changes after selective ankle ligament sectioning. *Sci Rep.* Feb 4 2019;9(1):1291. doi:10.1038/s41598-018-38101-5

46. Robinson S, Straatman L, Lee TY, Suh N, Lalone E. Evaluation of Four-Dimensional Computed Tomography as a Technique for Quantifying Carpal Motion. *J Biomech Eng.* Jun 1 2021;143(6)doi:10.1115/1.4050129
47. Kalia V, Obray RW, Filice R, Fayad LM, Murphy K, Carrino JA. Functional joint imaging using 256-MDCT: Technical feasibility. *AJR Am J Roentgenol.* Jun 2009;192(6):W295-9. doi:10.2214/AJR.08.1793
48. Kelly PM, Hopkins JG, Furey AJ, Squire DS. Dynamic CT scan of the normal scapholunate joint in a clenched fist and radial and ulnar deviation. *Hand.* 2018;13(6):666-670.
49. Brinkhorst M, Foumani M, van Rosmalen J, et al. Quantifying in vivo scaphoid, lunate, and capitate kinematics using four-dimensional computed tomography. *Skeletal Radiol.* Feb 2021;50(2):351-359. doi:10.1007/s00256-020-03543-4
50. Crompton PA, Sati M, Orr TE, Bourquin Y, Dumas GA, Nolte L-P. Animation of in vitro biomechanical tests. *J Biomech.* 2001;34:1091-1096.
51. Panjabi MM, Krag MH, Goel VK. A technique for measurement and description of three-dimensional six degree-of-freedom motion of a body joint with an application to the human spine. *J Biomech.* 1981;14:447-460.
52. Cescon C, Tettamanti A, Barbero M, Gatti R. Finite helical axis for the analysis of joint kinematics: comparison of an electromagnetic and an optical motion capture system. *Arch Physiother.* 2015;5:8. doi:10.1186/s40945-015-0008-7
53. Cescon C, Cattrysse E, Barbero M. Methodological analysis of finite helical axis behavior in cervical kinematics. *J Electromyogr Kinesiol.* Oct 2014;24(5):628-35. doi:10.1016/j.jelekin.2014.05.004
54. Ehrig RM, Heller MO. On intrinsic equivalences of the finite helical axis, the instantaneous helical axis, and the SARA approach. A mathematical perspective. *J Biomech.* Feb 14 2019;84:4-10. doi:10.1016/j.jbiomech.2018.12.034
55. Cescon C, Barbero M, Conti M, Bozzetti F, Lewis J. Helical axis analysis to quantify humeral kinematics during shoulder rotation. *Int Biomech.* Dec 2019;6(1):1-8. doi:10.1080/23335432.2019.1597642
56. Grip H, Hager C. A new approach to measure functional stability of the knee based on changes in knee axis orientation. *J Biomech.* Mar 15 2013;46(5):855-62. doi:10.1016/j.jbiomech.2012.12.015
57. Patterson RM, Nicodermus CL, Viegas SF, Elder KW, Rosenblatt J. High-speed, three-dimensional kinematic analysis of the normal wrist. *J Hand Surg Am.* 1998;23A(3):446-453.
58. Besl PJ, McKay ND. <Besl 1992- A method for registration of 3D shapes.pdf>. *IEEE Trans Pattern Anal Mach Intell.* 1992;14(2):239-256.
59. Wu G, van der Helm FC, Veeger HE, et al. ISB recommendation on definitions of joint coordinate systems of various joints for the reporting of human joint motion--Part II: shoulder, elbow, wrist and hand. *J Biomech.* May 2005;38(5):981-992. doi:10.1016/j.jbiomech.2004.05.042

60. Lalone EA, McDonald CP, Ferreira LM, Peters TM, King GW, Johnson JA. Development of an image-based technique to examine joint congruency at the elbow. *Comput Methods Biomech Biomed Engin.* 2013;16(3):280-90. doi:10.1080/10255842.2011.617006
61. Neu CP, Crisco JJ, Wolfe SW. In vivo kinematic behaviour of the radio-capitate joint during wrist flexion-extension and radio-ulnar deviation. *J Biomech.* 2001;34:1429-1438.
62. Garcia-Elias M, An KN, Cooney WP, 3rd, Linscheid MD, Chao EYS. Stability of the trasverse carpal arch: an experimental study. *J Hand Surg Am.* 1989;14(A):277-82.
63. Taleisnik J. The ligaments of the wrist. *The Journal of Hand Surgery.* 1976;1(2):110-118. doi:10.1016/s0363-5023(76)80004-4
64. Gauci MO, Waitzenegger T, Chammas PE, Coulet B, Lazerges C, Chammas M. Comparison of clinical outcomes of three-corner arthrodesis and bicolumnar arthrodesis for advanced wrist osteoarthritis. *J Hand Surg Eur Vol.* Sep 2020;45(7):679-686. doi:10.1177/1753193420905484
65. Delattre O, Goulon G, Vogels J, Wavreille G, Lasnier A. Three-Corner Arthrodesis With Scaphoid and Triquetrum Excision for Wrist Arthritis. *J Hand Surg Am.* Nov 2015;40(11):2176-82. doi:10.1016/j.jhsa.2015.07.032
66. Arvidsson I, Åkesson I, Hansson G-Å. Wrist movements among females in a repetitive, non-forceful work. *Applied Ergonomics.* 2003;34(4):309-316. doi:10.1016/s0003-6870(03)00042-5
67. Galley I, Bain GI, McLean JM. Influence of lunate type on scaphoid kinematics. *J Hand Surg Am.* Jul-Aug 2007;32(6):842-7. doi:10.1016/j.jhsa.2007.03.012
68. van de Giessen M, Foumani M, Streekstra GJ, et al. Statistical descriptions of scaphoid and lunate bone shapes. *J Biomech.* May 28 2010;43(8):1463-9. doi:10.1016/j.jbiomech.2010.02.006
69. Demehri S, Hafezi-Nejad N, Morelli JN, et al. Scapholunate kinematics of asymptomatic wrists in comparison with symptomatic contralateral wrists using four-dimensional CT examinations: initial clinical experience. *Skeletal Radiol.* Apr 2016;45(4):437-46. doi:10.1007/s00256-015-2308-0
70. Demehri S, Wadhwa V, Thawait GK, et al. Dynamic evaluation of pisotriquetral instability usng 4-dimensional computed tomography. *J Comput Assist Tomogr.* 2014;38(4)

# Appendices

## Appendix A: Ethics Approval



**Date:** 4 February 2020

**To:** Dr. Emily Lalone

**Project ID:** 111702

**Study Title:** Dynamic 4DCT to Examine the Effect of Mal-united Distal Radius Fractures on Carpal Contact Mechanics

**Application Type:** HSREB Amendment Form

**Review Type:** Delegated

**Full Board Reporting Date:** 25Feb2020

**Date Approval Issued:** 04/Feb/2020 10:00

**REB Approval Expiry Date:** 26/Sep/2020

---

Dear Dr. Emily Lalone ,

The Western University Health Sciences Research Ethics Board (HSREB) has reviewed and approved the WREM application form for the amendment, as of the date noted above.

**Documents Approved:**

Document Name	Document Type	Document Date	Document Version
LetterofInformationandConsent_V9_healthy	Consent Form	01/Feb/2020	9
Study Protocol_V9	Protocol	01/Feb/2020	9

REB members involved in the research project do not participate in the review, discussion or decision.

The Western University HSREB operates in compliance with, and is constituted in accordance with, the requirements of the TriCouncil Policy Statement: Ethical Conduct for Research Involving Humans (TCPS 2); the International Conference on Harmonisation Good Clinical Practice Consolidated Guideline (ICH GCP); Part C, Division 5 of the Food and Drug Regulations; Part 4 of the Natural Health Products Regulations; Part 3 of the Medical Devices Regulations and the provisions of the Ontario Personal Health Information Protection Act (PHIPA 2004) and its applicable regulations. The HSREB is registered with the U.S. Department of Health & Human Services under the IRB registration number IRB 00000940.

Please do not hesitate to contact us if you have any questions.

Sincerely,

Nicola Geoghegan-Morphet, Ethics Officer on behalf of Dr. Joseph Gilbert, HSREB Chair

## Appendix B: Glossary of Terms

Degrees-of-Freedom	Directions of motion in which independent motion can occur.
Antagonistic	To describe the actions of a muscle or group of muscles. An action which opposes the actions of another specified muscle or group of muscles.
Articulation	A joint or point of motion between two bones.
Axial	Generated by rotating around the axis of the body, a transverse planar image.
Biconcave	Concave on both sides.
Circumduction	The orderly combination of movements allowing rotation of a limb in a circle.
Composite	The sum of multiple parts, joints, motions.
Concave	Having a surface that curves inwards.
Coronal	In plane with the face.
Convex	Having a surface that curves outwards like a sphere.
Cuneiform	Wedge-shaped.
Deep	Away from the surface or further into the body.
Deviation (Radial or Ulnar)	Motion in the coronal plane bringing the part towards the body (ulnar), or away from the body (radial).
Displacement	Vector representing the distance travelled by an object between two points in time.

Distal	Farther from, or away from the head of the body.
Dominant (Hand)	The side preference (left vs right) which an individual prefers to use for gross and fine motor tasks of the upper extremity.
Dorsal	Towards the back of the body.
Dynamic	Characterized by motion, activity or progress.
Extension	Movement that increases the angle between two body parts. In reference to anatomic position.
Extrinsic	Muscle whose origin is in a different anatomic region than the part it moves.
Flexion	Movement that decreases the angle between two body parts. In reference to anatomic position.
Helical Axis ( <i>Screw Axis</i> )	A line that is simultaneously the axis of rotation and the line along which translation of a body in motion occurs.
Kinematics	The description of motion of points, bodies and systems of bodies without considering the forces that cause them to move.
In-Plane (Motion)	Motion constrained to two dimensions within a conventional coronal, sagittal or axial plane.
Insertion	The distal attachment of a muscle.
Intercalated	Inserted between two other bodies.
Intrinsic	Muscle who's contained wholly within the region it acts.
<i>In-vitro</i>	Process performed or taking place outside of a living organism.
<i>In-vivo</i>	Process performed or taking place within a living organism.

Lateral	Moving or away from the midline of the body.
Mean	The average.
Medial	Moving or towards the midline of the body.
Modelling	Generation of a conceptual or mathematical or visual representation of a real phenomenon or structure.
Neutral	In its original anatomic position.
Out-of-Plane (Motion)	Motion that occurs outside of the traditional two-dimensional coronal, sagittal or axial planes of motion.
Pronation	Rotation of the forearm, hand or wrist in a palm-down direction.
Proximal	Closer to, or towards to the head of the body.
Radial	Towards the radius bone; directionality term used as reference within the upper extremity irrespective of anatomic position.
Registration (Image)	The process of transforming different sets of data into one coordinate system.
Resolution	The fineness of detail in an image or ability to capture detail in an image.
Rotation	Motion around a center or axis.
Sagittal	In a plane parallel to the sagittal suture of the skull splitting the body into left and right halves.
Segmentation	To separate into defined parts.
Sharpey's Fibres	Fibres that attach a ligament or tendon to the periosteum of bone.
Static	Stationary; lacking in movement.

Stereotactic	Relating to techniques or treatments that permit accurate three-dimensional positioning in space with the use of markers and sensors.
Superficial	Towards the surface of the body.
Supination	Rotation of the forearm, hand or wrist in a palm-up direction.
Translation	Linear displacement or motion of a body.
Tubercle	Small, rounded protuberance on the surface of a bone.
Volar	Towards the palm of the hand; directionality term used as reference within the forearm, hand and wrist.
Voxel	In computer-based modelling. Element of volume that constitutes a notional three-dimensional space, especially the discrete base unit of which a three-dimensional image is divided.
Ulnar	Towards the ulna bone; directionality term used as reference within the upper extremity irrespective of anatomic position.
Unilateral	On one side of the body.



## Appendix C: Repeated-Measures ANOVA Pairwise Comparison by Kinematic Block

### Pairwise Comparisons

Measure: MEASURE\_1

(I) Group	(J) Group	Mean Difference (I-J)	Std. Error	Sig. <sup>b</sup>	95% Confidence Interval for Difference <sup>b</sup>	
					Lower Bound	Upper Bound
Capitate	Lunate	8.280 <sup>*</sup>	.520	.000	6.857	9.702
	Scaphoid	2.213 <sup>*</sup>	.655	.008	.423	4.002
	Trapezium	.904	.655	1.000	-.885	2.694
Lunate	Capitate	-8.280 <sup>*</sup>	.520	.000	-9.702	-6.857
	Scaphoid	-6.067 <sup>*</sup>	.687	.000	-7.946	-4.188
	Trapezium	-7.375 <sup>*</sup>	.687	.000	-9.254	-5.496
Scaphoid	Capitate	-2.213 <sup>*</sup>	.655	.008	-4.002	-.423
	Lunate	6.067 <sup>*</sup>	.687	.000	4.188	7.946
	Trapezium	-1.308	.794	.629	-3.478	.861
Trapezium	Capitate	-.904	.655	1.000	-2.694	.885
	Lunate	7.375 <sup>*</sup>	.687	.000	5.496	9.254
	Scaphoid	1.308	.794	.629	-.861	3.478

Based on estimated marginal means

\*. The mean difference is significant at the .05 level.

b. Adjustment for multiple comparisons: Bonferroni.

**Pass 1:** Repeated-measures ANOVA by kinematic block with pair-wise comparison between block for the first pass of FEM motion from 40 degrees of wrist extension to 40 degrees of wrist flexion. Lunate represents the proximal carpal block, capitate the distal carpal block, scaphoid the scaphoid block and trapezium the trapezium block. Significance is set at  $p < 0.05$ .

### Pairwise Comparisons

Measure: MEASURE\_1

(I) Group	(J) Group	Mean Difference (I-J)	Std. Error	Sig. <sup>b</sup>	95% Confidence Interval for Difference <sup>b</sup>	
					Lower Bound	Upper Bound
Capitate	Lunate	8.772 <sup>*</sup>	.569	.000	7.216	10.328
	Scaphoid	3.577 <sup>*</sup>	.732	.000	1.577	5.577
	Trapezium	1.502	.858	.512	-.843	3.847
Lunate	Capitate	-8.772 <sup>*</sup>	.569	.000	-10.328	-7.216
	Scaphoid	-5.195 <sup>*</sup>	.769	.000	-7.297	-3.092
	Trapezium	-7.270 <sup>*</sup>	.890	.000	-9.703	-4.837
Scaphoid	Capitate	-3.577 <sup>*</sup>	.732	.000	-5.577	-1.577
	Lunate	5.195 <sup>*</sup>	.769	.000	3.092	7.297
	Trapezium	-2.075	1.002	.257	-4.814	.664
Trapezium	Capitate	-1.502	.858	.512	-3.847	.843
	Lunate	7.270 <sup>*</sup>	.890	.000	4.837	9.703
	Scaphoid	2.075	1.002	.257	-.664	4.814

Based on estimated marginal means

\*. The mean difference is significant at the .05 level.

b. Adjustment for multiple comparisons: Bonferroni.

**Pass 2:** Repeated-measures ANOVA by kinematic block with pair-wise comparison between block for the second pass of FEM motion from 40 degrees of wrist flexion to 40 degrees of wrist extension. Lunate represents the proximal carpal block, capitate the distal carpal block, scaphoid the scaphoid block and trapezium the trapezium block. Significance is set at  $p < 0.05$ .

# **CURRICULUM VITAE**

**Dr. Manisha Mistry, MD, BMSc, FRCSC**

**Assistant Professor, The University of Ottawa Department of Surgery  
Orthopaedic Hand & Wrist Surgeon, Division of Orthopaedic Surgery  
Ottawa, Ontario, Canada  
MSc Candidate 2021**

## **PROFESSIONAL CERTIFICATION & LICENSURE**

---

<b>2019-Present</b>	<b>Fellow of the Royal College of Surgeons of Canada (FRCSC)- Orthopaedic Surgery</b>
<b>2019-Present</b>	<b>Independent Practice License</b> College of Physicians and Surgeons of Ontario 103221
<b>2020-Present</b>	<b>American Board of Orthopaedic Surgeons (ABOS) Board Eligible</b> ABOS Exam Part I Complete

## **POSTGRADUATE SURGICAL TRAINING**

---

<b>2020-2021</b>	<b>Clinical Fellowship</b> University of Western Ontario <i>Roth McFarlane Hand &amp; Upper Limb Centre, St. Joseph's Health Care, London, Ontario, Canada</i> Hand & Upper Extremity Surgery
------------------	--

- 2019- 2020**                    **Clinical Fellowship**  
*University of Toronto*  
*Sunnybrook Health Sciences Centre Toronto, Ontario,*  
*Canada*  
Upper Extremity & Trauma Surgery
- 2014-2019**                    **Residency: Orthopedic Surgery**  
*University of Ottawa*  
*The Ottawa Hospital Ottawa, Ontario, Canada*  
Division of Orthopaedic Surgery

## **GRADUATE EDUCATION**

---

- 2020-Present**                    **Master of Science (MSc), Surgery (Candidate)**  
*University of Western Ontario, London, Ontario,*  
*Canada*  
Department of Graduate Studies  
Thesis Topic: Use of 4-dimension computed tomography in analysis of carpal kinematics.

## **UNDERGRADUATE EDUCATION**

---

- 2010- 2014**                    **Medical Doctor (MD)**  
*University of Western Ontario, London, Ontario,*  
*Canada*  
Undergraduate Medical Education  
Schulich School of Medicine and Dentistry
- 2006-2010**                    **Honours Bachelor of Medical Science (BMSc. Hon)**  
*University of Western Ontario, London, Ontario,*  
*Canada*  
Honours Specialization Physiology  
Dept of Physiology and Pharmacology  
Graduated Dean's List

## **ACADEMIC APPOINTMENTS**

---

**2021 - Present**                      **Assistant Professor**  
*The University of Ottawa Department of Surgery*  
*Ottawa, Ontario, Canada*

## **HOSPITAL APPOINTMENTS**

---

**2021 - Present**                      **Associate Staff**  
Orthopaedic Hand & Wrist Surgeon  
*The Ottawa Hospital*  
*Ottawa, Ontario, Canada*

## **PROFESSIONAL MEMBERSHIPS**

---

Ontario Medical Association

Canadian Medical Association

College of Physicians and Surgeons of Ontario

Fellow of the Royal College of Surgeons of Canada

Medical Council of Canada

American College of Surgeons

Canadian Orthopaedic Association (COA)

Ontario Orthopaedic Association (OOA)

American Academy of Orthopaedic Surgeons (AAOS)

Canadian Shoulder and Elbow Society (CSES)

Orthopaedic Trauma Association (OTA)

AO North America

Wrist Evaluation Canada (WECAN)

## **COURSES & CERTIFICATIONS**

---

- 2018**                      **Canadian Shoulder Elbow Society Residents' Course**  
Ottawa, Ontario, Canada
- 2016**                      **AO Trauma Advanced**  
AO Foundation  
Orlando, Florida United States
- 2015**                      **Advanced Trauma Life Support Provider**  
Trauma Association of Canada  
Ottawa, Ontario, Canada
- 2014**                      **AO Trauma Basics**  
AO Foundation  
Markham, Ontario, Canada
- 2014**                      **Advanced Cardiac Life Support (ACLS) Provider**  
Heart and Stroke Foundation of Canada  
London, Ontario, Canada

## **PUBLICATIONS**

---

- 2013**                      V.A. Roach, **M.R. Mistry**, & T.D. Wilson. Spatial visualization ability and laparoscopic skills in novice learners: evaluating stereoscopic versus monoscopic visualizations. *Anatomical Sciences Education*. 2013. E- Published October 17<sup>th</sup>.
- 2013**                      **M. Mistry**, V.A. Roach, & T.D. Wilson. Application of stereoscopic visualization on novice laparoscopic skill acquisition. *Journal of Surgical Education*. 2013. 70(5):563-570.

## PRESENTATIONS

---

- 2021**                      **Canadian Orthopaedic Association Annual General Meeting**  
Podium Presentation  
Inadequate proximal screw fixation increases risk of mechanical failure following plate fixation of diaphyseal humerus fractures.
- 2020**                      **University of Toronto Fellows' Research Day**  
University of Toronto, Division of Orthopaedic Surgery  
Oral Presentation  
Failure characteristics following plate fixation of humeral shaft fractures.
- 2019**                      **Canadian Orthopaedic Residents Association (CORA) Meeting**  
Canadian Orthopaedic Association General Meeting 2019, Montreal QC  
Oral Presentation  
The influence of post-operative capillary blood glucose management on reoperation for infection following total joint arthroplasty
- 2018**                      **Collins Day**  
Department of Surgery, The University of Ottawa  
*Ottawa, ON*  
-Department of Surgery at the University of Ottawa, annual research day.  
Poster Presentation:  
The influence of post-operative capillary blood glucose management on reoperation for infection following total joint arthroplasty
- 2016**                      **Canadian Orthopaedic Association Annual General Meeting**  
*Vancouver, British Columbia*  
Poster Presentation:  
T1rho advanced cartilage mapping correlates with surgical outcome of patients treated for cam-type femoroacetabular impingement.

- 2015**                      **Collins Day**  
 Department of Surgery, The University of Ottawa  
*Ottawa, ON*  
 -Department of Surgery at the University of Ottawa,  
 annual research day.  
Poster Presentation:  
 T1rho mapping in hip cartilage: a two-year follow-up  
 after joint preserving surgery in hips with  
 femoracetabular impingement.
- 2015**                      **Hans K. Uhtoff Day**  
 The Department of Orthopaedic Surgery, The  
 University of Ottawa  
 Ottawa, ON  
 -Department of Orthopaedic Surgery annual research  
 day.  
Podium Presentation:  
 T1rho mapping in hip cartilage: a two-year follow-up  
 after joint preserving surgery in hips with  
 femoracetabular impingement.
- 2013**                      **Experimental Biology 2013; American Association  
 of Anatomists General Meeting**  
*Boston, Mass.*  
 -Annual general meeting of the American Association  
 of Anatomists.  
Poster Presentation:  
 Application of stereoscopic visualization on novice  
 laparoscopic skill acquisition
- 2011**                      **CSTAR Interprofessional Surgery & Anesthesia  
 School**  
*Canadian Surgical Technologies and Advanced  
 Robotics (CSTAR)*  
*London Health Sciences Centre*  
*London, Ontario*  
 -Hands on surgery and anesthesia training  
 symposium.



## CONTINUING EDUCATION

---

2020	<b>Canadian Arthroscopy Meeting</b> Virtual Forum (COVID Pandemic)
2020	<b>Ontario Orthopaedic Association General Meeting 2020</b> Virtual Forum (COVID Pandemic)
2020	<b>Orthopaedic Trauma Association General Meeting</b> <i>Virtual Forum (COVID Pandemic)</i>
2020	<b>Canadian Orthopaedic Association General Meeting</b> <i>Virtual Forum (COVID Pandemic)</i>
2019	<b>Ontario Orthopaedic Association General Meeting 2019</b> Toronto, Ontario, Canada
2019	<b>Canadian Orthopaedic Association General Meeting</b> Montreal, Quebec, Canada
2019	<b>Canadian Orthopaedic Resident Forum</b> Canadian Orthopaedic Association Calgary, Alberta, Canada
2019	<b>Orthopaedic Resident Review in Reconstruction</b> Canadian Orthopaedic Resident Review Toronto, Ontario, Canada
2019	<b>Orthopaedic Resident Review in Pediatrics</b> Canadian Orthopaedic Resident Review Toronto, Ontario, Canada
2018	<b>Orthopaedic Resident Review in Trauma</b> Canadian Orthopaedic Resident Review Toronto, Ontario, Canada
2018	<b>American Association of Orthopaedic Surgeons Annual General Meeting 2018</b> New Orleans, Louisiana, United States

- 2018                    **4<sup>th</sup> Biennial National Capital Knee Symposium**  
Ottawa, Ontario, Canada
- 2015                    **11<sup>th</sup> Symposium of Joint Preserving and Minimally  
Invasive Surgery of the Hip**  
Ottawa, Ontario, Canada

**ACADEMIC AWARDS/SCHOLARSHIPS**

---

- 2013                    **American Association of Anatomists /ASE  
Student/Postdoctoral Education Research Poster  
Presentation Award FINALIST**  
*Experimental Biology 2013 Conference, Boston Mass.*  
-Awarded to a graduate/professional with outstanding  
poster presentation presented at EB 2013 in the field of  
anatomic education.